ISSN 1732-9353 (suspended)
eISSN 2543-7496

Scientific Review

Engineering and Environmental Sciences

Przegląd Naukowy
Inżynieria i Kształtowanie Środowiska

Vol. 33 (3) 2024 Issue 105
Quarterly

SCIENTIFIC REVIEW
ENGINEERING AND ENVIRONMENTAL SCIENCES
Quarterly

EDITORIAL OFFICE ADDRESS
Wydział Budownictwa i Inżynierii Środowiska SGGW, ul. Nowoursynowska 159, 02-776 Warsaw, Poland
tel. (+48 22) 59 35 363, 59 35 210, 59 35 302
e-mail: srees@sggw.edu.pl
https://srees.sggw.edu.pl

Electronic version of the Scientific Review Engineering and Environmental Sciences is primary version

All papers are indexed in the data bases as follows: AGRO(Poznań), BazTech, Biblioteka Nauki, **CrossRef**, **DOAJ**, **Google Scholar**, **Index Copernicus**, INFONA, POL-Index, **SCOPUS**, SIGŻ(CBR)

Scientific Review

Engineering and Environmental Sciences

Przegląd Naukowy

Inżynieria i Kształtowanie Środowiska

Vol. 33 (3) 2024 Issue 105

Contents

Wydawnictwo SGGW, Warsaw 2024

Wydawnictwo SGGW wydawnictwosggw

Editorial work – Anna Dołomisiewicz, Tomasz Ruchniewicz

ISSN 1732-9353 (suspended) eISSN 2543-7496

Scientific Review Engineering and Environmental Sciences (2024), 33 (3), 227–242

Sci. Rev. Eng. Env. Sci. (2024), 33 (3) https://srees.sggw.edu.pl

ISSN 1732-9353 (suspended) eISSN 2543-7496 DOI 10.22630/srees.9824

Received: 25.05.2024
Accepted: 29.07.2024

Stefan WIEKE✉

Mendel University, Faculty of Business and Economics, Czech Republic

Decision-making in major investment projects with a life cycle cost: improvement with sensitivity analysis and sustainability assessment

Keywords: decision-making, life-cycle cost analysis, case studies, sensitivity analysis, weighted scoring, sustainability assessment, OPEX, energy costs

Introduction

Decision-makers need a reliable basis on which appropriate decisions for a company's business development can be made. In this context, decisions regarding investment in a company's technical facilities and equipment, which have a primary impact on a company's success and market assertions, are of crucial importance. In many cases, this investment is a strategic decision. Technical equipment, such as production facilities and machinery, represents a significant long-term financial investment. The evaluation of investment projects is primarily based on the discounted cash flow method, with the net present value (NPV) method constituting the most commonly applied approach. In some business areas, such as the energy sector, a life cycle cost (LCC) analysis and NPV are the preferred methods. For investment projects, decision-makers need a solid basis from which the best options can be selected.

✉xwieke@mendelu.cz

This also applies to transmission system operators (TSOs) in Germany, who operate in high-pressure natural gas pipeline networks. They plan to invest approximately 8 billion EUR by 2030 (Gasunie, 2021) and an additional investment of 20 billion EUR by 2032 for the hydrogen core network setup. To create a reliable basis for decision-making, the TSOs prepare case studies from which the best options for defined operation tasks, such as compressor station tasks, can be selected. Most case studies follow the LCC analysis procedure. In this context, reference should be made to the evaluation of operational expenditure (OPEX), such as energy and maintenance costs, and above all, to the future development of OPEX during the period under consideration. In the case studies, the period under consideration is generally set between 10 years and more than 20 or 30 years. These OPEX uncertainties, which constitute input data for the NPV calculation and future development of input data, create the risk of failing to select the best investment options, causing the misallocation of limited funds. An analysis of TSO case studies shows that the prediction of energy costs (among other cost drivers) involves high uncertainty and can lead to incorrect decisions. As these uncertainties and risks must be addressed in the evaluation, probabilistic and deterministic methods have been proposed.

This study introduces a sensitivity analysis as a deterministic method. The variation in the discount factor and operating hours allows for an assessment of the LCC outcome and provides a broader basis for decision-makers. Sustainability is becoming increasingly important and is key to a company's market success. Changes in economic, ecological, social, and technical decision-making requirements have been ignored in many case studies. Sustainability assessments with weighted scoring have been introduced, allowing for the incorporation of ecological and social aspects into decision-making. Seven case studies, performed by experts from consulting firms and reviewed by experts from the TSOs, are available for assessment. These case studies serve as the basis for decision-making on natural gas infrastructure investments and represent experts' opinions (i.e., experts from consulting firms and the TSOs). However, these case studies are not publicly accessible, which is generally the case with private sector case studies. Therefore, such case studies are typically not available for scientific research. This study focuses on investments in compressor stations in Germany's natural gas infrastructure. Its results are applicable to other investment decisions involving machinery, energy, and maintenance costs as drivers.

Material and method

Managing uncertainties using deterministic methods

Deterministic methods are used if the input data can be determined; for example, if historical data are available. However, the extrapolation of historical data for future development is associated with several uncertainties that must be quantified and evaluated. With the help of deterministic methods, the evaluation of the future development of input data can be conducted. Scope et al. (2016) suggest the following methods for mitigating uncertainties: rule of thumb/best guess and sensitivity analysis.

The rule of thumb procedure appears to have no stable foundation and is based solely on the experience of the study authors. It is a simplified procedure that is often used, as in the case studies examined herein. For example, historical data are simply extrapolated as percentages for the future. However, this does not represent an uncertainty assessment or risk analysis. A sensitivity analysis is a suitable method for estimating uncertainties because it is established, straightforward, easy to apply, and provides a comprehensive assessment of the input data's validity. The EN 15663 standard (European Committee for Standardization [CEN], 2017) refers to a sensitivity analysis method for evaluating uncertainties. Nábrádi and Szöllösi (2007) state that "given the uncertainty that may exist about the future, it is often useful to make a sensitivity analysis, which asks a number of 'what if' questions".

Moins et al. (2020) assert that deterministic methods are easy to apply because they involve the use of discrete variables that cause a single output value. If a sensitivity analysis is performed, a one-factor-at-a-time (OFAT) simulation is performed (Moins et al., 2020). The results can be evaluated and compared with those of the initial calculations to identify whether a change in the input affects the overall conclusion and ranking of the alternatives (Moins et al., 2020).

Weighted scoring

Zardari et al. (2014) provide a summary of the main categories of multi-criteria decision-making methods and the key issues that arise from their application. Zardari et al. (2014) describe a 'weighted summation' as the simplest form of a multi-attribute utility analysis that applies a linear relationship. It involves standardizing the scores across all criteria, assigning preference weights, multiplying the weights by the scores, adding up the resulting scores to obtain

Wieke, S. (2024). Decision-making in major investment projects with a life cycle cost: improvement with sensitivity analysis and sustainability assessment. *Sci. Rev. Eng. Env. Sci.*, *33* (3), 227–242. DOI 10.22630/srees.9824

total weighted scores for each alternative, and determining the ranking of the total weighted scores.

Although this method requires quantitative information on scores and priorities, only the relative values are used in the assessment. However, the method provides a complete ranking of options and information on the relative differences between options. The weighted summation results can be presented in bar graphs showing the relative contribution of all criteria or objectives compared to the overall rankings of alternatives. These rankings can be used to analyze the sensitivities of the rankings of alternatives to the overall uncertainties in both effects and priorities.

According to Baskaran (2018), weighted scoring is a multi-criteria decision--making method used to discover the relationship between the criteria and alternatives. When using this method, the weights of the criteria are multiplied by the values of alternatives, and the weighted sum indicates the overall sum of the process. Here, the terms 'option' and 'alternative' are synonyms.

Sustainability assessment

Companies are defined by their economic success and sustainability, and company policies designed to promote sustainability are becoming increasingly important. Visentin et al. (2020) assert that countless methods have been developed for assessing sustainability. In this context, a life cycle assessment (LCA) is an important tool for scientific investigations and is normalized using the ISO 14040 standard (International Organization for Standardization [ISO], 2006). However, it only includes the environmental dimension of sustainability. Due to the need to implement a broader and more complete approach to sustainability, the life cycle sustainability assessment (LCSA) method was developed (Visentin et al. 2020). According to Klöpffer (2008), LCSA combines LCA, LCC, and social life cycle assessment (S-LCA). Although LCA is the most popular tool, significant efforts have been made to develop methodologies for LCC and S-LCA (Visentin et al. 2020).

The Corporate Sustainability Reporting Directive (CSRD) was enacted by the European Union on January 5, 2023 (Directive (EU) 2022/2464). The following can be read on the European Union's website:

"The CSRD modernizes and strengthens the rules concerning the social and environmental information that companies have to report.

The new rules will ensure that investors and other stakeholders have access to the information they need to assess the impact of companies on people and the environment and for investors to assess financial risks and opportunities

arising from climate change and other sustainability issues." (European Commission [EC], n.d.).

This means that companies are not only assessed on the basis of their financial performance, but also on the basis of non-financial indicators.

The application of ESG criteria from ESG reporting makes the weighted scoring and thus the assessment of sustainability more objective. Oliver Yébenes (2024) provides an overview of the criteria. Environmental criteria include, for example, physical risks, transition risks or market risks. Social criteria include the company's social responsibility for the products, health and safety of the process.

Sensitivity analysis as a deterministic method

As described in the ISO 15663 standard (ISO, 2006), a sensitivity analysis involves testing LCC outcomes to establish whether the conclusion is sensitive to changes in assumptions. This study applies the OFAT method. Accordingly, this study applies a sensitivity analysis to the deterministic input data. In LCC, the following constitute key data to identify the best options for investments in compressors: the discount rate for calculating the NPV (and discounted cumulated expenditure [DCE]), and operating hours. As the discount rate is not easy to fix, a range is used to give decision-makers a broader basis from which they can choose. The operating hours of the equipment determine the energy and maintenance costs. The number of hours (i.e., 2,000 hours per year or 8,000 hours per year) significantly impacts these costs and the DCE. A high number of operating hours gives energy costs greater leverage over CAPEX.

In the DCE calculation, the discount rates are calculated for each option in each case study within a broad range of 4% and 15%. Figures 1 and 2 show their impacts on the magnitudes of the costs and rankings of the options. The DCE calculations for each option in every case study are undertaken with three selected assumptions for operating hours per year. The case studies' required operating hours per year are provided by the TSOs. Unfortunately, assumptions regarding the operating regime and projected annual operating hours are difficult to establish; therefore, they are associated with uncertainties. For this reason, the impact of the number of operating hours per year on the outcome provides valuable information for decision-makers. As explained earlier, operating hours significantly affect the OPEX and OPEX–capital expenditure (CAPEX) ratios. Moreover, similar to the discount rate, operating hours impact both the DCE amount and ranking of options.

Wieke, S. (2024). Decision-making in major investment projects with a life cycle cost: improvement with sensitivity analysis and sustainability assessment. *Sci. Rev. Eng. Env. Sci.*, *33* (3), 227–242. DOI 10.22630/srees.9824

Equal DCE for the ratio of energy costs

This study extends the sensitivity analysis to include further aspects of the energy costs evaluation as the main cost driver of OPEX. Thus, the electricity–natural gas cost ratio is calculated; the DCE is equal for both. The value of this ratio (which is a factor) gives decision-makers another indicator on which they can base their decisions regarding the options under consideration. This clarifies the factor that may lead to a form of energy (e.g., natural gas) becoming more expensive and cause the same DCE as that calculated for another energy form (i.e., electricity). This factor is implemented and evaluated based on the energy costs in the three case studies' options.

Sustainability assessment with weighted scoring

The economic, environmental, social, and technical decision-making requirements are rapidly changing. Germany's natural gas industry has been responding and adapting to these changing requirements for over a decade. In the decision-making process, LCC does not sufficiently reflect these aspects when selecting the best options. Climate protection issues are gaining importance, which, in this context, relate to the CO_2 emissions of the prime movers. However, these issues cannot be addressed using the LCC model alone. TSOs must also minimize emissions and select compressors/drivers with low-to-zero emissions. The selection of hermetically sealed compressors can support this goal. TSOs will continue to evolve from transporters of natural gas to hydrogen during decarbonization. The technical preconditions for this transformation must be implemented; thus, climate protection has become increasingly important. TSOs have already started to make green engineering a key factor. The social acceptance of this business sector is at stake. The preparation for hydrogen transport (H_2 readiness) and compliance with climate protection targets increase the public's acceptance of pipeline operators (i.e., TSOs). Every technical facility in Germany sits alongside a residential neighborhood. Smooth operations are guaranteed only if residents accept the technical facilities. The more sustainable the facility, the more acceptable it is. The facility operators depend on the neighborhoods; for example, in the case of a fire, support depends on voluntary fire departments.

TSOs are employers that provide high-quality jobs associated with the facilities. Providing good jobs with modern working conditions is an important aspect of a social assessment. Consumers are more likely to accept companies if they are sustainable. Raising funds from investors is easier if a company or sector is

considered sustainable. Meanwhile, good relationships with local communities are important because legal authorizations depend on them.

Accordingly, these aspects must be addressed when selecting the best investment options. An LCC analysis is important, but not the only criterion. The LCC results represent the economic part of a sustainability assessment, while the CAPEX, maintenance costs, and energy costs can be considered as the criteria. Moreover, TSOs have special characteristics that are not considered in the LCC model; for example, operating personnel's experience with new compressors and drivers to be installed. In this case, if the operating personnel are experienced only with gas turbines (GT), then installing an electric motor poses an organizational challenge. So, operating personnel must be retrained or supplemented with specialists. These criteria can be included in the weighted scoring. As these criteria are not associated with sustainability, they are omitted. The weighted scoring highlights other significant aspects apart from LCC. Economic considerations are of fundamental importance and must be included in a sustainability assessment. These questions and aspects, which are of great importance for a company's further development, cannot be sufficiently considered by the LCC model alone. Therefore, an established procedure must be introduced to consider these aspects. So, the sustainability assessment utilizes weighted scoring. In the course of the sustainability assessment, a full-scale life cycle assessment (LCA) could be included.

In the weighted scoring, the criteria are weighted, and the fulfilment of these criteria is assessed using points that represent the fulfilment degree of the criteria. The scores range from 1 to 10 (10 = 100% fulfilment). The criteria and weightings must be determined in advance by the team that prepares the case study, which forms the basis for the decision-makers. The methodology is as follows: the weighted scoring involves standardizing the scores for all criteria, assigning preference weights, multiplying the weights by the scores, adding the resulting scores to obtain the total weighted scores for each alternative, and ranking the total weighted scores (Zardari et al., 2014).

Results and discussion

Sensitivity analysis of discount rates and operating hours

Figures 1 and 2 illustrate the effects of different discount rates and operating hours per year on the DCE calculations of the case studies. Each graph depicts the DCE calculation as a function of the discount rate. The results for all case studies are not presented here due to space limitations. Instead, the results for the models used in

Wieke, S. (2024). Decision-making in major investment projects with a life cycle cost: improvement with sensitivity analysis and sustainability assessment. *Sci. Rev. Eng. Env. Sci.*, *33* (3), 227–242. DOI 10.22630/srees.9824

Case Studies 2 and 6 are shown. While Case Studies 2 and 6 are selected because the sensitivity analysis effects are significant, the other case studies also show significant sensitivity analysis effects. The graphs are based on real historical data for the energy and maintenance costs, and the discount rate is plotted for each option. For each of the two options, the operating hours per year range from approximately 6 to 15% and from 4 to 12%, respectively. In Figure 1 (Case Study 2), the three graphs show the calculated DCE as a function of the discount rates for 1,000, 2,880, and 8,000 operating hours.

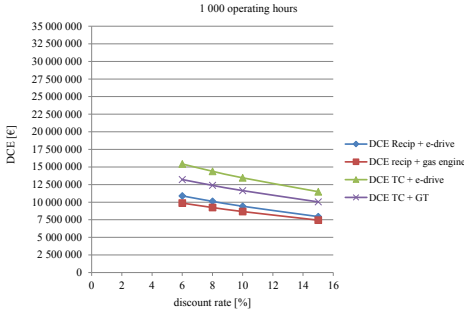

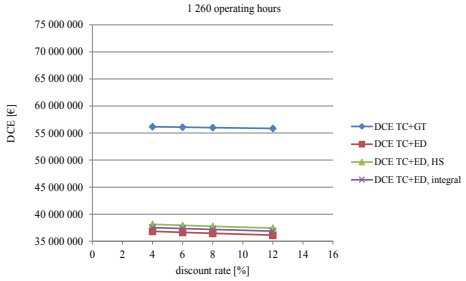

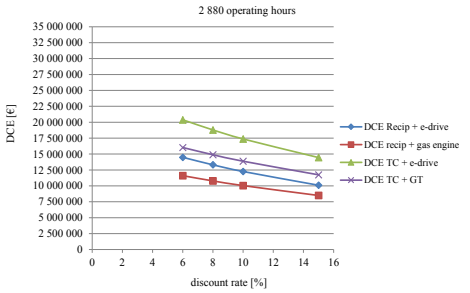

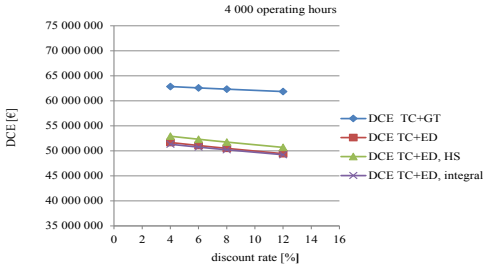

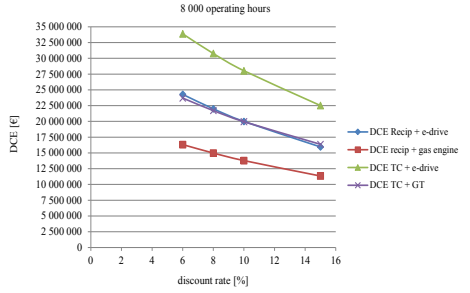

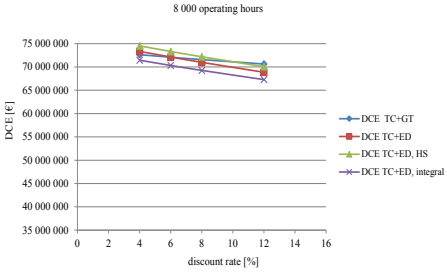

FIGURE 1. Case Study 2: DCE for real (historical) input data, calculated for several discount rates and three different operating hours per year

Source: own work.

FIGURE 2. Case Study 6: DCE for real (historical) input data, calculated for several discount rates and three different operating hours per year

Source: own work.

The DCEs of four different options are compared. The options constitute combinations of different compressor types and drivers. The drivers are powered by either electricity (electric drive) or natural gas (gas engine and GT). The option with the lowest DCE is the preferred option.

In Case Study 2, the dependency of DCE on the discount rate is immediately apparent. As the number of operating hours increases, the calculated DCE also increases, since the number of operating hours directly determines the energy and maintenance costs. At 1,000 and 2,880 operating hours, there are no changes in the option rankings. At 8,000 operating hours, DCE increases, and the ranking order changes. Compared with CAPEX, the influence of OPEX is clear when the compressors are almost fully utilized. Although the "Recip+Gas engine" option remains the most advantageous, the "TC+GT" and "Recip+ED-" variants switch positions at a discount rate of 9%. The gas engine option remains the best over the range of operating hours.

In Figure 2 (Case Study 6), the three graphs show the calculated DCE as a function of the discount rates for 1,260, 4,000, and 8,000 operating hours, respectively. In contrast to Case Study 2, only the turbo compressors (TC) and reciprocating compressors (Recip) are considered. The electric motors in the various designs (electric drive [ED], high speed [HS], and integral) and GT are examined as drivers.

Case Study 6 demonstrates the same pattern as that observed in Case Study 2. DCE increases with the operating hours. At 4,000 operating hours, the "TC+ED, integral" variant is equivalent to the "TC+ED" variant or is more advantageous, depending on the discount rate. At 8,000 operating hours, the "TC+ED, integral" variant is the variant to be selected for all discount rates. The graphs are not shown due to place constraints.

The discount rate and number of operating hours can change the ranking of options and affect the calculated DCE.

Decision-makers can use these measures to assess the changes in major cost drivers (i.e., electricity and natural gas) and analyze their impact on the calculated DCE using the cost model. Here, this study presents the effect of the discount rate. The decision--making can be effectively supported with the sensitivity analysis results, as the decision-makers can obtain a clearer picture of the impact of the main cost drivers.

Equal DCE for the ratio of energy costs

The main cost driver for OPEX are the energy costs combined with operating hours. While the electricity and natural gas costs greatly differ, they are still included in the model regardless. For the decision-makers, the quotient of the energy costs to achieve the same DCE is an additional valuable basis for securing their decisions.

Wieke, S. (2024). Decision-making in major investment projects with a life cycle cost: improvement with sensitivity analysis and sustainability assessment. *Sci. Rev. Eng. Env. Sci.*, *33* (3), 227–242. DOI 10.22630/srees.9824

To investigate the ratio of electricity to natural gas costs, DCE is considered equal, and two examples are selected to show the efficiency of the approach. For this purpose, this study analyzes the DCE calculations that use real historical data. It selects case studies that compare options and operate with different energy sources; no more than four options are compared to ensure clarity. Case Studies 2 and 4 fulfil these requirements.

Figure 3 shows the results for Case Study 2. This case study compares four options: two powered by electric energy and two powered by natural gas. Figure 1 (2,880 operating hours) demonstrates the DCE calculation using real historical energy data (factor 1 for increase of price of natural gas). In Figure 3, the costs for natural gas are increased by a factor of 2.3, such that the options for choosing natural gas and electric are (almost) congruent.

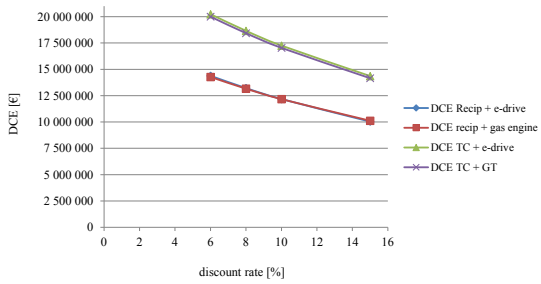

FIGURE 3. Case Study 2: equal DCE by increase in the price for natural gas
Source: own work.

The ranking in Figure 3 shows that the "Recip+Gas engine" option has the lowest DCE; thus, it is the most advantageous. This option is powered by natural gas. The following question arises: what factor must the natural gas price be increased by so that the DCE of the "Recip+Gas engine" option becomes equal to that of the "Recip-ED" option? If natural gas prices increase by a factor of 2.3, there is an almost complete match between the two curves of the "Recip+Gas engine" and "Recip+ED" options over the entire discount rate range. Moreover, a convergence of the curves for the "TC+GT" and "TC+ED" options can be observed.

Another example is Case Study 4 which examines two options. The approach is similar to that used in Case Study 2.

The natural gas option has a lower DCE, making it a suitable option for selection. Multiplying by a factor of 3.4 results in almost a full coverage of the two curves over the entire discount rate range. This result clearly supports the decision in favor of the natural gas-powered option, which, in this case, is the "GT-driven" option.

Sustainability assessment with weighted scoring

Table 1 shows the weighted scoring for the sustainability assessment of Case Study 4. This table shows the sustainability criteria as follows: environmental (30%), social (30%), and economic (40%). Weighting must be determined by TSO experts. The weighting and scoring setting clearly impact the outcome. So, the decision needs to be made before the process starts. The selection of the criteria and their weightings must not change during the decision-making process to ensure that the assessment is as objective as possible.

TABLE 1. Weighted scoring for options in Case Study 4

Sustainability	Weighting [%]	Option 2 TC + EM	Score	Weighted Score	Option 1 TC +GT	Score	Weighted Score
Environmental (LCA)	**30**			**2.15**			**0.75**
Emissions CO_2	15		8	1.2		2	0.3
Emissions CH_4	5		5	0.25		3	0.15
H_2 ready	10		7	0.7		3	0.3
Social	**30**			**2.4**			**0.95**
Neighborhood acceptance	5		8	0.4		3	0.15
High-quality jobs	5		8	0.4		8	0.4
Consumers	15		8	1.2		2	0.3
Local community	5		8	0.4		2	0.1
Economic (LCC)	**40**			**2.3**			**3.3**
CAPEX	10		4	0.4		10	1
Maintenance costs	10		9	0.9		5	0.5
Energy costs	20		5	1		9	1.8

Final weighted scoring (max. 10 points)	**Turbo compressor + Electric drive**	**6.85**	**Turbo compressor + Gasturbine**	**5.00**
Ranking	**1**		**2**	

Source: own work.

The criteria and associated weighting show that the "TC+EM" option is preferable to the "TC+GT" option. The EM is equivalent to the ED. Overall, the former has a higher sustainability assessment score. LCC is included

Wieke, S. (2024). Decision-making in major investment projects with a life cycle cost: improvement with sensitivity analysis and sustainability assessment. *Sci. Rev. Eng. Env. Sci.*, *33* (3), 227–242. DOI 10.22630/srees.9824

in the sustainability assessment at 40% only. This leads to a different ranking from that of the LCC-only analysis. The DCE calculation for Case Study 4 shows that the "TC+GT" variant is more beneficial according to the LCC analysis. A sustainability assessment can change the ranking of options when compared with a pure LCC analysis, and can provide a more comprehensive approach to assessments.

Table 2 shows only the input values, which are made up of the sustainability criteria and their weighting.

Once the scores have been entered, the weighted scores are calculated, resulting in the ranking.

TABLE 2. Input values for weighted scoring

Sustainability	Weighting [%]	Option 2 TC + EM	Score	Weighted Score	Option 1 TC +GT	Score	Weighted Score
Environmental (LCA)	**30**			**0**			**0**
Emissions CO_2	15			0			0
Emissions CH_4	5			0			0
H_2 ready	10			0			0
Social	**30**			**0**			**0**
Neighborhood acceptance	5			0			0
High-quality jobs	5			0			0
Consumers	15			0			0
Local community	5			0			0
Economic (LCC)	**40**			**0**			**0**
CAPEX	10			0			0
Maintenance costs	10			0			0
Energy costs	20			0			0

Final weighted scoring (max. 10 points)	**Turbo compressor + Electric drive**	**0.00**	**Turbo compressor + Gasturbine**	**0.00**
Ranking				

Source: own work.

Conclusions

The decision-making process for Germany's natural gas infrastructure investments is based on LCC. This study's investigation of seven LCC-based case studies on investment decisions in compressor stations shows that incorrect decisions are made due to the input data used and the predictions of the input data's future development.

To reduce the risk of incorrect decisions, this study examines various methods via a sensitivity analysis of the discount factor and operating hours. The number of operating hours directly influences the energy and maintenance costs. The analysis shows the effects of variations in the input data. Both the calculated DCE and ranking of the options change. A higher DCE means a higher OPEX, which can affect the cash flow and subsequent investment decisions. The effects of the different discount factors are illustrated.

To further validate the investment decisions, the energy costs are set in relation to each other with the same DCE for the options. If the factor is 2.3, as in Case Study 2, then the cost of natural gas can increase by a factor of 2.3 compared to the cost of electricity, until the electricity options are more advantageous than those of the natural gas options. These measures provide decision-makers with additional information regarding the sensitivity of the input data and its influence on profitability.

In addition to the economic criteria, a sustainability assessment can determine a company's market success. Sustainable companies achieve higher levels of social acceptance, which, in turn, affects their economic results. For this reason, this study presents decision-makers with a sustainability assessment that considers social, ecological, and economic aspects. The sustainability assessment is based on a weighted scoring method, as demonstrated in Case Study 4, considering that weighted scoring in sustainability assessments can lead to a change in the ranking of options. Weighted scoring can include a full scale LCA to address the environmental impact.

The definition of the criteria primarily considers the subjective assessment of the team. The criteria should not be subjective, but objective. One possibility is to use ESG reporting, which is based on the Corporate Sustainability Reporting Directive (CSRD) of the EU. Further research shall integrate sustainability assessment with weighted scoring and objective criteria for environmental and social requirements based on LCA and ESG reporting.

In the examined case studies, this study only conducted sensitivity analyses for three studies; specifically, for operating hours. It did not conduct sustainability

assessments. Therefore, decision-makers could only receive a limited overview of the effects of their decisions, which could lead to a misallocation of investment funds. To prevent this, the basis for decision-making must be expanded. Sensitivity analyses and sustainability assessments are effective measures that provide decision-makers with much broader bases for their decision-making. Sensitivity analyses are among the deterministic methods used for reducing uncertainties. The effectiveness of probabilistic methods, such as the Monte Carlo simulation for risk mitigation, should also be included in the case studies. Accordingly, the key risk mitigation measures can be implemented, and the decision-makers can obtain a comprehensive overview of investments together with the measures described in this study. Although this study relates to LCC in Germany's natural gas infrastructure, the suggested process can be adopted for other investment projects comprising CAPEX and OPEX.

References

Baskaran, S. M. (2018). Ranking of lean tools using weighted scoring method. *Transportation*, *30*, 0–30.

Directive (EU) 2022/2464 of the European Parliament and of the Council of 14 December 2022 amending Regulation (EU) No 537/2014, Directive 2004/109/EC, Directive 2006/43/EC and Directive 2013/34/EU, as regards corporate sustainability reporting. PE/35/2022/REV/1 (OJ L 322, 16.12.2022, p. 15–80).

European Commission [EC], [n.d.]. *Corporate sustainability reporting*. https://finance.ec.europa.eu/capital-markets-union-and-financial-markets/company-reporting-and-auditing/company-reporting/corporate-sustainability-reporting_en

European Committee for Standardization (2017). *Railway applications. Vehicle reference masses* (EN 15663).

Gasunie (2021). *Transmission system operators want to invest 7.8 billion euros in secure and fit for future networks*. Gasunie. https://www.gasunie.de/news/fernleitungsnetzbetreiber-wollen-78-milliarden-euro-in-versorgungssichere-und-zukunftsfaehige-netze-investieren

International Organization for Standardization [ISO], (2006). *Environmental management. Life cycle assessment. Principles and framework* (ISO 14040).

Klöpffer, W. (2008). Life cycle sustainability assessment of products (with comments by Helias A. Udo de Haes, p. 95). *The International Journal of Life Cycle Assessment*, *13*, 89–95. https://doi.org/10.1065/lca2008.02.376

Moins, B., France, C., Van den bergh, W., & Audenaert, A. (2020). Implementing life cycle cost analysis in road engineering: A critical review on methodological framework choices. *Renewable and Sustainable Energy Reviews*, *133*, 110284. https://doi.org/10.1016/j.rser.2020.110284

Nábrádi, A., & Szöllösi, L. (2007). Key aspects of investment analysis. *APSTRACT: Applied Studies in Agribusiness and Commerce*, *1* (1), 53–56. http://dx.doi.org/10.22004/ag.econ.43577

Oliver Yébenes, M. (2024). Climate change, ESG criteria and recent regulation: challenges and opportunities. *Eurasian Economic Review*, *14* (1), 87–120. https://doi.org/10.1007/s40822-023-00251-x

Scope, C., Ilg, P., Muench, S., & Guenther, E. (2016). Uncertainty in life cycle costing for long-range infrastructure. Part II: guidance and suitability of applied methods to address uncertainty. *The International Journal of Life Cycle Assessment*, *21*, 1170–1184. https://doi.org/10.1007/s11367-016-1086-9

Visentin, C., Silva Trentin, A. W. da, Braun, A. B., & Thomé, A. (2020). Life cycle sustainability assessment: A systematic literature review through the application perspective, indicators, and methodologies. *Journal of Cleaner Production*, *270*, 122509. https://doi.org/10.1016/j.jclepro.2020.122509

Zardari, N. H., Ahmed, K., Shirazi, S. M., & Yusop, Z. B. (2014). *Weighting methods and their effects on multi-criteria decision making model outcomes in water resources management*. Springer.

Summary

Decision-making in major investment projects with a life cycle cost: improvement with sensitivity analysis and sustainability assessment. This study focuses on compressor station investments in Germany's natural gas infrastructure, offering insights applicable to machinery, energy, and maintenance cost-driven decisions. A life cycle cost (LCC) analysis can guide investment choices; however, uncertainties in input data and future developments pose risks. The LCC-based studies encounter questions impacting their results and optimal selections. These uncertainties may lead to misallocations, emphasizing the need for careful consideration of investment decisions to avoid potential consequences and efficiently allocate limited funds. Various measures are available to mitigate the uncertainties and risks in LCC analyses. Recognized measures are deterministic and probabilistic. Seven case studies on investments in the natural gas infrastructure in Germany were analyzed in this context. In addition to the executed case studies, a case study from a scientific journal (published in 2001) was included in the analysis. The case studies were conducted by transmission system operators from 2005–2015, and a retrospective view made it possible to recognize whether the best options (due to the LCC analysis) were identified. Simulations were conducted with generated models using real historical input data such as energy costs. The re-calculation of the net present value or better discounted cumulated expenditure with real input data shows that the LCC analysis results are significantly dependent on the reliability of the input data and the prediction of their development. Therefore, validating the results using appropriate measures is mandatory. This study illustrates how sensitivity analysis can be used as a deterministic method to evaluate the LCC analysis

results. A company's success is increasingly determined by its sustainability. A pure LCC analysis is insufficient, so social, ecological, and economic sustainability assessments must be conducted. This study demonstrates the effectiveness of the weighted scoring method for sustainability assessments. Although this study relates to LCC in Germany's natural gas infrastructure, the suggested process can be adopted for other investment projects comprising capital and operational expenditures.

Scientific Review Engineering and Environmental Sciences (2024), 33 (3), 243–260

Sci. Rev. Eng. Env. Sci. (2024), 33 (3) https://srees.sggw.edu.pl

ISSN 1732-9353 (suspended) eISSN 2543-7496 DOI 10.22630/srees.9780

Received: 26.04.2024
Accepted: 24.06.2024

Abderrahim GUETTECHE[1, 2]✉
Salaheddine BENSEBTI[1]
Samy MEZHOUD[1]
Tien-Tung NGO[2]
El-Hadj KADRI[2]

[1] University Mentouri of Constantine, Department of Civil Engineering, Laboratoire Matériaux et Durabilité des Constructions, Algérie
[2] University Cergy Pontoise, Department of Civil Engineering, Laboratoire de Mécanique et Matériaux du Génie Civil (L2MGC), France

Structural evaluation and durability potential of cementitious materials based on expanded clay kiln dust

Keywords: characterization, expanded clay kiln dust (ECKD), mortar, strength, substitution

Introduction

The construction industry heavily relies on cement as a fundamental element, particularly in the production of concrete, the most widely used construction material globally (Akhtar & Sarmah, 2018). However, despite its undeniable benefits in terms of strength and durability, cement production carries significant environmental impacts, primarily attributed to carbon dioxide (CO_2) emissions from limestone calcination. Construction activities contribute to approximately 20% of CO_2 emissions worldwide (Gao et al., 2015). With rapid urbanization

✉abderrahime.guetteche@doc.umc.edu.dz

and increasing infrastructure demands, pressure on natural resources and the environment escalates. Hence, there is an urgent need to explore sustainable alternatives to conventional cement to mitigate the construction industry's carbon footprint.

The substitution of cement with alternative materials or innovative construction techniques emerges as a promising solution to alleviate the environmental impacts associated with cement production (Kumar & Sharma, 2018). Materials such as fly ash, blast furnace slag, construction and demolition waste residues, as well as geopolymer-based binders, have been investigated as potential substitutes for traditional portland cement (Faleschini et al., 2016). These materials not only offer environmental benefits by reducing CO_2 emissions, but also have the potential to enhance concrete properties such as durability and resistance to chemical attacks.

Expanded clay kiln dust (ECKD) is a derivative of the cement production process, similar to CKD, but with a distinct composition and properties. This substance is obtained from the expanded clay manufacturing process, where raw clay undergoes thermal treatment to create lightweight aggregate. During this process, fine particles are generated and collected as ECKD. While ECKD shares similarities with CKD, its unique characteristics, including particle size distribution and mineralogy, offer opportunities for alternative applications in cementitious materials (Abdel-Gawwad et al., 2021).

Expanded clay kiln dust, considered pozzolanic due to its significant silica content, presents a viable option for cement substitution. While CKDs have demonstrated to be effective in stabilizing soils and materials, very little has been done to understand the mechanisms responsible for the improved behavior (Sreekrishnavilasam & Santagata, 2006). Similarly, the mechanisms underlying the effectiveness of ECKD as a cement substitute remain to be clarified. Furthermore, research into the utilization of ECKD in cement, mortar, and concrete has shown promising results. Studies have investigated its potential as a supplementary cementitious material, exploring its effects on hydration kinetics, mechanical properties, and durability of concrete (Kaminskas & Savickaite, 2023). Pozzolanic and hydraulic properties of ECKD contribute to the formation of additional cementitious phases, leading to improved strength development and reduced permeability in concrete mixtures (Ogila, 2021). Moreover, ECKD's lightweight nature can enhance the workability and reduce the density of concrete, making it particularly suitable for applications where weight reduction is desired (Shoaei et al., 2017). In addition to its use in concrete, ECKD has been studied as

a partial replacement for cement in mortar formulations. Studies have demonstrated the potential of ECKD to enhance the performance of mortar by improving its workability, bond strength, and resistance to sulfate attack (Al-Bakri et al., 2022). Incorporating ECKD into mortar mixtures not only reduces the environmental impact associated with cement production, but also provides economic benefits by utilizing a waste material effectively (Luhar et al., 2021).

The objectives of this study are twofold: first, to assess the efficacy of ECKD as a cement substitute in mortars, and second, to understand the mechanisms underlying its performance enhancement. Through a comprehensive evaluation of ECKD's properties and its impact on mortar characteristics, this research endeavors to contribute to the advancement of sustainable construction practices.

Research significance

The significance of this research lies in addressing pressing environmental and economic challenges associated with the cement industry while advancing sustainable practices in construction materials. Cement production is a major contributor to greenhouse gas emissions, with the calcination process alone accounting for a significant portion of CO_2 emissions worldwide. By exploring the potential of using ECKD as a substitute or supplement element for conventional cement, this research seeks to mitigate the environmental impact of cement production by reducing CO_2 emissions and promoting resource efficiency. Furthermore, the utilization of ECKD offers opportunities for waste valorization and circular economy principles within the cement industry. As a byproduct of the expanded clay manufacturing process ECKD presents an underutilized resource that can be repurposed in cementitious materials, thus reducing reliance on raw materials and minimizing waste generation.

Implementing ECKD in cement, mortar, and concrete formulations not only diversifies the feedstock for construction materials, but also contributes to cost savings and resource conservation. Moreover, the findings of this research are expected to inform industry stakeholders, policymakers, and researchers about the feasibility and practicality of incorporating ECKD into cement, mortar, and concrete production. By demonstrating the technical feasibility, economic viability, and environmental benefits of using ECKD in construction materials, this research paves the way for wider adoption and implementation of sustainable practices in the cement industry.

Guetteche, A., Bensebti, S., Mezhoud, S., Ngo, T-T., Kadri, E-H. (2024). Structural evaluation and durability potential of cementitious materials based on expanded clay kiln dust. *Sci. Rev. Eng. Env. Sci.*, *33* (3), 243–260. DOI 10.22630/srees.9780

Methodology

The methodology employed in this study comprises three distinct phases aimed at comprehensively evaluating the potential of expanded clay kiln dust (ECKD) in cementitious materials. The initial phase involved preliminary inspections and the preparation of study materials, including the collection and characterization of ECKD samples. This phase also encompassed the meticulous preparation of specimens according to predetermined mix proportions to ensure consistency and reproducibility in subsequent testing procedures. The second phase focused on the characterization of specimens through the microstructural analysis, which involved techniques such as energy dispersive X-ray spectroscopy (EDX) for chemical analysis, scanning electron microscopy (SEM) for morphology analysis, and thermal analysis (DTA-TGA) for understanding the thermal behavior of materials. Differential thermal analysis (DTA) and thermogravimetric analysis (TGA) were utilized to investigate the morphology, phase composition, and hydration products within the cementitious matrix. This characterization step provides valuable insights into the interactions between ECKD and other components of the cementitious system, elucidating its potential influence on material properties.

Subsequently, the third stage of the methodology involved mechanical testing to assess the performance of ECKD-incorporated specimens in terms of compressive and flexural strength. Standardized testing protocols were employed to measure the mechanical properties of the specimens, including ASTM International standards for compressive strength – ASTM C39-19 (ASTM International [ASTM], 2019), and for flexural strength – ASTM C78-18 (ASTM, 2018). The obtained data were analyzed to evaluate the effects of ECKD on the mechanical behavior of cementitious materials, comparing results with control specimens containing conventional cement. Additionally, a step was taken to evaluate the long-term durability of specimens in seawater compared to conservation in normal conditions in ambient air or normal water. This step aimed to understand the effects of environmental exposure on the performance of ECKD-incorporated specimens over time.

A comprehensive analysis of the results and findings from each phase of the study facilitated the formulation of meaningful conclusions regarding the efficacy and potential applications of ECKD in cement and mortar. The flowchart and experimental setup depicting the methodology employed in this research are illustrated in Figure 1, providing a visual representation of the sequential steps involved in the study. Through this systematic approach, this study contributes valuable insights into the utilization of ECKD as a sustainable alternative in cementitious materials.

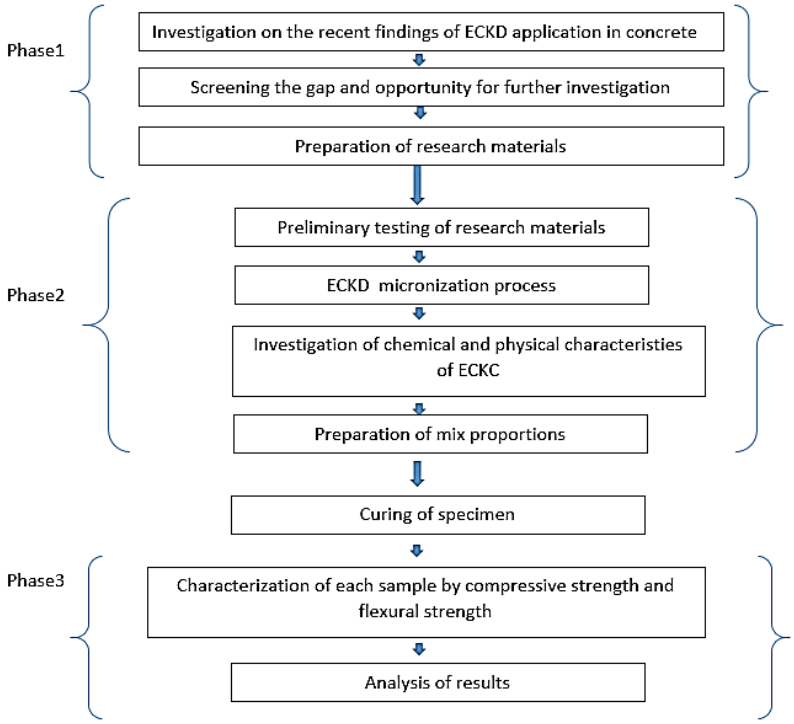

FIGURE 1. Flowchart of the methodology
Source: own work.

Experimental procedure

Materials

The cement utilized in this study is CEM I 42.5R, without any additives (95% clinker with 5% gypsum), manufactured by the industrial group of cements of SPA Biskria Ciment located in Biskra, Algeria, and compliant with the NF EN 197-1 standard (Association française de normalisation [AFNOR], 2000). This cement is employed for formulating mortars, with a water-to-cement ratio (w/c) of 0.5. The cement constituents according to the Bogue formula are as follows: C3S between 60–65%, C3A between 6–10%, and gypsum at 5%. In terms of mechanical properties, it exhibits a compressive strength of 23–26 MPa at 2 days and 45–50 MPa at 28 days. The chemical compositions and physical characteristics are detailed in Table 1.

Guetteche, A., Bensebti, S., Mezhoud, S., Ngo, T-T., Kadri, E-H. (2024). Structural evaluation and durability potential of cementitious materials based on expanded clay kiln dust. *Sci. Rev. Eng. Env. Sci.*, *33* (3), 243–260. DOI 10.22630/srees.9780

TABLE 1. Chemical and physical characteristics of the cement

Chemical composition		Physical properties	
component	value	parameter	value
C3S	55–65%	normal consistency	25.4–26%
C2S	10–25%	hot expansion	< 1.0 mm
C3A	8–12%	initial setting	150 min
C4AF	9–13%	final setting	260 min

Source: own work.

In this study, a superplasticizer type Sika Viscocrete Tempo 12 was used for mortar mixes. This is a non-chlorinated superplasticizer provided by the Sika group. This high-range water-reducing admixture, compliant with NF EN 934-2 standard (AFNOR, 2002), is based on acrylic copolymer and is renowned for its versatility in enhancing the properties of ready-mix concrete.

The sand utilized for mortar formulation was sourced from the region of El Khroub in the Constantine Province (National Aggregates Company – Khroub unit, Algeria). This sand, characterized by a granular class of 0/4 mm, was derived from crushed limestone rock. This specific type of sand was selected for its suitability in mortar formulations, offering the necessary particle size distribution to enhance workability and mechanical properties. The choice of sand plays a critical role in determining the overall performance and characteristics of the mortar, making it essential to use high-quality aggregates with appropriate grading for optimal results.

In this study, one type of fine powder of ECKD is used (Fig. 2). The source of the raw material is derived from a deposit exploited by a public local enterprise, it is a by-product of expanded clay production. The fine powder is collected from electrostatic precipitators during the production of expanded clay pellets.

FIGURE 2. Source of expanded clay kiln dust (ECKD) raw material

Source: own work.

Methods

Granulometric analysis

This study test aims to determine the distribution of different grain sizes within a sample, which is crucial for characterizing the physical and mechanical properties of ECKD. In this study, two methods to evaluate the granularity of ECKD were employed: Air jet sieving and sedimentation in a liquid under the effect of gravity. The distribution of different grain sizes for ECKD powder sample is presented in Figure 3.

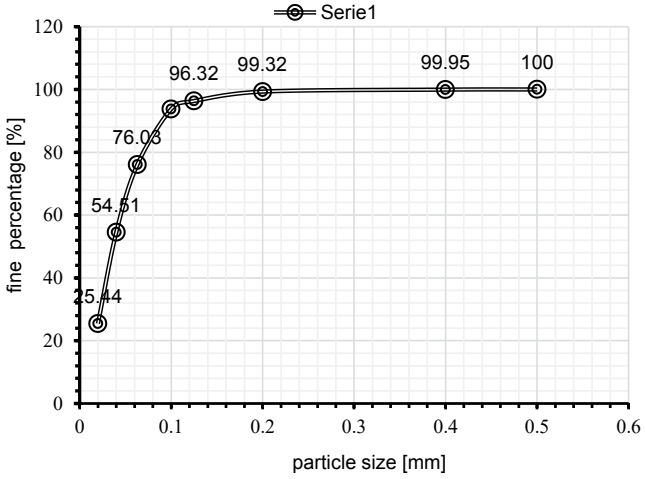

FIGURE 3. Analysis sieve of expanded clay kiln dust (ECKD) powder
Source: own work.

Chemical composition and microstructural structure analysis

The results of identifying the chemical composition by EDX showed that the ECKD powder are composed of several components. The chemical composition of six samples of ECKD powder is represented in Table 2.

In addition to characterizing the ECKD powder, several chemical tests were conducted according to the requirements of the EN 1744-1 standard (European Committee for Standardization [CEN], 2019). These tests allowed for the determination of calcium carbonate content, chloride content, water-soluble sulfate content, insoluble residues, and loss on ignition. The results of these tests are presented in Table 3.

Guetteche, A., Bensebti, S., Mezhoud, S., Ngo, T-T., Kadri, E-H. (2024). Structural evaluation and durability potential of cementitious materials based on expanded clay kiln dust. *Sci. Rev. Eng. Env. Sci.*, *33* (3), 243–260. DOI 10.22630/srees.9780

TABLE 2. Chemical composition of expanded clay kiln dust (ECKD) powder

Component	Content [%]
SiO_2	46.85–64.46
Na_2O	0.33–1.04
Al_2O_3	12.06–21.07
Fe_2O_3	5.91–11.56
MgO	1.27–2.57
K_2O	3.33–4.42
CaO	1.04–4.10
SO_3	1.83–5.25
TiO_2	0.84–0.60
SiO_2	46.85–64.46
Na_2O	0.33–1.04

Source: own work.

TABLE 3. Chemical analysis of expanded clay kiln dust (ECKD) powder

Designation	Result	Requirement
Calcium carbonate ($CaCO_3$) content	2.46%	–
Chlorides (Cl) content – Volhard method	0.00089%	Cl < 0.01
Water-soluble sulfates (SO_3) content	2.35%	SO_3 < 0.8
Loss on ignition	5.30%	–
Insoluble residues	79.85%	–
Methylene blue test (MBf)	16.67 g·kg^{-1}	–

Source: own work.

Microstructure analysis

It is necessary to conduct structural characterization of ECKD using scanning electron microscopy (SEM). To do this, ECKD samples were prepared by metallography. They were then observed under the SEM, which provides high-resolution images of material surfaces. These results are important as they allow for a better understanding of the composition and structure of ECKD powder. This information is useful for developing new materials based on ECKD. The observation results showed that ECKD consists of particles of various sizes and shapes. The results are presented in Figure 4.

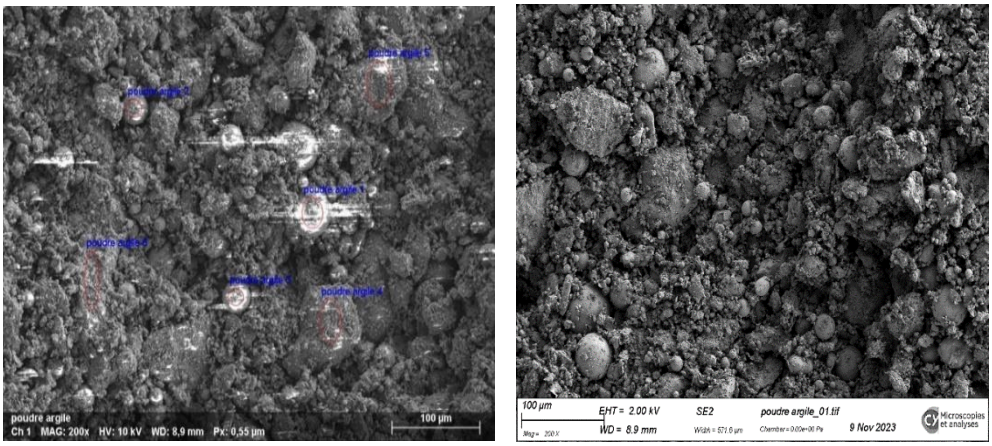

FIGURE 4. Scanning electron microscopy (SEM) analysis for expanded clay kiln dust (ECKD) powder
Source: own work.

Endurance tests

To prepare different types of mortar, a standardized mixer with a capacity of 5 l was utilized, following the EN 196-1 standard (CEN, 2016). The placement of the specimens was conducted according to the procedure outlined in the standard. To monitor the mechanical behavior of the mortars, four series were carried out, with a constant water-to-cement ratio (w/c) of 0.5. The water-to-binder ratio (w/b) was varied (0.5, 0.45, 0.425, 0.4). The dosage of ECKD was also varied (0%, 10%, 15%, 20%). The mass composition of the studied mortars is presented in Table 4.

TABLE 4. Mortar mixes design (c/w ratio: 0.5) [g]

Component	Cement	ECKD	Sand	Water	Superplasticizer
Mo-CTRL	450	0	1350	225	5.85
ECKD-10%	405	45	1350	202.5	5.26
ECKD-15%	382.5	67.5	1350	191.25	4.97
ECKD-20%	360	90	1350	180	4.68

Source: own work.

The introduction of a new material into concrete can have various influences, among others on the strength, durability, workability, or thermal conductivity of the concrete. This strongly depends on the characteristics of the new material in question and the way it interacts with the mortar components. For this reason, a series of tests were conducted on the incorporation of ECKD to better understand

Guetteche, A., Bensebti, S., Mezhoud, S., Ngo, T-T., Kadri, E-H. (2024). Structural evaluation and durability potential of cementitious materials based on expanded clay kiln dust. *Sci. Rev. Eng. Env. Sci.*, *33* (3), 243–260. DOI 10.22630/srees.9780

their chemical and mechanical behavior as well as their impact on mortars. They consist of two parts: rheological tests and mechanical tests.

Rheological tests. These tests of fresh-state mixes were conducted on different types of mortars to characterize their workability and compactness. The slump test was used to measure the flowability of the mortars. This test involves filling an Abrams cone with fresh mortar and then compacting the concrete downward using a piston. The distance between the top of the concrete and the edge of the cone after piston removal is measured. A higher slump indicates a more fluid mortar. The spread test was also used to measure the flowability of the mortars. A greater diameter indicates a more fluid mortar. The mortar workability test was used to measure the ease of handling of the mortars. This test involves measuring the time required to mix a volume of the mortar. A longer mixing time indicates a more difficult-to-mix mortar. The air content of the mortars was measured using an air entrainment measuring device. This measurement determines the amount of air trapped in the mortar. A higher air content indicates a more porous mortar. Finally, the density of fresh-state mortar specimens was measured. This measurement determines the density of the mortar. A higher density indicates a more compact mortar.

Mechanical tests. These tests were conducted according to the EN 196-1 standard (CEN, 2016) to characterize the mortars at different ages. According to the aforementioned standard, three specimens of 4 × 4 × 16 cm^3 were used for each bending test. The given results are the average values obtained. Each specimen of 4 × 4 × 16 cm^3 generates two 4 × 4 × 4 cm^3 cubes for the compression tests. The sample preparation and compression test are shown in Figure 5.

FIGURE 5. Mechanical test: a – sample preparation; b – compression strength measurement
Source: own work.

Results and discussion

Expanded clay kiln dust mixes in fresh condition

The effect of ECKD dosage on the fresh state of mortars was analyzed. Table 5, Figures 6 and 7 summarize all the obtained results.

TABLE 5. Expanded clay kiln dust (ECKD) mixes in fresh condition

Test	ECKD dosage			
	0%	10%	15%	20%
Mini cone slump [cm]	1	0.5	0.5	0.5
Mini cone spread [cm]	0	0	0	0
Workability [s]	3.25	23.98	–	–
Entrapped air [%]	4.7	12.8	5.6	6.9
Density [kg·l^{-1}]	2.45	2.44	2.37	2.29

Source: own work.

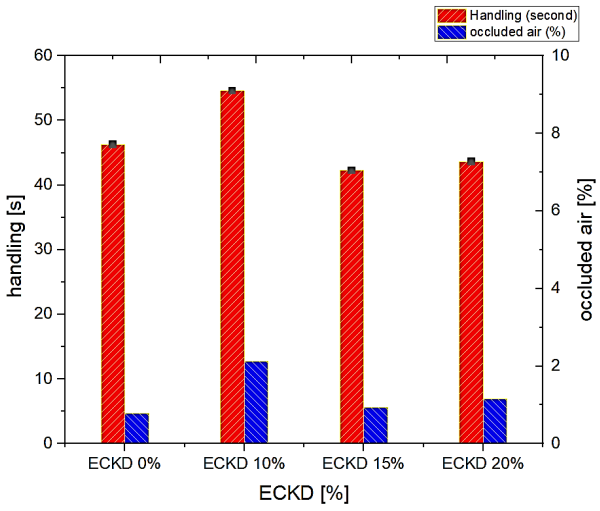

FIGURE 6. Results of handling and occluded air tests

Source: own work.

Guetteche, A., Bensebti, S., Mezhoud, S., Ngo, T-T., Kadri, E-H. (2024). Structural evaluation and durability potential of cementitious materials based on expanded clay kiln dust. *Sci. Rev. Eng. Env. Sci.*, *33* (3), 243–260. DOI 10.22630/srees.9780

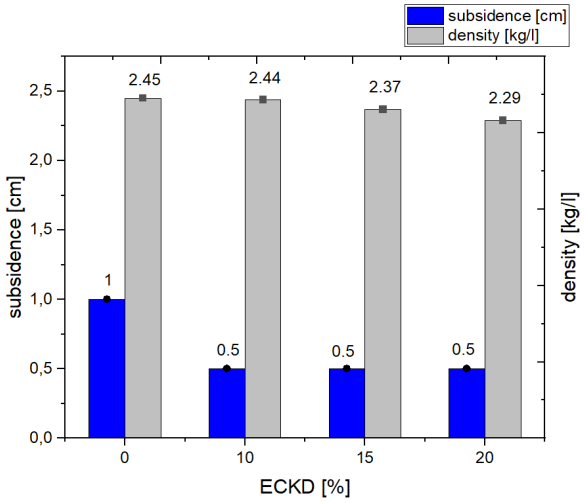

FIGURE 7. Results of density and subsidence tests
Source: own work.

Results revealed a decrease in slump flow with increasing ECKD content, indicating an increase in mortar viscosity. Conversely, the flow spread was not significantly affected by ECKD, which could be attributed to the mortar's nature. In addition, the workability of the mortar was significantly reduced by the addition of ECKD, with the workability time increasing from 3.25 s to 23.98 s. However, the amount of entrapped air slightly increased with the increasing ECKD content, ranging from 4.7% to 6.9%, even reaching 12.8% for mortars containing 10% of ECKD. Furthermore, the density of the mortar decreased with increasing ECKD content, decreasing from 2.45 g·cm^{-3} to 2.29 g·cm^{-3}. This observation can be attributed to the presence of air voids in the mortar, which reduce its bulk density. These findings suggest that the addition of ECKD impacts various properties of fresh mortars, influencing their workability, air entrainment, and density.

Compressive test results

Figure 8 depicts the compressive strength results of mortars containing ECKD as a substitute for cement at different curing ages. It is evident that the compressive strength increases logically from 7 days to 120 days for all mortars. Mortars containing 10% of ECKD show an increase in compressive strength compared to the control mortar for all ages, with percentages ranging from 17.9% to 19.23% at 7 days, 28 days, and 120 days, representing an increase from 14% to 19%.

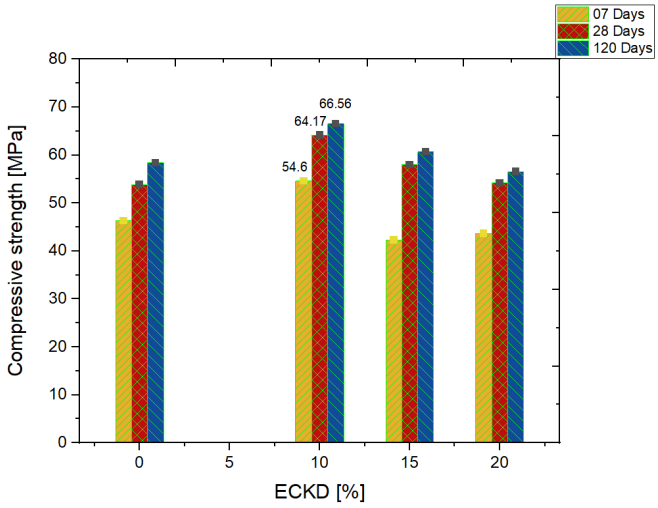

FIGURE 8. Compressive tests for several curing ages
Source: own work.

The flexural strength results at 120 days suggest that a dosage of 10% of ECKD yields the highest obtained results, with Rc_{max} = 66.65 MPa under the tested experimental conditions with cement without the addition of CEM I 42.5 R class. However, mortars containing 15% or 20% of ECKD exhibit a decrease in flexural strength compared to the control mortar. This decrease can reach values lower than the control mortar without ECKD, particularly for mortars containing 20% of ECKD at 7 days and 120 days. At 28 days, the strength remains almost constant at 54 MPa. These results suggest that the use of 10% of ECKD allows for the best flexural strength of substitute mortars.

Flexural strength test results

The results of the flexural strength test of ECKD substitute mortars are presented in Figure 9. These results demonstrate that the flexural strength of all specimens increases with age, from 7 days to 120 days. Mortars containing 10% of ECKD exhibit a significant increase in the flexural strength compared to the control mortar for all ages. This increase is 6.82% at 7 days, 34.75% at 28 days, and 20.86% at 120 days. Such enhancement is attributed to the effect of ECKD, which strengthens the mortar structure and provides better resistance to rupture.

Guetteche, A., Bensebti, S., Mezhoud, S., Ngo, T-T., Kadri, E-H. (2024). Structural evaluation and durability potential of cementitious materials based on expanded clay kiln dust. *Sci. Rev. Eng. Env. Sci.*, *33* (3), 243–260. DOI 10.22630/srees.9780

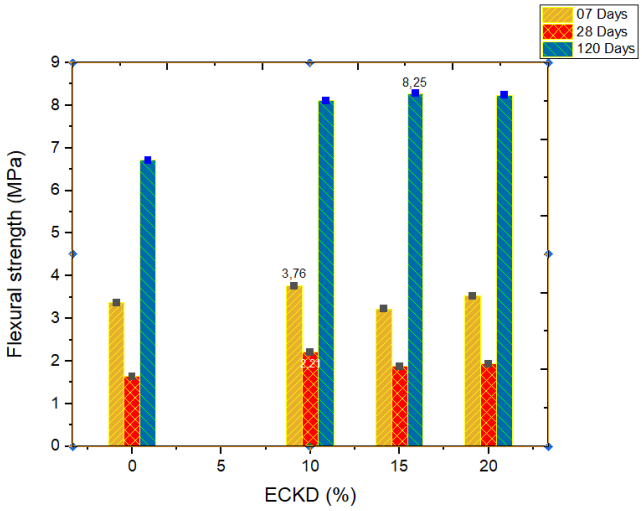

FIGURE 9. Results of flexural strength tests for several curing ages
Source: own work.

In addition, mortars containing 15% and 20% of ECKD also show an increase in flexural strength compared to the control mortar. However, the increase is less significant than for mortars containing 10% of ECKD. At 120 days, the mortar containing 15% of ECKD exhibits the highest flexural strength, with a value of 8.28 MPa.

These results suggest that the use of 10% of ECKD enables the best flexural strength of substitute mortars.

Durability in fresh water and sea water

In this section, the long-term durability assessment of ECKD mortar samples under two distinct conservation conditions is explored: immersion in seawater versus standard preservation in fresh water. Specifically, the investigation spans over 120 days, during which the performance of mortar samples containing 10% of ECKD under both fresh water and seawater immersion is compared.

The findings (Fig. 10) from the compression and flexural strength tests conducted at the 120-day mark show a substantial enhancement in performance for mortar compositions incorporating 10% of ECKD when subjected to seawater, while observing a slight decrease in strength for samples conserved in fresh water, as compared to the control mixes (0% of ECKD). This notable

enhancement in mechanical properties serves as strong evidence supporting the effectiveness of ECKD integration into mortar formulations to enhance long-term durability, regardless of the water environment, whether it be normal or seawater conditions.

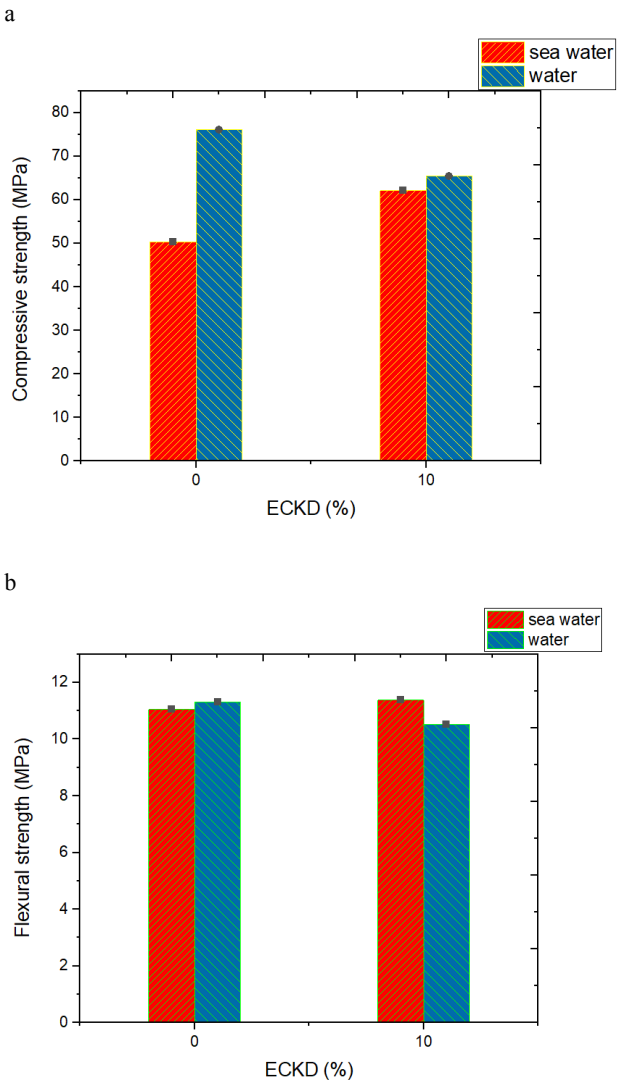

FIGURE 10. Mechanical performance at 120 days: a – compressive test; b – indirect tensile strength
Source: own work.

Conclusion

The utilization of expanded clay kiln dust (ECKD) as a sustainable alternative in cementitious materials offers promising prospects for addressing environmental concerns associated with traditional cement production. Through a comprehensive evaluation encompassing material characterization, mechanical testing, and microstructural analysis, this study has provided valuable insights into the potential applications and performance of ECKD in mortar formulations.

The results obtained from fresh-state mortar tests revealed that the addition of ECKD influenced various properties of the mortar, including workability, air entrainment, and density. While ECKD dosage led to a decrease in slump flow and workability, it also resulted in an increase in entrapped air and a reduction in mortar density. However, these changes did not significantly compromise the overall performance of the mortar. Mechanical testing demonstrated that mortar mixes containing 10% of ECKD exhibited enhanced compressive and indirect tensile strength compared to control mixes at various curing ages. This improvement in mechanical properties emphasizes the effectiveness of ECKD as a cement substitute in mortar formulations. Notably, mortars with 10% of ECKD displayed superior performance in terms of strength development, indicating its potential for structural applications in construction. Moreover, the long-term durability of ECKD samples in seawater revealed promising results. They show a substantial enhancement in performance for mortar compositions incorporating 10% of ECKD when subjected to seawater, while observing a slight decrease in strength for samples conserved in fresh water, as compared to the control mixes.

Finally, the findings of this study demonstrate the feasibility and efficacy of incorporating ECKD as a cement substitute in mortar formulations.

References

Abdel-Gawwad, H. A., Rashad, A. M., Mohammed, M. S., & Tawfik, T. A. (2021). The potential application of cement kiln dust-red clay brick waste-silica fume composites as unfired building bricks with outstanding properties and high ability to CO_2-capture. *Journal of Building Engineering*, *42*, 102479. https://doi.org/10.1016/j.jobe.2021.102479

Akhtar, A., & Sarmah, A. K. (2018). Construction and demolition waste generation and properties of recycled aggregate concrete: A global perspective. *Journal of Cleaner Production*, *186*, 262–281. https://doi.org/10.1016/j.jclepro.2018.03.085

Al-Bakri, A. Y., Ahmed, H. M., & Hefni, M. A. (2022). Cement kiln dust (CKD): potential beneficial applications and eco-sustainable solutions. *Sustainability*, *14* (12), 7022. https://doi.org/10.3390/su14127022

Association française de normalisation [AFNOR], (2000). *Cement. Part 1: composition, specifications and conformity criteria for common cements* (EN 197-1).

Association française de normalisation [AFNOR], (2002). *Admixtures for concrete, mortar and grout. Part 2: concrete admixtures. Definitions, requirements, conformity, marking and labeling* (EN 934-2).

ASTM International [ASTM], (2018). *Standard test method for flexural strength of concrete (using simple beam with third-point loading)* (ASTM C78-18).

ASTM International [ASTM], (2019). *Standard test method for compressive strength of cylindrical concrete specimens* (ASTM C39-19).

European Committee for Standardization [CEN], (2016). *Methods of testing cement. Determination of strength* (EN 196-1).

European Committee for Standardization [CEN], (2019). *Tests for chemical properties of aggregates. Part 1: chemical analysis* (EN 1744-1).

Faleschini, F., Zanini, M. A., Pellegrino, C., & Pasinato, S. (2016). Sustainable management and supply of natural and recycled aggregates in a medium-size integrated plant. *Waste Management*, *49*, 146–155. https://doi.org/10.1016/j.wasman.2016.01.013

Gao, T., Shen, L., Shen, M., Chen, F., Liu, L., & Gao, L. (2015). Analysis on differences of carbon dioxide emission from cement production and their major determinants. *Journal of Cleaner Production*, *103*, 160–170. https://doi.org/10.1016/j.jclepro.2014.11.026

Kaminskas, R., & Savickaite, B. (2023). Expanded clay production waste as supplementary cementitious material. *Sustainability*, *15* (15), 11850. https://doi.org/10.3390/su151511850

Kumar, J. S., & Sharma, P. (2018). Geotechnical properties of pond ash mixed with cement kiln dust and polypropylene fiber. *Journal of Materials in Civil Engineering*, *30* (8), 04018154. https://doi.org/10.1061/(ASCE)MT.1943-5533.0002334

Luhar, S., Luhar, I., Abdullah, M. M. A. B., & Hussin, K. (2021). Challenges and prospective trends of various industrial and solid wastes incorporated with sustainable green concrete. In *Advances in Organic Farming* (pp. 223–240). Woodhead Publishing. https://doi.org/10.1016/B978-0-12-822358-1.00001-8

Ogila, W. A. M. (2021). Effectiveness of fresh cement kiln dust as a soil stabilizer and stabilization mechanism of high swelling clays. *Environmental Earth Sciences*, *80* (7), 283. https://doi.org/10.1007/s12665-021-09589-4

Shoaei, P., Zolfaghary, S., Jafari, N., Dehestani, M., & Hejazi, M. (2017). Investigation of adding cement kiln dust (CKD) in ordinary and lightweight concrete. *Advances in Concrete Construction*, *5* (2), 101. https://doi.org/10.12989/acc.2017.5.2.101

Sreekrishnavilasam, A., & Santagata, M. C. (2006). *Development of criteria for the utilization of cement kiln dust (CKD) in highway infrastructures* (Final report FHWA/IN/JTRP-2005/10). Joint Transportation Research Program. https://docs.lib.purdue.edu/cgi/viewcontent.cgi?article=1743&context=jtrp

Guetteche, A., Bensebti, S., Mezhoud, S., Ngo, T-T., Kadri, E-H. (2024). Structural evaluation and durability potential of cementitious materials based on expanded clay kiln dust. *Sci. Rev. Eng. Env. Sci.*, *33* (3), 243–260. DOI 10.22630/srees.9780

Summary

Structural evaluation and durability potential of cementitious materials based on expanded clay kiln dust. This paper investigates the potential of expanded clay kiln dust (ECKD) as a sustainable alternative in cementitious materials, aiming to address environmental concerns associated with traditional cement production. The study conducts a comprehensive evaluation, including material characterization, mechanical testing, and microstructural analysis, to assess the performance of ECKD in mortar formulations. Results indicate that ECKD influences various mortar properties, such as workability, air entrainment, and density. Mortar mixes containing 10% of ECKD show enhanced compressive and tensile strength compared to control mixes, indicating its effectiveness as a cement substitute. Moreover, the long-term durability of ECKD samples in seawater revealed promising results, confirming their favorable durability. In conclusion, the study demonstrates the feasibility and efficacy of incorporating ECKD in mortar formulations to mitigate the environmental impact of cement production while enhancing mechanical properties.

Scientific Review Engineering and Environmental Sciences (2024), 33 (3), 261–277

Sci. Rev. Eng. Env. Sci. (2024), 33 (3) https://srees.sggw.edu.pl

ISSN 1732-9353 (suspended) eISSN 2543-7496 DOI 10.22630/srees.9810

Received: 18.05.2024
Accepted: 10.07.2024

Mourad SERIKMA[1]✉
Baizid BENAHMED[2]
Salim KENNOUCHE[3]
Mohd Hisbany MOHD HASHIM[4]
Salem MERABTI[5]

[1, 2] University of Djelfa, Department of Civil Engineering, Development Laboratory in Mechanics and Materials, Algeria
[3] University of Bouira, Department of Civil Engineering, Algeria
[4] Universiti Teknologi MARA Selangor, School of Civil Engineering, Malaysia
[5] University of Khemis-Miliana, Acoustics and Civil Engineering Laboratory, Algeria

Valorization of glass powder as filler in self-compacting concrete

Keywords: compressive strength, limestone filler, mechanical properties, recycled glass powder, self-compacting concrete, workability

Introduction

Self-compacting concretes appeared in 1980, and continue to be the subject of several research projects aimed at formulating more environmentally friendly self-compacting concretes with improved technical characteristics. However, this progress can only be realized with the development of new formulation approaches, the use of new additions, and the recovery of waste. Also, self-compacting concrete (SCC) is currently an appealing product because it can significantly reduce labor and time requirements (Ruslan et al., 2024).

✉mourad.serikma@univ-djelfa.dz

In Algeria, household waste annual production is around 13.5 million tons per year, and the recovery of glass is estimated at 41,724 tons per year, or about 1.04% of the annual production. This rate remains relatively low compared to other sectors. Unfortunately, glass is ranked last compared to other recycled materials (National Waste Agency [NWA], 2020). The limestone filler is largely used as an addition to SCC (Petersson, 2001; Jiang et al., 2024; Martinez-Echevarria et al., 2024). Research has thus shown that fillers exhibit some physical-chemical activity, which promotes the acceleration of clinker hydration and contributes to a pozzolanic reaction (Zhu & Gibbs, 2005; Diederich et al., 2013). The valorization of glass waste in the field of materials could be an interesting ecological and economical solution (Zhao et al., 2024). Glass powder (GP) has now become an effective addition to the field of building materials. Its rheological performance, strength, and durability have been proven in several types of concrete (Carlswärd et al., 2003). The introduction of GP in concrete dates back to the 1960s and the use of glass as aggregates in concrete has been investigated (Pike et al., 1960). Johnston (1974) used GP as an addition to cement for ordinary concrete. Nishikawa et al. (1995) showed that the strength of ordinary concretes would increase with the content of glass mixtures and that the simultaneous use of glass and natural pozzolan to partially replace cement was of interest in the research. The strength testing and durability of ordinary concrete using glass waste as aggregate yielded acceptable results (Polley et al., 1998). The prediction of the glass aggregate effect size on concrete swelling has been investigated by Zhang et al. (2021). The chemical composition of glass plays a significant role in its mechanical properties, including compressive strength (Karamberi & Moutsatsou, 2005). Batayneh et al. (2007) studied sand substitutions rather than cement by comparing glass to other pozzolanic materials. Mourad and Tahar (2013) invested in partial cement substitution with GP in SCC. The work of Malafalda Matos and Sousa-Coutinho (2016) consisted of collecting relevant information on the sustainability of SCS manufactured using GP addition. Arabi et al. (2019) examined the possible incorporation of both coarse recycled concrete aggregates and coarse recycled windshield glass aggregates in the composition of SCS. Singh and Siddique (2022) studied the possible utilization of glass waste in the production of SCC and showed that the rheological parameters were improved. Ahmad et al. (2023b) explore sustainable alternatives for self-compacting concrete by using waste glass powder as a cement substitute and incorporating marble waste as a filler material. The levels of powder glass replacement ranged from 0% to 20%, in 5% increments, while 10% marble waste was added to enhance SCC flowability. All waste glass powder substituted mixes met SCC's standards and exhibited improved filling and passing abilities. The study shows mechanical

performance was enhanced with waste glass powder substitution due to micro--filling and pozzolanic actions. Scanning electron microscopy and Fourier transform infrared analysis provided visual and chemical evidence of the microstructural improvements from pozzolanic reactions and micro-filling effects.

The research work conducted by Ahmad et al. (2023a) has concluded that self-compacting concrete with 22.5% glass powder shows the highest increases in compressive, tensile, and flexural strengths (16.99%, 23.53%, and 17.65%, respectively) compared to other mix designs. Although there is a slight reduction in strength parameters, concretes with 30% glass powder still outperform the control design, and the same analysis confirms that the replacement of cement with glass powder addresses environmental issues related to cement production and glass waste disposal, while also enhancing concrete properties and lowering production costs by approximately 23.67%.

Indeed, formulations were prepared by substituting the filler with glass powders up to 100%, which is not the case in current literature. Fresh and hardened tests were conducted to achieve a more suitable SCC in terms of workability and compressive strength.

Experimental procedure

Materials

The aggregates are crushed limestone obtained from a Béjaia quarry in Algeria. The sand (S) used is of alluvial origin, with a nominal particle size of 4 mm; the gravel (G) used has two fraction sizes (4/8 and 8/16 mm). The physical properties of fine and coarse aggregates are shown in Table 1. The grading of aggregate mixtures is presented according to references issued by the NF EN 933-1 standard (Association française de normalization [Afnor], 2012). Furthermore, the cement (C) utilized is CPJ-CEMII-42.5A, originating from the local cement plant in Ain Kebira, Setif. The chemical analysis of the cement used in the study is given in Table 2. The additive used is a high-performance water-reducing superplasticizer of the new generation, known as MEDAFLOW 30, produced by GRANITEX Building Chemicals Company. It is a polycarboxylate solution with a 30% solid content, a light brown color, and a pH ranging between 6 and 6.5. The filler (F) used is the limestone UF5-type filler from the ENG El-Khroub quarry. Its chemical composition is presented in Table 2. The GP used in this study was obtained by crushing glass waste from public landfills (Figs 1 and 2). Its chemical composition is listed in Table 2.

Serikma, M., Benahmed, B., Kennouche, S., Mohd Hashim, M. H., Merabti, S. (2024). Valorization of glass powder as filler in self-compacting concrete. *Sci. Rev. Eng. Env. Sci.*, *33* (3), 261–277. DOI 10.22630/srees.9810

TABLE 1. Physical properties of various used materials

Characteristics	Standard	Fine aggregate	Coarse aggregate	C	F	GP
Fineness modulus	NF EN 12620	2.91	–	–	–	3.12
Absolute density [g·cm^{-3}]	NF EN 1097-6	2.63	2.67	3.11	2.45	2.55
Bulk density [g·cm^{-3}]	NF EN 1097-6	1.45	1.41	1.12	0.85	0.89
Sand equivalent [%]	NF EN 933-8	81.12	–	–	–	71.38
Compactness [%]	NF EN 1097-6	58	–	–	–	–
Water absorption [%]	NF EN 1097-6	1	0.03	–	0.00	–

Source: own work.

TABLE 2. Chemical compositions of cement, filler, glass powder, and aggregate

The samples (100%)	Cement	Filler	Glass powder	Aggregate
Silicon dioxide (SiO_2)	21.26	0.39	73.89	–
Aluminum oxide (AI_2O_3)	3.83	0.11	1.72	–
Iron oxide (Fe_2O_3)	2.91	0.06	1.24	–
Calcium oxide (CaO)	61.22	57.94	10.12	–
Magnesium oxide (MgO)	1.17	0.17	2.44	–
Sodium oxide (Na_2O)	2.05	0.07	9.05	–
Potassium oxide (K_2O)	–	0	0.25	–
Sulfur trioxide (SO_3)	1.18	0.05	0.21	–
Chromium oxide (CrO_2)	–	–	0.12	–
Calcium carbonate ($CaCO_3$)	–	–	–	96.18
Other	–	–	–	2.95
Loss on ignition	6.24	40.65	0.95	–

Source: own work.

FIGURE 1. Glass in the landfill
Source: own photo

FIGURE 2. Glass crushing
Source: own photo

A granulometric analysis (Fig. 3) was conducted to validate the computation and ensure that the analysis curve aligns with the specified range outlined in the NF EN ISO 17892-4 standard (Afron, 2018).

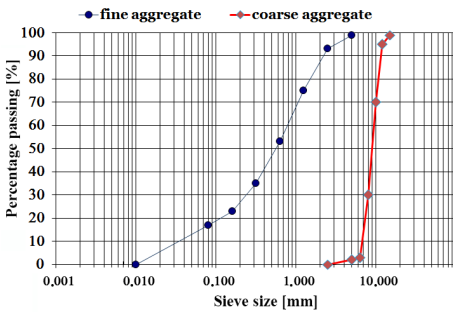

FIGURE 3. Grain size of fine and coarse aggregates distribution

Source: own work.

Concrete mixtures

For the experimentation, eleven types of concrete mixes were made. In each mix, filler was replaced by (GP) at the rates of 0%, 10%, 20%, 30%, 40%, 50%, 60%, 70%, 80%, 90% and 100% by weight.

The preliminary mix design was carried out using a prescribed method reported by Okamura and Ouchi (2003).

The dosage of the superplasticizer, as well as the water-to-cement and filler-to-cement ratios, remained consistent for all SCC mixtures; $\frac{W}{C}+F=0.35$; $\frac{F}{C}=0.2$; $\frac{SP}{C+F}=0.014$; and $\frac{F}{F+C}=0.2$. The compositions of different mixes are given in Table 3.

TABLE 3. Self-compacting concrete mix proportions

Mixture	Cement [kg·m^{-3}]	Filler [kg·m^{-3}]	Glass powder [kg·m^{-3}]	Coarse aggregate [kg·m^{-3}]	Fine aggregate [kg·m^{-3}]	Super-plasticizer [kg·m^{-3}]	Water [l·m^{-3}]
SCC0	400	100	0	783	779	7	175
SCC1		90	10				
SCC2		80	20				
SCC3		70	30				
SCC4		60	40				
SCC5		50	50				
SCC6		40	60				
SCC7		30	70				
SCC8		20	80				
SCC9		10	90				
SCC10		0	100				

Source: own work.

Test method

After the mix design, the formulated concretes must satisfy several standard tests, such as the NF EN 206-9 standard (Afron, 2010b). The trial mixes were prepared and tested to assess two characteristics: workability and mechanical strength.

Workability

Workability refers to the ease of handling fresh concrete. These characteristics can be divided into three measurable criteria through empirical tests:

- The concrete filling capacity is a criterion directly influenced by its fluidity and was evaluated using the slump flow test according to the NF EN 12350-8 standard (Afron, 2010a).
- The flow, which denotes the ability to pass through obstacles such as narrow sections of formwork or closely spaced reinforcement bars, is primarily influenced by the characteristics of the aggregates and the volume of paste, as evaluated by the L-box test according to the NF EN 12350-11 standard (Afron, 2010d).
- The resistance to segregation of SCC is attributed to its high fluidity and paste content. Ensuring the stability of fresh materials is necessary to guarantee the uniformity of mechanical characteristics in the final structure. The stability was evaluated with sieve segregation test according to the NF EN 12350-10 standard (Afron, 2010c), which allowed checking the resistance against segregation of our concretes.

Mechanical strengths

The compressive strength was measured using cylindrical specimens for each type of SCC. It should be noted that six specimens were used for each test. Thus, a total of 66 (11 × 22 cm) concrete cylinders were prepared. The concrete was poured into the molds without the use of vibration. The specimens were then kept in their molds for 24 hours before being demolded and then fully immersed in water at a temperature of 20°C for curing periods of 7 days and 28 days, respectively. The results are presented in Table 4.

TABLE 4. Characterization experimental results

Mixture	Slump flow test [mm]	L-box test (H_2/H_1) [%]	Sieve segregation test [%]	Compressive strength test [MPa]	
				CS_7 (7 days)	CS_{28} (28 days)
SCC_0	761	0.98	16.4	27.49	37.19
SCC_1	743	0.96	15.6	28.37	38.45
SCC_2	735	0.93	13.8	31.76	39.68
SCC_3	726	0.91	12.7	31.89	40.34
SCC_4	694	0.90	10.9	31.73	38.87
SCC_5	685	0.89	9.3	30.86	37.56
SCC_6	679	0.87	8.8	30.33	36.88
SCC_7	668	0.85	7.5	29.85	36.45
SCC_8	643	0.82	6.8	28.61	35.96
SCC_9	627	0.80	5.6	28.92	35.89
SCC_{10}	612	0.79	3.2	29.12	35.16

Source: own work.

Results and discussion

Fresh concrete results

Effect of glass powder on slump flow

The results obtained are presented in Figure 4. They show that all concrete has spreading values located within the field of SCC. The influence of GP on the spreading of concrete is a function of its dosage in all mixtures studied. It can be noted that the more GP content increases, the more the spreading decreases. This can be explained by the fact that the GP amount decreases the granular compactness of the mixes due to its lower fineness than that of the limestone filler. The lack of free water between the particles makes the mixture heavier and thus affects the fluidity, which can reduce the workability of the concrete.

Serikma, M., Benahmed, B., Kennouche, S., Mohd Hashim, M. H., Merabti, S. (2024). Valorization of glass powder as filler in self-compacting concrete. *Sci. Rev. Eng. Env. Sci.*, *33* (3), 261–277. DOI 10.22630/srees.9810

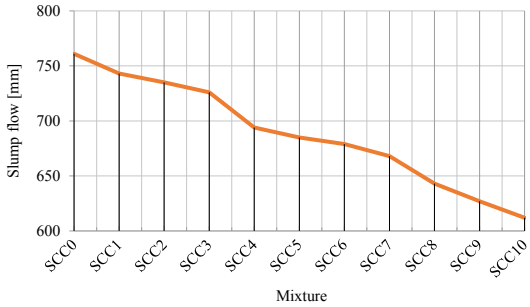

FIGURE 4. Spreading evaluation depending on glass powder filler content
Source: own work.

The GP filler reduces the spreading up to 80.4% [761 mm for SCC0 (0%) and 612 mm for SCC10 (100%)], but it is acceptable because the SCC spreading varies between 550 and 850 mm following the tests to the NF EN 206-9 standard (Afron, 2010b). It is then possible to replace the limestone filler with GP to ensure normalized spreading.

Effect of glass powder on passing ability (L-box test)

Figure 5 shows the results of the L-box test. All mixtures give filling rates that fall within the range of SCC, except SCC10, which is formulated entirely with GP filler. These results confirm the interest in increasing the paste volume by adding fines to the composition of SCC. Increasing the GP filler content leads to a linear decrease in the filling rate.

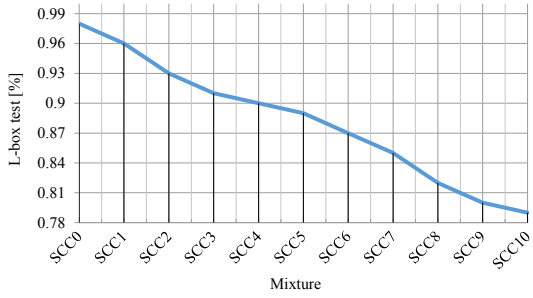

FIGURE 5. Filling evaluation depending on glass powder filler content
Source: own work.

The GP filler reduces the spreading up to 80.6% – 0.98 for SCC0 (0%) and 0.79 for SCC10 (100%) – but remains above 0.8, the limit value defined by the standard tests of the NF EN 206-9 standard (Afron, 2010b). It is thus possible to replace the limestone fillers by (GP) up to 90% to ensure that the filling follows the standards.

Effect of glass powder on sieve segregation

The results obtained by the sieve segregation test are shown in Figure 6. All mixtures have a segregation rate that falls within the range of SCC, except SCC0 and SCC1, which are higher than 15%; the other mixtures (from SCC2 to SCC10) have a segregation rate of less than 15%, thus confirming good stability.

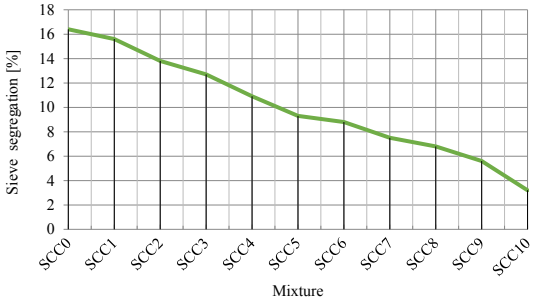

FIGURE 6. Static segregation depending on glass powder filler content
Source: own work.

It can be noted that beyond the 10% GP filler content, the mixture does not present any risk of static segregation, and concrete based on glass waste (SCC% GP) in an unconfined environment is more stable than concrete based on limestone fillers. These results confirm the interest in increasing the paste volume by adding fines to the composition of SCC.

Relationship between workability parameters

The workability of SCC mixes is assessed using slump flow test, L-box test, and the sieve segregation test, as per the NF EN 206-9 standard (Afron, 2010b).

Serikma, M., Benahmed, B., Kennouche, S., Mohd Hashim, M. H., Merabti, S. (2024). Valorization of glass powder as filler in self-compacting concrete. *Sci. Rev. Eng. Env. Sci.*, *33* (3), 261–277. DOI 10.22630/srees.9810

Relationship between slump flow and passing ability (L-box test)

The analysis of Figure 7 indicates that Eq. (1) gives an adequate representation of the actual relationship between slump flow test and L-box test.

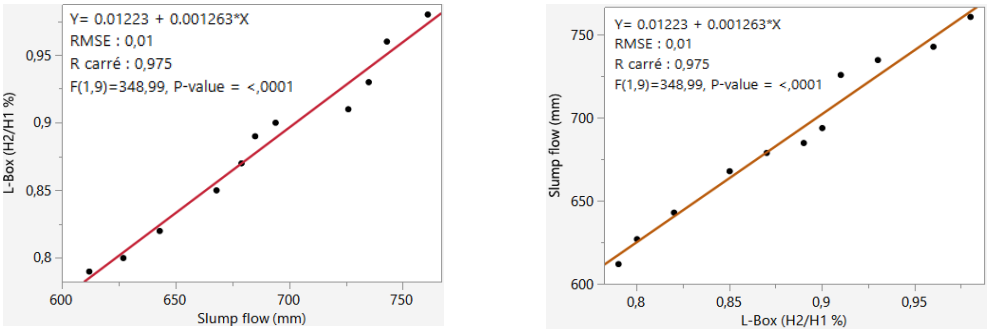

FIGURE 7. Relation between slump flow test and L-box test results
Source: own work.

It is evident from the excellent correlations between the tests. The mathematical models used in slump test and L-box test are given by the following equations:

$$SF = 7.866 + 771.80 \cdot (H_2/H_1),$$

$$H_2/H_1 = 0.0122 + 0.0013 \cdot (SF), \quad (1)$$

$$R^2 = 0.975.$$

Relation between slump flow and sieve segregation

The analysis of Figure 8 indicates that Eq. (2) gives an adequate representation of the actual relationship between the slump flow test and sieve segregation test.

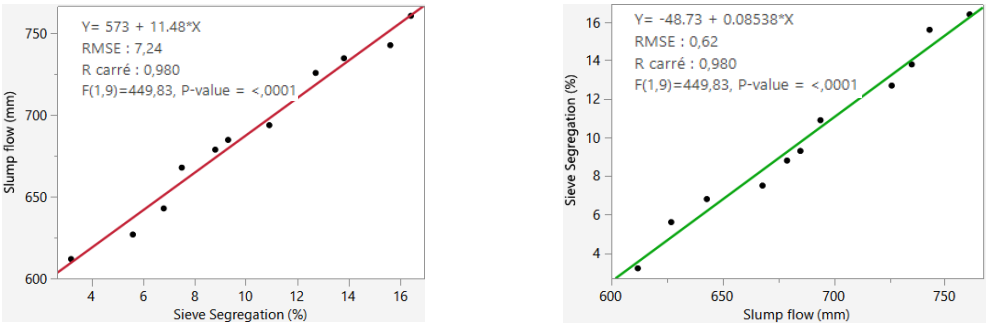

FIGURE 8. Relation between slump flow test and sieve segregation test results
Source: own work.

The mathematical models used in the slump test and sieve segregation test are given by the following equations:

$$SS = -48.73 + 0.0854 \cdot (SF),$$

$$SF = 573 + 11.480 \cdot (SS), \quad (2)$$

$$R^2 = 0.98.$$

Relation between sieve segregation and passing ability (L-box test)

Examining Figure 9, it can be seen that Eq. (3) gives an adequate representation of the actual relationship between sieve segregation test and the L-box test.

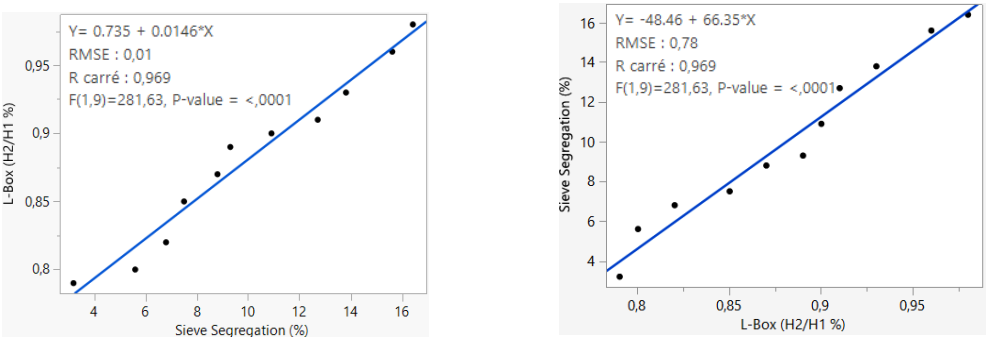

FIGURE 9. Relation between sieve segregation test and L-box test results
Source: own work.

The mathematical models used for the sieve segregation test and L-box test are given by the following equations:

$$SS = -48.460 + 66.350 \cdot (H_2/H_1),$$

$$H_2/H_1 = 0.735 + 0.0146 \cdot (SS), \quad (3)$$

$$R^2 = 0.969.$$

Recapitulative analysis

Figures 7, 8, and 9 show that SCC (slump flow test, L-box test, and sieve segregation test) parameters have exponential functions with correlation coefficients $R^2 > 0.96$. The ANOVA results show that $P < 0.001$, implying that

the coefficients R and adjusted (R^2_{adj}) were calculated to assess the adequacy and relevance of the model. The R^2 and R^2_{adj} values are close to 1. A positive correlation exists between these parameters that move in tandem; when one parameter decreases, the other parameter decreases, or one parameter increases while the other increases. Because these different variables move in the same direction, they are practically influenced by the same (GP) filler quantity. Despite losing their workability depending on the addition of GP fillers, concrete remains workable; these correlations are in agreement with the results of the study by Roussel (2006).

Hardened concrete test results

Effect of glass powder on strengths

The test results obtained for compressive strength after 7 days and 28 days are shown in Figures 10 and 11. The compressive strength curing at 28 days shows that the concrete specimen without GP is 37.19 MPa. Thus, it can be noted that compressive strength grows as the proportion of GP in concrete increases up to 30%. This can be explained by the consumption of portlandite [$Ca(OH)_2$] at around 30% glass powder, which is a crucial component for the pozzolanic reaction, and the production of C-S-H, responsible for mechanical strength (Shi, 2001). In the case of using 10% GP addition, the observed increase is 3.38%; however, for 20% addition, the increase is 6.70%, whereas for an addition of 30% GP, an increase of 8.47% is reached, and that corresponds to the optimum. It has been noticed that compressive strength decreases; in the case of using a 40% addition of GP compared to the optimum, an increase of 4.51% of the initial compressive strength has been observed. The same trend has been obtained for 50% GP content, where an increase of 0.99 is reached.

However, from 60% GP content, a decrease in strength of 0.83% is noticed. When the proportion of GP is up to 70%, a decrease of 1.98% is obtained. However, when this proportion increases to 100%, a decrease in compressive strength of 5.45% is noted, giving a strength value of 35.16 MPa at the end.

Despite these losses in strength, concrete samples still have acceptable strength according to the current standards.

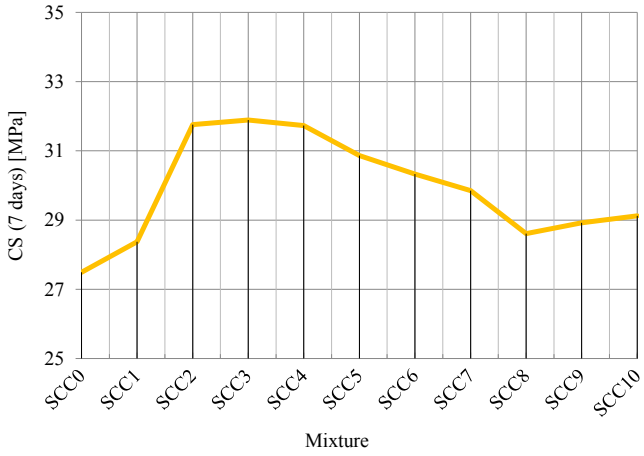

FIGURE 10. Compressive strength at 7 days depending on the GP filler content
Source: own work.

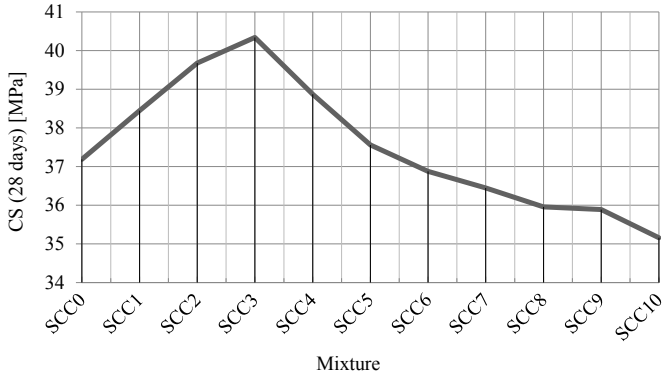

FIGURE 11. Compressive strength at 28 days depending on the GP filler content
Source: own work.

Conclusions

The main objective of this study was to evaluate the effects of incorporating glass powder (GP) waste, by substituting the filler up to 100%, on the rheological and mechanical properties of self-compacting concrete (SCC). This was achieved

through conducting experimental tests and analyzing each formulation, which included varying substitution levels. The following conclusions have been drawn:

- A positive correlation exists between the workability parameters (slump flow test, L-box test and sieve segregation test) due to the obtained results that fall within the range of SCC, except for two mixtures (SCC0 and SCC1 greater than 15%) in the sieve segregation test with a segregation rate of less than 15%. For this purpose, to ensure good concrete workability, the addition of GP filler must exceed 10% incorporation by weight in the replacement of the limestone filler.
- The gain in compressive strength compared to the concrete specimen without GP. The incorporation must be between 10 and 50%, and the optimum remains at 30% with a gain of 8.47%;
- The obtained results showed the advantage of substituting the limestone filler in SCC with GP waste in the same proportions of 10–50%, inducing potential technical interests and environmental benefits;
- The addition of GP can have effects on the fresh concrete by improving stability and eliminating segregation risks about the dosage, whereas for the hardened concrete, substitutions that exceed 50% increase the mechanical strength.
- The gain in strength generated by the addition of GP through the filling and pozzolanic effect, is a durability property that allows us to consider the valorization of the glass in SCC.
- The durability of the improvements made by incorporating GP in cementitious matrix materials needs to be validated through further research, particularly by applying this concrete (SCC) in more challenging environments. Additionally, it is essential to conduct more in-depth investigations into the environmental and economic impacts.

Acknowledgments

The author wishes to express gratitude to Professor Bali Abderahmane for his valuable remarks.

References

Ahmad, S., Upadhyay, S., Umar, A., & Al-Osta, M. A. (2023a). Effect of recycled crushed glass and recycled coarse aggregate on the properties of self-compacting concrete. *Case Studies in Construction Materials*, *19*, e02532. https://doi.org/10.1016/j.cscm.2023.e02532

Ahmad, J., Zhou, Z., & Deifalla, A. F. (2023b). Self-compacting concrete with partially substitution of waste marble: a review. *International Journal of Concrete Structures and Materials*, *17* (1), 25. https://doi.org/10.1186/s40069-023-00585-5

Arabi, N., Meftah, H., Amara, H., Kebaïli, O., & Berredjem, L. (2019). Valorization of recycled materials in development of self-compacting concrete: Mixing recycled concrete aggregates – Windshield waste glass aggregates. *Construction and Building Materials*, *209*, 364–376. https://doi.org/10.1016/j.conbuildmat.2019.03.024

Association française de normalization [Afnor], (2010a). *Test for fresh concrete. Part 8: Self-compacting concrete – Abrams cone spreading test* (NF EN 12350-8).

Association française de normalization [Afnor], (2010b). *Self-compacting concrete. Part 9: Additional rules for self-compacting concrete* (NF EN 206-9).

Association française de normalization [Afnor], (2010bc). *Test for fresh concrete. Part 10: Self-compacting concrete – L-box test* (NF EN 12350-10).

Association française de normalization [Afnor], (2010d). *Test for fresh concrete. Part 11: Self-compacting concrete – sieve stability test* (NF EN 12350-11).

Association française de normalization [Afnor], (2012). *Tests for geometrical properties of aggregates. Part 1: Determination of particle size distribution – sieving method* (NF EN 933).

Association française de normalization [Afnor], (2018). *Physical properties of soils. Part 4: Determination of grain size distribution* (NF EN ISO 17892-4).

Batayneh, M., Marie, I., & Asi, I. (2007). Use of selected waste materials in concrete mixes. *Waste Management*, *27* (12), 1870–1876. https://doi.org/10.1016/j.wasman.2006.07.026

Behim, M., & Ali Boucetta, T. (2013).Valorisation du verre à bouteille comme addition fine dans les bétons autoplaçants. *Environnement, Ingénierie & Développement*, *65*, *20–28.* https://doi.org/10.4267/dechets-sciences-techniques.932

Carlswärd, J., Emborg, M., Utsi, S., & Öberg, P. (2003, August 17-20). Effects of constituents on the workability and rheology of self-compacting concrete. In O. Wallevik & I. Nielsson (Eds), *International RILEM Symposium on Self-Compacting Concrete* (pp. 143–153). RILEM Publications SARL.

Diederich, P., Mouret, M., & Ponchon, F. (2013). Simple tools for achieving self-compacting ability of concrete according to the nature of the limestone filler. *Construction and Building Materials*, *48*, 840–852. https://doi.org/10.1016/j.conbuildmat.2013.07.071

Jiang, Z., Yang, Q., Wang, B., Li, C., Zhang, J., & Ren, Q. (2024). Limestone filler as a mineral additive on the compressive strength and durability of self-compacting concrete with limestone manufactured sand. *Journal of Building Engineering*, *94*, 109965. https://doi.org/10.1016/j.jobe.2024.109965

Johnston, C. D. (1974). Waste glass as coarse aggregate for concrete. *Journal of Testing and Evaluation*, *2* (5), 344–350. https://doi.org/10.1520/JTE10117J

Karamberi, A., & Moutsatsou, A. (2005). Participation of coloured glass cullet in cementitious materials. *Cement and Concrete Composites*, *27* (2), 319–327. https://doi.org/10.1016/j.cemconcomp.2004.02.021

Malafalda Matos, A. M., & Sousa-Coutinho, J. (2016). Waste glass powder in cement: Macro and micro scale study. *Advances in Cement Research*, *28* (7), 423–432. https://doi.org/10.1680/jadcr.14.00025

Martinez-Echevarria, M. J., Del Castillo, J. P., Rodríguez Montero, J., & López-Alonso, M. (2024). Reinforcement corrosion in self-compacting concrete made with waste filler of bituminous mixtures. *Construction and Building Materials*, *411*, 134623. https://doi.org/10.1016/j.conbuildmat.2023.134623

National Waste Agency [NWA] (2020). *The annual report on the state of waste management in Algeria fiscal year 2020.* National Waste Agency.

Nishikawa, T., Takatsu, M., & Daimon, M. (1995). Fracture behavior of hardened cement paste incorporating mineral additions. *Cement and Concrete Research*, *25* (6), 1218–1224. https://doi.org/10.1016/0008-8846(95)00114-R

Okamura, H., & Ouchi, M. (2003). Self-compacting concrete. *Journal of Advanced Concrete Technology*, *1* (1), 5–15. https://doi.org/10.3151/jact.1.5

Petersson, O. (2001). *Limestone powder as filler in self-compacting concrete-frost resistance and compressive strength*. Proceeding of 2nd International RILEM, Symposium on Self-Compacting Concrete, Tokyo, Japan.

Pike, R. G., Hubbard, D., & Newman, E. S. (1960). Binary silicate glasses in the study of alkali-aggregate reaction. *Highway Research Board Bulletin*, *275*, 39–44.

Polley, C., Cramer, S. M., & Cruz, R. V. de la (1998). Potential for using waste glass in Portland cement concrete. *Journal of materials in Civil Engineering*, *10* (4), 210–219. https://doi.org/10.1061/(ASCE)0899-1561(1998)10:4(210)

Roussel, N. (2006). Correlation between yield stress and slump: comparison between numerical simulations and concrete rheometers results. *Materials and Structures*, *39* (4), 501–509. https://doi.org/10.1617/s11527-005-9035-2v

Ruslan, H. N., Muthusamy, K., Yahaya, F. M., Fauzi, M. A., Ismail, M. A., & Ali, Z. (2024). Review on performance of self compacting concrete containing solid waste and bibliometric properties: a review. *Journal of Building Engineering*, *86*, 108752. https://doi.org/10.1016/j.jobe.2024.108752

Shi, C. (2001). An overview on the activation of reactivity of natural pozzolans. *Canadian Journal of Civil Engineering*, *28* (5), 778–786. https://doi.org/10.1139/l01-041

Singh, H., & Siddique, R. (2022). Utilization of crushed recycled glass and metakaolin for development of self-compacting concrete. *Construction and Building Materials*, *348*, 128659. https://doi.org/10.1016/j.conbuildmat.2022.128659

Zhang, J., Li, C., Ding, L., & Li, J. (2021). Performance evaluation of cement stabilized recycled mixture with recycled concrete aggregate and crushed brick. *Construction and Building Materials*, *296*, 123596. https://doi.org/10.1016/j.conbuildmat.2021.123596

Zhao, X., Lu, J. X., Lv, X., Tian, W., Cyr, M., Tagnit-Hamou, A., & Sun Poon, C. (2024). Recycling of contaminated waste glass in ultra-high performance concrete: Impurities impact. *Construction and Building Materials*, *437*, 136971. https://doi.org/10.1016/j.conbuildmat.2024.136971

Zhu, W., & Gibbs, J. C. (2005). Use of different limestone and chalk powders in self-compacting concrete. *Cement and Concrete Research*, *35* (8), 1457–1462. https://doi.org/10.1016/j.cemconres.2004.07.001

Summary

Valorization of glass powder as filler in self-compacting concrete. In Algeria, glass waste is underutilized in the industrial sector; however, its potential use in civil engineering offers a significant ecological and economic opportunity. This approach could be a solution to eliminating illegal dumping sites, reduce pollution, and provide a new source of sustainable construction materials. In this context, this research aimed to produce self-compacting concrete (SCC) mixtures using recycled glass powder as a replacement for limestone filler. This research presents an experimental study investigating the impact of glass powder waste as a replacement for the traditionally used limestone filler in self-compacting concrete. To investigate the workability and compressive strength of the SCC studied, eleven concrete mixtures were prepared with varying substitution rates of limestone filler (0%, 10%, 20%, 30%, 40%, 50%, 60%, 70%, 80%, 90%, and 100%) with powder glass. The use of powdered glass waste has beneficial effects, as the pozzolanic reaction generates an additional amount of hydrated calcium silicates. The results of the investigation showed an increase in compressive strength compared to the control concrete specimen (without glass powder). The best results were observed when incorporation ranged between 10% and 50%, with the optimal level being 30%, resulting in an 8.47% strength gain. This study contributes to the valorization of glass powder as a substitute for limestone filler. The results demonstrate positive effects on both fresh and hardened characteristics when using glass powder in proportions ranging from 10% to 50% of the filler mass.

Scientific Review Engineering and Environmental Sciences (2024), 33 (3), 278–288

Sci. Rev. Eng. Env. Sci. (2024), 33 (3) https://srees.sggw.edu.pl

ISSN 1732-9353 (suspended) eISSN 2543-7496 DOI 10.22630/srees.9816

Received: 04.06.2024
Accepted: 20.07.2024

Givi GAVARDASHVILI[1, 2]✉
Eduard KUKHALASHVILI[1, 2]
Nana KURTSIKIDZE[2]
Keti DADIANI[1]

[1] Ts. Tsotne Mirtskhulava Water Management Institute of Georgian Technical University, Georgia
[2] Ecocenter for Environmental Protection, the Organization in Category of Consultative Status with the Economic and Social Council (ECOSOC) of UN, Georgia

Mathematical model for the capacity of the mud flow with wave regime taking into account its rheological properties

Keywords: mudflow, power, wave motion, rheology, energy properties

Introduction

The process of driving a mudflow mass originating from a mudflow center and the prediction of the expected value is a complex problem.

Therefore, as soon as the hydrological, hydraulic and energy characteristics of the mudflow are known, the choice of engineering measures for flood control is no longer difficult.

Recently, frequent impact of mudflows on the environment has become intense. Frequent occurrences of incitement of mudflow masses in the mudflow centers and impacts on facilities have been identified. The process corresponding to the onset

✉givi_gava@yahoo.com

of movement from the epicenter is very complex. Therefore, it is difficult to predict the volume and discharge of alluvial mass driven from the erosion center.

As it is confirmed by the statistics of studying the alluvial processes, the formation of a mudflow from erosion centers and the beginning of movement occurs as a continuous dynamic or monoclinal wave. Continuous or stepwise changes in hydraulic and hydrological parameters of the flow are typical to the cases of mudflow movement as a wave, accompanied by a gradual process of "increase--and-decrease" of energy parameters, in particular discharge, velocity and levels, as well as cases of discontinuous changes or wave-like motion (Gavardashvili, 2022; Gavardashvili et al., 2023).

Flood formation as a wave is always associated with the violation of the equilibrium state of the mudflow forming mass in the center, overcoming the barriers of the encountered resistances in the transit zone, or impulses caused by the influence of other external forces. A mudflow moves as a continuous wave when the current is transformed from one stationary state to another. The development of the motion process in this way is similar to a quasi-stationary event, and this is to be expected when gravitational forces are gradually balanced by resistance forces.

Material and methods

The disruption of the deformed state of the mudflow mass formed in the erosion center corresponds to a certain phase of the equilibrium state of its body and is associated with certain limits of the mutual ratio of the constituent components. Accordingly, the violation of equilibrium and the beginning of movement are related to the value of the active transverse force, and the dynamics of movement is related to the filling of the pores of the mudflow mass with water, capillary moisture, effective flow and cohesion forces.

In order to obtain the calculation equation for the power of the mudflow mass, the limit stress state of the solid inert mass accumulated in the erosive banks as a result of negative geomorphological processes on the mountain slopes (erosion of the mountain slopes, landslides, rock falls, snow avalanches, etc.) is considered, using the basic equations of ground mechanics and hydrodynamics.

In connection with the above, the study of the tensed state of the mudflow mass can be considered analogous to the problems of soil mechanics (Fig. 1).

Gavardashvili, G., Kukhalashvili, E., Kurtsikidze, N., Dadiani, K. (2024). Mathematical model for the capacity of the mud flow with wave regime taking into account its rheological properties. *Sci. Rev. Eng. Env. Sci.*, *33* (3), 278–288. DOI 10.22630/srees.9816

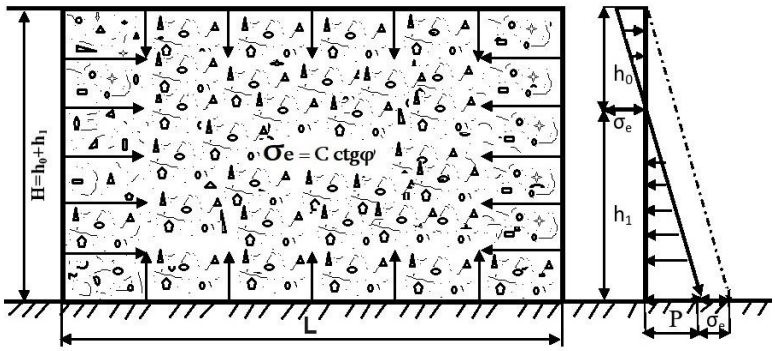

FIGURE 1. Calculation scheme
Source: own work.

When the density of the mudflow-forming mass (ρ), the gravity acceleration (g), the angle of internal friction (φ), the height of layer (h') of adherence pressure (Pe), the height of the mudflow-forming mass (H), the intensities of transverse pressure (P), and cohesiveness (C) are known, the value of active pressure is (Gregoretti et al., 2011; Natishvili et al., 2020):

$$P = \rho g\left(H + h'\right)\mathrm{tg}^2\left(45° - \frac{\phi}{2}\right) - Pe, \tag{1}$$

when the value of cohesion pressure: $Pe = \gamma h' = pgh'$ and the equivalent depth of cohesion: $h' = \dfrac{C}{\rho g\,\mathrm{tg}\,\phi}$, the value of active pressure is calculated by the following relation (Kailey et al., 2011):

$$P = \rho gH\,\mathrm{tg}^2\left(45° - \frac{\phi}{2}\right) - 2C\,\mathrm{tg}^2\left(45° - \frac{\phi}{2}\right). \tag{2}$$

Based on the principle of inert mass tension, the effect of the active pressure in the cohesive mudflow-forming mass on the ultimate resistance starts at a certain depth from its surface. Hence, when $P = 0$, $H = h_0$, we will have:

$$h_0 = \frac{2C}{\gamma\,\mathrm{tg}\left(45° - \frac{\phi}{2}\right)}, \tag{3}$$

where h_0 is the depth, corresponding to the zero value of the tension.

If we introduce notation $\mathrm{tg}^2\left(45° - \frac{\phi}{2}\right) = \psi$, the maximum tension distribution in the stressed zone is calculated:

$$P = \gamma H\left(1 - \frac{h_0}{H}\right)\psi \tag{4}$$

and the depth corresponding to the stressed state is calculated:

$$\frac{P}{\gamma} = h_1\left(1 - \frac{h_0}{H}\right)\psi. \tag{5}$$

Based on the active pressure, the magnitude of its corresponding transverse force is:

$$P = \frac{\gamma H^2}{2}\left(1 - \frac{h_0}{H}\right)^2 \psi. \tag{6}$$

The active force P is the force destructing the equilibrium resistance of the mudflow mass and the volume of the mudflow mass moved under its action when the width of its hearth is B. In this case:

$$W = \frac{P}{\gamma} = \frac{BH^2}{2}\left(1 - \frac{h_0}{H}\right)^2 \psi, \tag{7}$$

when the length of the hearth is L, the volume of the mudflow mass moved is:

$$BHL = \frac{BH^2}{2}\left(1 - \frac{h_0}{H}\right)^2 \psi. \tag{8}$$

Accordingly, the length of the active force exposure is equal to:

$$L = \frac{H}{2}\left(1 - \frac{h_0}{H}\right)\psi \tag{9}$$

and the active height of mudflow's hearth is: $H_a = H\left(1 - \frac{h_0}{H}\right)\psi$.

Gavardashvili, G., Kukhalashvili, E., Kurtsikidze, N., Dadiani, K. (2024). Mathematical model for the capacity of the mud flow with wave regime taking into account its rheological properties. *Sci. Rev. Eng. Env. Sci.*, *33* (3), 278–288. DOI 10.22630/srees.9816

The disturbance of the equilibrium state of the mudflow mass in the erosion center and the value of the discharge of the onset of movement (Kaitna et al., 2011) is:

$$Q = \frac{W}{t}. \tag{10}$$

If we introduce the value of Eq. (10) into Eq. (8), we get:

$$Qt = \frac{BH^2}{2}\left(1 - \frac{h_0}{H}\right)^2 \psi. \tag{11}$$

For the ratio of unit width and length of the mudflow-forming center $Q = q'_{nc}$. Consequently:

$$q'_m t = H\left(1 - \frac{h_0}{H}\right)\psi. \tag{12}$$

The relationship between the discharge and intensity of possible mudflow that started from the erosion center is:

$$q'_m = \frac{2Q}{H\left(1 - \frac{h_0}{H}\right)\psi}. \tag{13}$$

If we differentiate equation (12) with limit condition $q'_{nc} = const$, we will obtain:

$$q'_m dt = \left(1 - \frac{h_0}{H}\right)\psi dH, \tag{14}$$

when the resistance coefficient of the mudflow mass that started from the center is a constant value and $\varphi = 1$ and $h_0 = 0$, then:

$$q'_m = \frac{dH}{dt}. \tag{15}$$

Hence, by integrating (15), we obtain:

$$q'_m\left(t - t_0\right) = H - H_0 \tag{16}$$

and

$$q'_m\left(1-\frac{h_0}{H}\right)=\psi q'_n. \tag{17}$$

If we substitute the value of Eq. (16) into Eq. (17), we obtain:

$$q'_m\left(t-t_0\right)=\left(1-\frac{h}{H}\right)\psi\left(H-H_0\right). \tag{18}$$

The occurrence of mudflow movement onset from the erosion center is described by Eq. (14) as a wave what can be represented as follows:

$$q'_m\left(1-\frac{h_0}{H}\right)\phi\frac{dHdx}{dx\cdot dt}=\left(1-\frac{h_0}{H}\right)\psi V_B\frac{dH}{dx}. \tag{19}$$

In the case of uniform steady motion, the mudflow discharge is a function of its depth. In the case of motion as a continuous wave, the wave velocity, following the continuity condition, is three times its mean velocity $\overline{V}$ and accordingly, by integrating the nineteenth equation including mathematical transformations, we will get (Arnold et al., 2011):

$$q'_m=3\left(1-\frac{h_0}{H}\right)\psi\overline{V}\frac{dH}{dx}=H-H_0. \tag{20}$$

Based on the generalized Shvedov–Bingham model, the value of the average velocity is calculated by the following relation (Steger & Warming, 1981):

$$\overline{V}=\frac{\gamma iH^2}{3\mu}\left(1-\frac{h_0}{H}\right)^2\psi\left(1+\frac{1h_0}{2H}\right). \tag{21}$$

By inserting the value of Eq. (22) into the relation (21) and transforming it, we obtain:

$$q'_{nc}=\left(1-\frac{h_0}{H}\right)^3\phi^2\frac{\gamma iH^2}{\mu}\left(1-\frac{1h_0}{2H}\right)\frac{dH}{dx}. \tag{22}$$

Gavardashvili, G., Kukhalashvili, E., Kurtsikidze, N., Dadiani, K. (2024). Mathematical model for the capacity of the mud flow with wave regime taking into account its rheological properties. *Sci. Rev. Eng. Env. Sci.*, *33* (3), 278–288. DOI 10.22630/srees.9816

Based on the simplification and transformation of Eq. (23), when $\beta = \frac{h_0}{H}$ and $f(\beta) = (1-\beta)^2\left(1+\frac{1h_0}{2H}\right)\psi$, we obtain:

$$q'_m = \frac{\mathrm{g}iH^2}{\nu}\left(1-\frac{h_0}{H}\right)\psi\, f(\beta)\frac{dH}{dx}. \tag{23}$$

For a particular mudflow wave when the 0X axis coincides with direction of mudflow motion, by integrating Eq. (23), we obtain:

$$\frac{\left(H^3 - H_0^3\right)\left(1-\frac{h_0}{H}\right)\psi\, f(\beta)\mathrm{g}i}{\nu} = q'_m\left(x - x_0\right). \tag{24}$$

The resulting formula (24) is the equation of the free surface of the wave in plane *Hx*. If calculating the value of the mudflow depth *H* by the relation (23), we obtain:

$$\left[H_0 + \frac{q'_m\left(t-t_0\right)}{\left(1-\frac{h_0}{H}\right)\psi}\right]^3 = H_0^3 + \frac{q'_m\left(x-x_0\right)\nu}{\mathrm{g}if(\beta)\left(1-\frac{h_0}{H}\right)\psi}. \tag{25}$$

If excluding H_0 from the relation (24), the value *H* can be determined in time *t* and the profile of the free surface of the wave can be described by the following equation:

$$H^3 = \left[H - \frac{q'_m\left(t-t_0\right)}{\left(1-\frac{h_0}{H}\right)\psi}\right]^3 = \frac{q'_m\left(x-x_0\right)\nu}{\mathrm{g}if(\beta)\left(1-\frac{h_0}{H}\right)\psi}. \tag{26}$$

In the case of starting the mudflow motion from the initial position when $x = 0$, and $t_0 = 0$, in the case of different values of *H* at the first mudflow wave formation, from Eq. (24) we have:

$$H^3 = H_0^3 + \frac{q'_m x\nu}{\mathrm{g}if(\beta)\left(1-\frac{h_0}{H}\right)\psi}. \tag{27}$$

The propagation length of the wave in the plane *xt* can be determined from equation:

$$\left[H_0 + \frac{q'_m t}{\left(1-\frac{h_0}{H}\right)\psi}\right]^3 = H_0^3 + \frac{q'_m x\nu}{\mathrm{g}if\left(\beta\right)\left(1-\frac{h_0}{H}\right)\psi}. \tag{28}$$

The profile of the wave surface $x = 0$, and $t = 0$, is determined by Eq. (26):

$$H^3 = \left[H - \frac{q'_m t}{\left(1-\frac{h_0}{H}\right)\psi}\right]^3 + \frac{q'_m x\nu}{\mathrm{g}if\left(\beta\right)\left(1-\frac{h_0}{H}\right)\psi}. \tag{29}$$

At a later time moment when $x = 0$ and $H_0 = 0$, the wave surface profile is defined by equation:

$$H_0^3 = \frac{q'_m x\nu}{\mathrm{g}if\left(\beta\right)\left(1-\frac{h_0}{H}\right)\psi}. \tag{30}$$

Accordingly, the wavelength of wave propagation is calculated by Eq. (24) and the time *t* is calculated by the following equation:

$$t = t_0 + \sqrt[3]{\frac{x\nu\left(1-\frac{h_0}{H}\right)^2\psi}{q^2{}_m \mathrm{g}if\left(\beta\right)}}, \tag{31}$$

where *i* is the gradient of the uniform motion of mudflow.

In the first approximation, it is possible to analyze the process of mudflow formation from erosion foci. By means of the methodology used and the obtained Eq. (27), the formation of micropower floods can be predicted.

For the first destructive mudflow wave when $t = 0$ and $x = 0$, the wave propagation length can be described by equation, and for microwaves in plane *xt* when $H_0 = 0$, $x = 0$, and $t_0 = 0$, it is calculated by Eq. (31).

Gavardashvili, G., Kukhalashvili, E., Kurtsikidze, N., Dadiani, K. (2024). Mathematical model for the capacity of the mud flow with wave regime taking into account its rheological properties. *Sci. Rev. Eng. Env. Sci.*, *33* (3), 278–288. DOI 10.22630/srees.9816

Assessment of stability violation of the mudflow mass formed in the erosion center, when on the basis of the theory of stresses the beginning of movement and movement of one part of the formation onto another is predicted, the discharge change dynamics during the movement is non-stationary. The mathematical model of mass movement in an erosion center corresponding to the reduction of its depth H to h can be determined by relating the mudflow formed by the active force to the stability characteristics.

Based on the natural reality, due to the multicomponent nature of the mudflow mass formed in the erosion center and different effects of weather and climatic factors as confirmed by the real event, the value of the discharge formed by the active lateral force is variable.

To evaluate the process of the motion onset of the mudflow mass and to represent the shear surface in a nonlinear form, the length of active wave propagation in relation to rheology can be calculated by Eq. (28).

In the case of using Eq. (24) to estimate the wave surface profile, when the characteristics of initial conditions are 0 and, accordingly, the change in its depth in relation to the intensity of the discharge change is represented by the dependence (27), the mudflow discharge for center height H_k can be determined by the formula:

$$Q = \frac{\mathrm{g}i\left(1-\frac{h_0}{H_k}\right)\psi f(\beta) H_k^3}{L}. \tag{32}$$

In the wave zone, when the magnitude of energy loss is a function of rheological characteristics, the relationship from depth H_k to h value can be defined as follows:

$$h = \frac{4H_k}{\left[2+\left(1-\frac{h_0}{H_k}\right)\psi\right]^2}. \tag{33}$$

Substituting the ratio (33) into Eq. (32), we obtain:

$$Q = \frac{\mathrm{g}i\left(1-\frac{h_0}{h}\right)\psi f(\beta)\left[1+\left(1-\frac{h_0}{H}\right)\psi\right]^6 h^3}{L}. \tag{34}$$

Based on the deduced dependence to calculate the discharge, the mudflow capacity is calculated by the following ratio:

$$N = \gamma Q H_k = \frac{4\gamma g i \left(1-\frac{h_0}{h}\right)\psi f(\beta)\left[1+\left(1-\frac{h_0}{H}\right)\psi\right]^6\left[2+\left(1-\frac{h_0}{h}\right)\psi\right]^2 h^4}{L}. \quad (35)$$

Based on the obtained ratio (35), it is possible to estimate the total capacity of the mudflow mass accumulated in erosion gullies, taking into account the main rheological properties of the solid mass eroded from the mountain slopes.

Conclusion

By taking into account the dynamics of wave motion of mudflows and rheological properties of the solid mass eroded from the mountain slopes, on the basis of theoretical studies, the equation to calculate the full capacity of the mudflow mass is deduced in the present paper.

When calculating the mudflow strength, attention is focused on the assessment of stability violation of the mudflow mass accumulated in the center of erosion when the onset of the mudflow mass movement predicted on the basis of the stress theory is non-stationary.

The derived formula (35) is currently being tested for particular cases of mudflow mass accumulated in erosion gullies identified in the river catchment basins in natural conditions.

Acknowledgements

The research was financial supported by Shota Rustaveli National Science Foundation of Georgia, Grant # AR-18-1244 “Elastic debris flow-regulating barrage” Solid Sediments Movement Regulating Innovative Debris Flow Elastic Barrage.

References

Arnold, A., Hübl, J., Suriñach, E., Vilajosana, I., Zhang, S., Yun, N., & McArdell, B. (2011). A study of infrasonic signals of debris flows. *Italian Journal of Engineering Geology and Environment*, *2011*, 563–572. https://doi.org/10.4408/IJEGE.2011-03.B-062

Gavardashvili, G. V. (2022). *Predicting erosive and debris flow processes and the innovative measures to control them.* Cambridge Scholars Publishing.

Gavardashvili, G. V., Kukhalashvili, E. G., & Gavardashvili, N. G. (2023, September 26–29). *Solid sediments movement regulating innovative debris flow elastic barrage.* 20th International Conference on Transport and sedimentation of solid particles. Wrocław, Poland.

Gregoretti, C., Furlan, M., & Degetto, M. (2011). GIS-based cell model for simulating debris flow routing and deposition phases on a fan. *Italian Journal of Engineering Geology and Environment*, *2011*, 425–434. https://doi.org/10.4408/IJEGE.2011-03.B-048

Kailey, P., Bowman, E., Laue, J., & Springman, S. M. (2011). Modelling debris flow processes with geotechnical centrifuge. *Italian Journal of Engineering Geology and Environment*, *2011*, 339–349. https://doi.org/10.4408/IJEGE.2011-03.B-039

Kaitna, R., Hsu, L., Rickenmann, D., & Dietrich, W. E. (2011). On the development of an unsaturated front of debris flow. *Italian Journal of Engineering Geology and Environment*, *2011*, 351–358. https://doi.org/10.4408/IJEGE.2011-03.B-040

Natishvili, O., Kukhalashvili, E., & Gavardashvili, G. (2020). One-dimension mathematical model of energy parameters of a hyper concentrated mudflow. *Annals of Agrarian Science*, *18* (3), 251–257. https://journals.org.ge/index.php/aans/issue/view/19/23

Steger, J. L., & Warming, R. (1981). Flux vector splitting of the inviscid gasdynamic equations with application to finite-difference methods. *Journal of Computational Physics*, *40* (2), 263–293. https://doi.org/10.1016/0021-9991(81)90210-2

Summary

Mathematical model for the capacity of the mud flow with wave regime taking into account its rheological properties. The paper presents particular issues of mudflow dynamics, one of the hazardous natural disasters, namely the theoretical study of the flow power during mudflow movement in the wave regime taking into account its rheological properties. The paper discusses the physical process of mudflow mass impetus accumulated in erosion banks, taking into account the impact of the tense state of the eroded mass, in particular, similar to soil mechanics problems, the density of the mudflow-forming mass (ρ), the free fall acceleration (g), angle of internal friction (φ), the adhesive force (Pe), the height equivalent to pressure (h'), the height of the mudflow-forming mass (H), the intensity of transverse pressure (P), and the value of the active pressure of the inertial mass cohesion (C) on the deformation mode of the mudflow mass. On the basis of the basic equations of mudflow dynamics and theoretical studies, an equation is obtained to calculate the values of flow power when mudflows move in the wave mode, taking into account the main rheological properties of a mudflow mass.

Scientific Review Engineering and Environmental Sciences (2024), 33 (3), 289–303

Sci. Rev. Eng. Env. Sci. (2024), 33 (3) https://srees.sggw.edu.pl

ISSN 1732-9353 (suspended) eISSN 2543-7496 DOI 10.22630/srees.9765

Received: 15.04.2024
Accepted: 13.06.2024

Erika HURAJOVÁ[1]
Petra MARTÍNEZ BARROSO[2]
Ladislav HAVEL[1]
Igor DĚKANOVSKÝ[3]
Jan WINKLER[1]✉

[1] Mendel University in Brno, Faculty of AgriSciences, Department of Plant Biology, Czech Republic
[2] Mendel University in Brno, Faculty of AgriSciences, Department of Applied and Landscape Ecology, Czech Republic
[3] University Hospital Brno, Czech Republic

Vegetation succession and changes in carabid beetle (Coleoptera: Carabidae) communities in vineyards in Moravia, Czech Republic

Keywords: vineyard ecosystem, insects, succession, vegetation

Introduction

The structure of a plant community is the basis for a spatial and structural heterogeneity of a habitat. Vegetation provides diverse niches (microhabitats) offering different opportunities to animals, including insects, for acquiring food and shelter from predators (Gardiner et al., 2002; Schaffers et al., 2008; Badenhausser & Cordeau, 2015). Habitat fragmentation and destruction caused by agricultural

✉jan.winkler@mendelu.cz

intensification is one of the main drivers of arthropod decline in agroecosystems (Tscharntke et al., 2005; Bianchi et al., 2006; Landis, 2017). The loss of habitat complexity and diversity due to intensive agricultural practices results in fewer niches and less protection for arthropods, contributing to their decline.

Although vineyards belong to intensively managed agroecosystems, they still offer diverse habitats for a number of organisms (Geldenhuys et al., 2021). The mosaic of different microhabitats found in vineyards, combined with the alternation of bare soil and higher vegetation, meets the needs of different life stages of insects (Ingrisch & Köhler, 1998; Fischer et al., 2020). Different types of management can be found in the vineyards, e.g. a highly intensive inter-row management using a combination of herbicides and tillage; on the other hand, sowing of cover crops or allowing local vegetation to flourish (Winkler et al., 2017; Winter et al., 2018).

Greater microhabitat diversity leads to greater plant diversity and typically increases arthropod diversity, thereby enhancing the likelihood of introducing beneficial arthropods into the vineyard. Spontaneous vegetation, which is well adapted to local conditions, particularly supports this relationship in vineyards (Bischoff et al., 2016).

Inter-row vegetation of vineyards contributes to richness of native plant species (Beaumelle et al., 2021; Blaise et al., 2022) and increases arthropod biodiversity (Blaise et al., 2022; Rocher et al., 2022). Semi-natural habitats are very important for communities of arthropods, which are the key organisms in agroecosystems (Tscharntke et al., 2005; Saunders, 2018; Cahenzli et al., 2019). Spontaneous vegetation in vineyards increases the abundance of other insects that have the ability to engage in natural protection against pests in agroecosystems (Sáenz-Romo et al., 2019). Carabid beetles (Coleoptera: Carabidae) also increase arthropod richness in vineyards and are considered valuable contributors to integrated pest management (Rainio & Niemelä, 2003; Adamski et al., 2019). The composition and richness of vegetation are essential factors to be considered when assessing not only biodiversity, but also the sustainable development of agriculture and viticulture (Isaacs et al., 2009). The method of vineyard management is very specific and provides space for increasing the heterogeneity of the landscape. The inter-row vegetation is an integral part of the vineyard, which undergoes natural changes (successions) over time. Long-term vineyard management combined with the natural succession of vegetation changes the conditions of microhabitats.

Vegetation succession in vineyards plays a crucial role in shaping carabid beetle communities. Studies have shown that different inter-row ground cover treatments, such as bare soil, alternating, and full vegetation cover, can significantly affect carabid beetle density and species richness (Uzman et al., 2020; Porter et al., 2022).

In addition, structural heterogeneity of vegetation has been found to be a key factor influencing carabid beetle diversity, with vegetation structure explaining a significant proportion of the variation in species richness (Brose, 2003). Furthermore, the response of carabid beetles to changing conditions during succession varies, with different responses observed in diverse habitat types such as fallow and grassland (Taranto et al., 2023). Maintaining a balance between dense and sparsely vegetated elements in vineyard interrow may be optimal for supporting diverse carabid beetle communities and promoting biodiversity in vineyard ecosystems.

Despite the recognized importance of vegetation and habitat heterogeneity in supporting arthropod diversity, there is a lack of detailed understanding of how vegetation succession in vineyards of different ages influences carabid beetle communities. This study aims to fill this research gap by exploring the following questions: (i) What are the trends in carabid beetle communities in vineyards over the course of the year? (ii) How does vegetation succession affect these trends? (iii) What is the effect of vineyard age on carabid beetle biodiversity? Addressing these questions will not only improve our understanding of arthropod dynamics in vineyard ecosystems, but will also contribute to the development of sustainable viticultural practices.

Material and methods

Study area

The evaluated vineyards are located in Moravia in the Czech Republic. The area is located at the transition between Jevišovská vrchovina and Dyjskosvratecký úval. The average altitude is 280 m above sea level. The long-term air temperature is between 9°C and 10°C and the long-term precipitation is between 500 mm and 600 mm. The probability of dry seasons is 30–50%. Cambisols and Chernozems are the predominant soils (Culek, 1996; Czech Geotechnical Society, 2017, 2018). Table 1 gives an overview of the wine-growing villages, wine routes and years of establishment of the surveyed vineyards. The selected vineyards are conventionally farmed and have similar management practices. The selection of the monitored vineyards was based on several criteria. Vineyards were selected only in neighboring wine-producing villages with the same climatic and pedological conditions. Vineyards that were physically accessible and for which the year of planting was known were selected. The intention was to create a set of vineyards of different ages, with management conditions that could create different conditions for the occurrence of the carabid beetle community.

Hurajová, E., Martínez Barroso, P., Havel, L., Děkanovský, I., Winkler, J. (2024). Vegetation succession and changes in carabid beetle (Coleoptera: Carabidae) communities in vineyards in Moravia, Czech Republic. *Sci. Rev. Eng. Env. Sci.*, *33* (3), 289–303. DOI 10.22630/srees.9765

TABLE 1. General characteristics of selected vineyards

Winery village (vine lines)	GPS	Years of establishment of evaluated vineyards
Horní Dunajovice (Frédy, Stará hora)	48°56′41.153″N, 16°10′41.676″E	1995 (2 vineyards), 2000, 2002, 2009, 2016, 2018, 2020, 2021
Hostěradice (Volné pole)	48°57′17.479″N, 16°17′12.790″E	1972, 2003, 2014, 2015, 2016, 2017, 2018, 2020, 2021
Miroslav (U vinohradu, Weinperky)	48°56′37.223″N, 16°17′59.253″E	1996, 1998, 1999, 2001, 2002, 2003, 2004, 2007, 2011, 2014, 2015, 2017, 2019
Miroslavské Knínice (Stará hora, Zolos)	48°58′16.344″N, 16°19′50.606″E	2001, 2011

Source: own work.

Method of vegetation assessment

In 37 vineyards of different ages, plots were established to assess both the vegetation and carabid beetle community. These plots were located in the inter-rows of the vineyards. The vegetation in these inter-rows developed naturally through spontaneous revegetation and was managed through mulching practices. The vegetation evaluation was carried out in areas close to where the evaluation of the carabid community took place. Vegetation was assessed using phytocoenological relevés, according to the standard principles of the Zürich–Montpellier approach (Biondi, 2011). The extent of cover for each plant species was estimated and documented as a percentage of the total cover. Observations were conducted annually from 2020 to 2023, with assessments made during three separate periods each year: spring, summer, and fall. Within every vineyard, three phytocoenological relevés were captured, each covering an area of 2 × 4 m. The taxonomic naming of the plants adhered to the system outlined by Kaplan et al. (2019). The plant species identified were categorized into four groups: (i) annual dicotyledons, (ii) perennial dicotyledons, (iii) annual grasses, and (iv) perennial grasses.

Methodology of carabid beetle community assessment

Carabid beetles were captured in areas immediately adjacent to the areas of vegetation assessment. Capturing of carabid beetles was performed during the same period as the vegetation assessment in order to facilitate correlation of carabid beetle abundance with vegetation characteristics. Vegetation was removed from the area where carabid beetles were observed and captured. Subsequently, soil

traps of 0.3 × 0.3 m in size and 0.3 m depth were excavated in 3 replicates. The carabid beetles were observed by direct observation of individuals for 30 min, at noon of the evaluated day and in sunny weather. Trapping was limited in time so that the abundance of beetle populations would not be affected by excessive trapping during the multi-year observation. The number of individuals occurring in the vineyard was recorded. The carabid beetles were captured and put in a bottle containing a medium impregnated with a lethal poison (ethyl acetate) in order to allow a later species identification of the collected individuals in a laboratory. Identification was performed according to Hůrka (1996).

Statistical data treatment

The data obtained on vegetation and carabid beetle populations were processed using weighted averages. The averages were calculated from 3 phytocenological relevé and 3 trap plots recorded in vineyards of the same age for 4 years of observation. The average vegetation cover and the average number of carabid beetle populations are graphically presented further in the text.

The basic data from individual observations were used for statistical processing. Data from each season (spring, summer, autumn) were analyzed separately. Multivariate analyses of ecological data were used to analyze the results of the assessment in terms of carabid abundance and coverage of different plant species groups.

The first analysis was the detrended correspondence analysis (DCA), which influences the selection of the most appropriate analysis. The result of the DCA is the length of the gradient. For the spring data, the response data were compositional and have a gradient length of 2.0 SD units, so the linear method is recommended. For the summer data, the response data are compositional and have a gradient length of 1.8 SD units, so the linear method is recommended. For the autumn data, the response data are compositional and have a gradient of 2.1 SD units in length, so the linear method is recommended.

A redundancy analysis was chosen based on the recommendations of the Canoco 5.0 software and the methodological approach. Computed axes 4, detrending none, hybrid analysis not performed, response data (species) transformation log (log transformation formula: $Y' = 1 \times Y + 1$), center and standardize by species yes. Statistical significance was assessed using the Monte Carlo test with 999 permutations. All multivariate analyses and necessary calculations were performed using Canoco 5.0 software (ter Braak & Šmilauer, 2012).

Hurajová, E., Martínez Barroso, P., Havel, L., Děkanovský, I., Winkler, J. (2024). Vegetation succession and changes in carabid beetle (Coleoptera: Carabidae) communities in vineyards in Moravia, Czech Republic. *Sci. Rev. Eng. Env. Sci.*, *33* (3), 289–303. DOI 10.22630/srees.9765

Results and discussion

The vegetation in the monitored vineyards consisted of 48 species of annual dicotyledons, 63 species of perennial dicotyledons, 9 species of annual grasses, and 10 species of perennial grasses.

The average coverage of plant groups in the vineyards is illustrated in Figure 1. Among the annual dicot taxa with dominant representation were *Amaranthus retroflexus*, *Geranium pusillum*, *Stellaria media*, *Chenopodium album*, and *Conyza canadensis*. Perennial dicot plant taxa with dominant presence included *Convolvulus arvensis*, *Trifolium repens*, *Achillea millefolium*, *Trifolium pratense*, *Cirsium arvense* and *Plantago lanceolata*. Annual grass taxa with dominant presence included *Hordeum murinum*, *Setaria pumila*, *S. viridis*, and

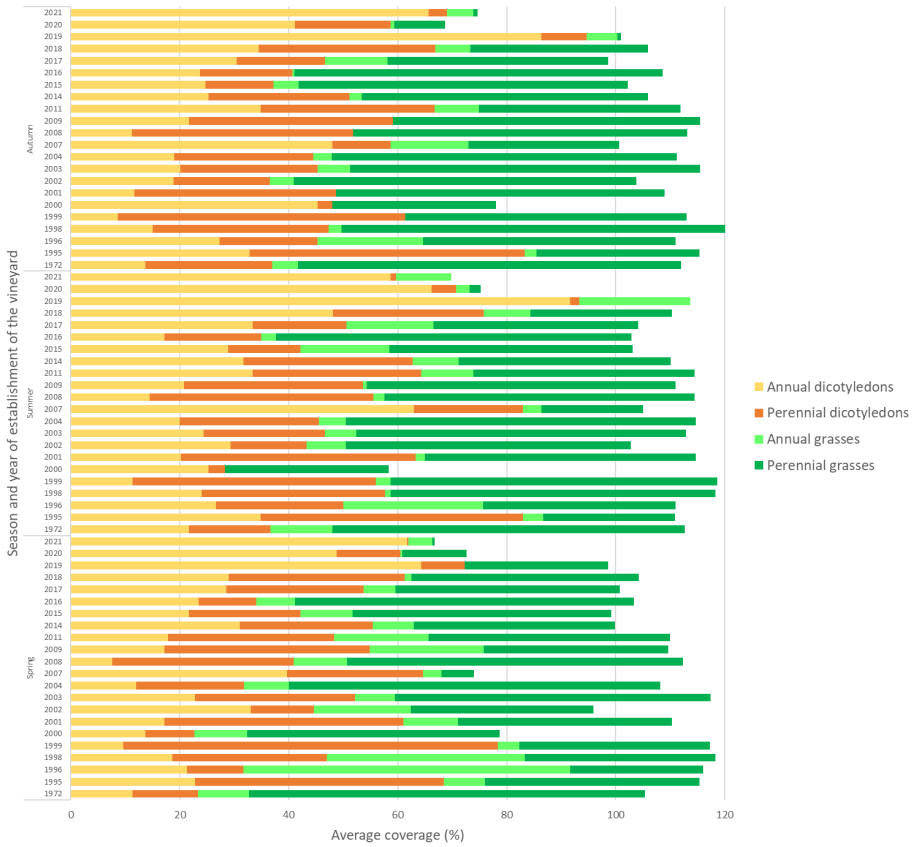

FIGURE 1. Representation of plant groups in monitored seasons in vineyards of different

Source: own work.

Echinochloa crus-galli. Perennial grass taxa with a dominant presence included *Lolium perenne*, *L. multiflorum*, and *Festuca rubra.*

In the monitored vineyards, 9 species of carabid beetles were captured during the observation; the total number of captured individuals is given in brackets, namely, namely *Anchomenus dorsalis* (172 individuals), *Dolichus halensis* (212 individuals), *Europhilus fuliginosus* (256 individuals), *Harpalus affinis* (132 individuals), *H. hospes* (264 individuals), *Leistus ferrugineus* (12 individuals), *Platynus assimilis* (300 individuals), *Poecilus cupreus* (440 individuals), and *Pseudoophonus rufipes* (972 individuals). The average number of captured carabid beetles is demonstrated in Figure 2.

FIGURE 2. Carabid beetle community in monitored seasons in vineyards of different ages
Source: own work.

Hurajová, E., Martínez Barroso, P., Havel, L., Děkanovský, I., Winkler, J. (2024). Vegetation succession and changes in carabid beetle (Coleoptera: Carabidae) communities in vineyards in Moravia, Czech Republic. *Sci. Rev. Eng. Env. Sci.*, *33* (3), 289–303. DOI 10.22630/srees.9765

The influence of the age of the vineyards on the coverage of plant groups and on the number of carabid beetles was statistically significant in all three monitored seasons. The results of data processing by RDA analysis are shown in Figure 3.

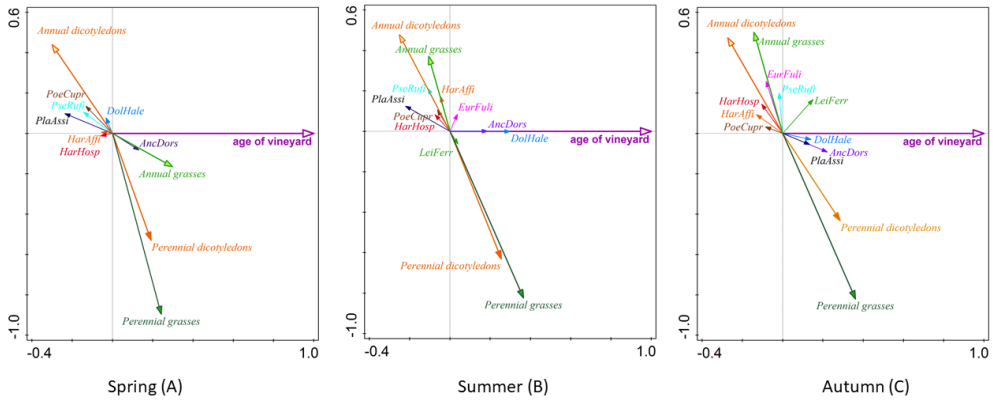

AncDors – Anchomenus dorsalis, *DolHale – Dolichus halensis*, *EurFuli – Europhilus fuliginosus*, *HarAffi – Harpalus affinis*, *HarHosp – Harpalus hospes*, *LeiFerr – Leistus ferrugineus*, *PlaAssi – Platynus assimilis*, *PoeCupr – Poecilus cupreus*, *PseRufi – Pseudoophonus rufipes*.

FIGURE 3. Relationship between vineyard age, plant groups and carabid beetle community for period of spring (A), summer (B), autumn (C), (result RDA; Fig. A: total explained variability = 6.3%, F-ratio = 8.7, P-value = 0.001; Fig. B: total explained variability = 7.1%, F-ratio = 9.9, P-value = 0.001; Fig. C: total explained variability = 7.4%; F-ratio = 10.3, P-value = 0.001)

Source: own work.

In the spring season, the younger vineyards create more favorable conditions for annual dicotyledons plant taxa. Higher numbers of the following carabid beetle species were recorded: *Dolichus halensis*, *Europhilus fuliginosus*, *Harpalus affinis*, *H. hospes*, *Leistus ferrugineus*, *Platynus assimilis*, *Poecilus cupreus*, and *Pseudoophonus rufipes*. Older vineyards provide more favorable conditions during the spring season for annual grasses, perennial dicotyledons, perennial grasses, and for carabid beetles of the species *Anchomenus dorsalis*.

In summer season, younger vineyards create more favorable conditions for the following plant taxa: annual dicotyledons and annual grasses. A higher number of the following carabid beetle species was recorded: *Europhilus fuliginosus*, *Harpalus affinis*, *H. hospes*, *Leistus ferrugineus*, *Platynus assimilis*, *Poecilus cupreus*, and *Pseudoophonus rufipes*. Older vineyards offer more favorable conditions during the summer season for perennial dicotyledons, perennial grasses, and for a higher number of carabid beetles of the species *Anchomenus dorsalis*, *Dolichus halensis*, and *Leistus ferrugineus.*

In autumn, younger vineyards create more favorable conditions for the following plant taxa: annual dicotyledons and annual grasses. A higher number of carabid beetles of the following species was recorded: *Europhilus fuliginosus*, *Harpalus affinis*, *H. hospes*, *Leistus ferrugineus*, *Poecilus cupreus*, *Pseudoophonus rufipes.* In autumn, older vineyards provide more favorable conditions for the plant groups: perennial dicotyledons, perennial grasses, and for carabid beetles of the species *Anchomenus dorsalis*, *Dolichus halensis*, *Leistus ferrugineus*, and *Platynus assimilis.*

The biodiversity of carabid beetles is mainly supported by the presence of spontaneous vegetation in the vineyards. Additionally, carabid beetles are affected by the management applied in the vineyard, which alters the ecosystem services provided by carabid beetles (Porter et al., 2022). Changes in inter-row vegetation in vineyards can negatively affect the biodiversity and the number of invertebrate insect species (Ragasová et al., 2021). According to our results, it is evident that carabid beetle communities change seasonally. The composition of the vegetation changes with the age of the vineyards. During the aging of vineyards, representatives of perennial dicotyledons and perennial grasses groups increase and representatives of the annual dicotyledons group decrease. Members of the annual grasses group change markedly during the seasons. In spring, they have a higher coverage in older vineyards, while in summer and autumn, they reach higher coverage in younger vineyards. The species composition of the vegetation corresponds to the grassed inter-row vegetation in the observed region, which occurs in vineyards (Ragasová et al., 2021) and in orchards (Winkler et al., 2023).

A higher quantity of carabid beetles was recorded in summer and autumn, which might be attributed to a higher food supply and a sufficiency of microhabitats enabling wintering. The age of the vineyards also affected the community of carabid beetles – the species *Anchomenus dorsalis* was more common in older vineyards during the monitored seasons. The species *Dolichus halensis*, *Leistus ferrugineus*, and *Platynus assimilis* were recorded with a higher frequency in summer and autumn in older vineyards. The other species preferred younger vineyards. Vegetation does not form a continuous cover in younger vineyards, therefore it creates habitats favorable for a number of carabid beetle species (Kromp, 1999; Holland, 2002; Kotze et al., 2011).

Gradual changes in the composition of the vegetation combined with the age of the vineyards can also impact the carabid beetles. Older vineyards were dominated by grasses, which may be the cause of a smaller food supply for carabid beetles. Grasses are less attractive for a number of arthropods (Del-Claro et al., 2016), which may be reflected in a decrease in abundance and species diversity of carabid beetles, as noticeable from our results.

Taxa from the annual dicotyledons group had a higher share in the vegetation of young vineyards. These plants produce large amounts of biomass, which die relatively quickly due to dry and warm weather. The biomass of these plants serves as a food source for a number of organisms. Gaigher and Samways (2010) found that biomass creates structural diversity in vineyards and supports different arthropod species. As our results show, thanks to the higher presence of arthropods, the food supply offer for predatory carabid beetles increased and a higher frequency of carabid beetles was recorded mainly in summer and autumn. The total number of beetles captured is relatively low in our observation, which is a consequence of our method and particularly of the short period of time during which the beetles were captured. The sample of beetles caught had only a limited influence on their occurrence in subsequent years. Despite the low number of beetles caught, our results show trends that characterize changes in the beetle population in vineyards of different ages.

According to Porter et al. (2022), seasonal changes in carabid beetle community composition are affected by applied inter-row management in vineyards. The timing of management operations should take into account the carabid beetle community dynamics to minimize harm caused to their communities. Predatory carabid beetles reduce the occurrence of a number of agricultural pests (Rainio & Niemelä, 2003; Adamski et al., 2019). The species of the *Harpalus* genus contribute to the predation of weed seeds, thereby reducing unwanted vegetation in vineyards (Rusch et al., 2015; De Heij & Willenborg, 2020). Protection of carabid beetle communities in the form of limited vineyard management creates synergies for wine production and reduced pesticide applications.

Conclusions

The succession of vineyards induces a dynamic transformation of the ecosystem, which is manifested by a change in the species composition of the vegetation and the carabid beetle community. The composition and changes in the vegetation of the vineyards provoke a response in the community of carabid beetles that use the vineyards as their habitat:

– The community of carabid beetles in vineyards changes with the season. Carabid beetles find more favorable conditions in young vineyards during summer and autumn.

– This is mainly due to the biomass growth of the annual dicotyledons plant group in summer and fall. The biomass of living and dead vegetation increases the food supply for carabid beetles, and thus their abundance and the attractiveness of vineyards.
– The proportion of perennial grasses, which are not so attractive to carabid beetles, increases with the aging of vineyards.
– The study of vineyard biodiversity must take into account the temporal dynamics of changes in vegetation and carabid beetle communities.
– The age of vineyards affects the representation of certain plant and animal species.

The vineyard ecosystem changes dynamically over time, both during the changing seasons and over a longer time span. When assessing the carabid beetles community in vineyards, it is essential to consider the dynamics of development and to understand the changes in the biodiversity of vineyard ecosystems over time.

Acknowledgments

This research was created within the project: IGA-ZF/2021-ST2001 – Evaluation of ecosystem services of vegetation in permanent crops.

References

Adamski, Z., Bufo, S. A., Chowanski, S., Falabella, P., Lubawy, J., Marciniak, P., Pacholska-Bogalska, J., Salvia, R., Scrano, L., Słocinska, M., Spochacz, M., Szymczak, M., Urbański, A., Walkowiak-Nowicka, K., & Rosiński, G. (2019). Beetles as model organisms in physiological, biomedical and environmental studies – a review. *Frontiers in Physiology*, *10*, 431695. https://doi.org/10.3389/fphys.2019.00319

Badenhausser, I., & Cordeau, S. (2015). Sown grass strip – a stable habitat for grasshoppers (Orthoptera: Acrididae) in dynamic agricultural landscapes. *Agriculture, Ecosystems & Environment*, *159*, 105–111. https://doi.org/10.1016/j.agee.2012.06.017

Beaumelle, L., Auriol, A., Grasset, M., Pavy, A., Thiéry, D., & Rusch, A. (2021). Benefits of increased cover crop diversity for predators and biological pest control depend on the landscape context. *Ecological Solutions and Evidence*, *2* (3), e12086. https://doi.org/10.1002/2688-8319.12086

Bianchi, F. J. J. A., Booij, C. J. H., & Tscharntke, T. (2006). Sustainable pest regulation in agricultural landscapes: a review on landscape composition, biodiversity and natural pest control. *Proceedings of the Royal Society B: Biological Sciences*, *273* (1595), 1715–1727. https://doi.org/10.1098/rspb.2006.3530

Biondi, E. (2011). Phytosociology today: methodological and conceptual evolution. *Plant Biosystems – an International Journal Dealing with All Aspects of Plant Biology*, *145* (1), 19–29. https://doi.org/10.1080/11263504.2011.602748

Bischoff, A., Pollier, A., Lamarre, E., Salvadori, O., Cortesero, A. M., Le Ralec, A., Tricault, Y., & Jaloux, B. (2016). Effects of spontaneous field margin vegetation and surrounding landscape on *Brassica oleracea* crop herbivory. *Agriculture, Ecosystems & Environment*, *223*, 135–143. https://doi.org/10.1016/j.agee.2016.02.029

Blaise, C., Mazzia, C., Bischoff, A., Millon, A., Ponel, P., & Blight, O. (2022). Vegetation increases abundances of ground and canopy arthropods in Mediterranean vineyards. *Scientific Reports*, *12* (1), 3680. https://doi.org/10.1038/s41598-022-07529-1

Braak, C. J. F. ter, & Šmilauer, P. (2012). *Canoco reference manual and user's guide: software for ordination (version 5.0)*. Microcomputer Power.

Brose, U. (2003). Bottom-up control of carabid beetle communities in early successional wetlands: mediated by vegetation structure or plant diversity? *Oecologia*, *135* (3), 407–413. https://doi.org/10.1007/s00442-003-1222-7

Cahenzli, F., Sigsgaard, L., Daniel, C., Herz, A., Jamar, L. Kelderer, M., Jacobsen, S. K., Kruczyńska, D., Matray, S., Porcel, M., Sekrecka, M., Świergiel, W., Tasin, M., Telfser, J., & Pfiffner, L. (2019). Perennial flower strips for pest control in organic apple orchards – A pan-European study. *Agriculture, Ecosystems & Environment*, *278*, 43–53. https://doi.org/10.1016/j.agee.2019.03.011

Czech Geological Society (2017). *Map of soil types of the Czech Republic, 1:50 000*. Czech Geological Society. https://mapy.geology.cz/pudy/

Czech Geological Society (2018). *Geological Map of the Czech Republic, 1:50 000*. Czech Geological Society. https://mapy.geology.cz/geocr50/

Culek, M. (Ed.) (1996). *Biogeografické členění České republiky* [*Biogeographical division of the Czech Republic*]. Enigma.

De Heij, S. E., & Willenborg, C. J. (2020). Connected carabids: network interactions and their impact on biocontrol by carabid beetles. *Bioscience*, *70* (6), 490–500. https://doi.org/10.1093/biosci/biaa039

Del-Claro, K., Rico-Gray, V., Torezan-Silingardi, H. M., Alves-Silva, E., Fagundes, R., Lange, D., Dáttilo, W., Vilela, A., & Rodriguez-Morales, D. (2016). Loss and gains in ant–plant interactions mediated by extrafloral nectar: fidelity, cheats, and lies. *Insectes Sociaux*, *63*, 207–221. https://doi.org/10.1007/s00040-016-0466-2

Fischer, J., Steinlechner, D., Zehm, A., Poniatowski, D., Fartmann, T., Beckmann, A., & Stettmer, C. (2020). *Die Heuschrecken Deutschlands und Nordtirols: Bestimmen – Beobachten – Schützen* [*The locusts of Germany and North Tyrol: identify – observe – protect*]. Quelle & Meyer Verlag.

Gaigher, R., & Samways, M. J. (2010). Surface-active arthropods in organic vineyards, integrated vineyards and natural habitat in the Cape Floristic Region. *Journal of Insect Conservation*, *14*, 595–605. https://doi.org/10.1007/s10841-010-9286-2

Gardiner, T., Pye, M., Field, R., & Hill, J. (2002). The influence of sward height and vegetation composition in determining the habitat preferences of three Chorthippus species (Orthoptera: Acrididae) in Chelmsford, Essex, UK. *Journal of Orthoptera Research*, *11* (2), 207–213.

Geldenhuys, M., Gaigher, R., Pryke, J. S., & Samways, M. J. (2021). Diverse herbaceous cover crops promote vineyard arthropod diversity across different management regimes. *Agriculture, Ecosystems and Environment*, *307*, 107222. https://doi.org/10.1016/j.agee.2020.107222

Holland, J. M. (2002). Carabid beetles: their ecology, survival and use in agroecosystems. In J. M. Holland (Ed.), *The agroecology of carabid beetles* (pp. 1–40). Intercept.

Hůrka, K. (1996). *Carabidae* České *a Slovenské republiky* [*Carabidae of the Czech and Slovak Republics*]. Kabourek.

Ingrisch, S., & Köhler, G. (1998). *Die Heuschrecken Mitteleuropas* [*The locusts of Central Europe*]. Westarp Wissenschaften.

Isaacs, R., Tuell, J., Fiedler, A., Gardiner, M., & Landis, D. (2009). Maximizing arthropod-mediated ecosystem services in agricultural landscapes: the role of native plants. *Frontiers in Ecology and the Environment*, *7* (4), 196–203. https://doi.org/10.1890/080035

Kaplan, Z., Danihelka, J., Chrtek, J., Kirschner, J., Kubát, K., Štěch, M. A., & Štěpánek, J. (Eds). (2019). *Klíč ke Květeně* České *republiky* [*Key to the flora of the Czech Republic*]. Academia.

Kotze, D. J., Brandmayr, P., Casale, A., Dauffy-Richard, E., Dekoninck, W., Koivula, M., Lövei, G., Mossakowski, D., Noordijk, J., Paarmann, W., Pizzolotto, R., Saska, P., Schwerk, A., Serrano, J., Szyszko, J., Taboada, A., Turin, H., Venn, S., Vermeulen, R., & Zetto, T. (2011). Forty years of carabid beetle research in Europe – From taxonomy, biology, ecology and population studies to bioindication, habitat assessment and conservation. *ZooKeys*, *100*, 55–148. https://doi.org/10.3897/zookeys.100.1523

Kromp, B. (1999). Carabid beetles in sustainable agriculture: a review on pest control efficacy, cultivation impacts and enhancement. *Agriculture, Ecosystems & Environment*, *74* (1–3), 187–228. https://doi.org/10.1016/S0167-8809(99)00037-7

Landis, D. A. (2017). Designing agricultural landscapes for biodiversity-based ecosystem services. *Basic and Applied Ecology*, *18*, 1–12. https://doi.org/10.1016/j.baae.2016.07.005

Porter, L., Khalil, S., Forneck, A., Winter, S., & Griesser, M. (2022). Effects of ground cover management, lndscape elements and local conditions on carabid (Coleoptera: Carabidae) diversity and vine vitality in temperate vineyards. *Agronomy*, *12* (6), 1328. https://doi.org/10.3390/agronomy12061328

Ragasová, L., Kopta, T., Winkler, J., Šefrová, H., Sochor, J., & Pokluda, R. (2021). The impact of vineyard inter-row vegetation on plant and insect diversity. *European Journal of Horticultural Science*, *86* (4), 360–370. https://doi.org/10.17660/eJHS.2021/86.4.3

Rainio, J., & Niemelä, J. (2003). Ground beetles (Coleoptera: Carabidae) as bioindicators. *Biodiversity & Conservation*, *12*, 487–506. https://doi.org/10.1023/A:1022412617568

Rocher, L., Melloul, E., Blight, O., & Bischoff, A. (2024). Effect of spontaneous vegetation on beneficial arthropods in Mediterranean vineyards. *Agriculture, Ecosystems & Environment*, *359*, 108740. https://doi.org/10.1016/j.agee.2023.108740

Rusch, A., Binet, D., Delbac, L., & Thiéry, D. (2016). Local and landscape effects of agricultural intensification on Carabid community structure and weed seed predation in a perennial cropping system. *Landscape Ecology*, *31*, 2163–2174. https://doi.org/10.1007/s10980-016-0390-x

Sáenz-Romo, M. G., Veas-Bernal, A., Martínez-García, H., Campos-Herrera, R., Ibáñez-Pascual, S., Martínez-Villar, E., Pérez-Moreno, I., & Marco-Mancebón, V. S. (2019). Ground cover man-

agement in a Mediterranean vineyard: impact on insect abundance and diversity. *Agriculture, Ecosystems & Environment*, *283*, 106571. https://doi.org/10.1016/j.agee.2019.106571

Saunders, M. E. (2018). Ecosystem services in agriculture: understanding the multifunctional role of invertebrates. *Agricultural & Forest Entomology*, *20* (2), 298–300. https://doi.org/10.1111/afe.12248

Schaffers, A. P., Raemakers, I. P., Sýkora, K. V., & Braak, C. ter (2008). Arthropod assemblages are best predicted by plant species composition. *Ecology*, *89* (3), 782–794. https://doi.org/10.1890/07-0361.1

Taranto, L., Rodrigues, I., Santos, S., Villa, M., & Pereira, J. A. (2023). Intermediate fragmentation surrounding vineyards favours the Coleoptera community within the crop. *Agricultural and Forest Entomology*, *25* (1), 9–19. https://doi.org/10.1111/afe.12527

Tscharntke, T., Klein, A. M., Kruess, A., Steffan-Dewenter, I., & Thies, C. (2005). Landscape perspectives on agricultural intensification and biodiversity – ecosystem service management. *Ecology Letters*, *8* (8), 857–874. https://doi.org/10.1111/j.1461-0248.2005.00782.x

Uzman, D., Entling, M. H., Leyer, I., & Reineke, A. (2020). Mutual and opposing responses of carabid beetles and predatory wasps to local and landscape factors in vineyards. *Insects*, *11* (11), 746. https://doi.org/10.3390/insects11110746

Winkler, J., Ježová, M., Punčochář, R., Hurajová, E., Martínez Barroso, P., Kopta, T., Semerádová, D., & Vaverková, M. D. (2023). Fire hazard: undesirable ecosystem function of orchard vegetation. *Fire*, *6* (1), 25. https://doi.org/10.3390/fire6010025

Winkler, K. J., Viers, J. H., & Nicholas, K. A. (2017). Assessing Ecosystem Services and Multifunctionality for Vineyard Systems. *Frontiers in Environmental Science*, *5*, 15. https://doi.org/10.3389/fenvs.2017.00015

Winter, S., Bauer, T., Strauss, P., Kratschmer, S., Paredes, D., Popescu, D., Landa, B., Guzmán, G., Gómez, J. A., Guernion, M., Zaller, J. G., & Batáry, P. (2018). Effects of vegetation management intensity on biodiversity and ecosystem services in vineyards: a meta-analysis. *Journal of Applied Ecology*, *55* (5), 2484–2495. https://doi.org/10.1111/1365-2664.13124

Summary

Vegetation succession and changes in carabid beetle (Coleoptera: Carabidae) communities in vineyards in Moravia, Czech Republic. Vineyards provide space for microhabitats and require a very specific way of management. Vineyard vegetation undergoes succession over time, which affects insect communities. The selected vineyards are located in Moravia in the Czech Republic. The vegetation of the vineyards consisted of 48 species of annual dicotyledons, 63 species of perennial dicotyledons, 9 species of annual grasses, and 10 species of perennial grasses. During the observation, 9 species of carabid beetles were recorded in the monitored

vineyards. The composition of the vegetation in the vineyards changes with the age of the vineyard. Over time, representatives of the perennial dicotyledons, perennial grasses groups increase and representatives of the group annual dicotyledons decrease. The age of the vineyards also changed the carabid beetle community – the *Anchomenus dorsalis* species was more common in older vineyards. The *Dolichus halensis*, *Leistus ferrugineus* and *Platynus assimilis* species were more frequently recorded in summer and fall in older vineyards. The other species preferred younger vineyards. A higher abundance was recorded in summer and fall, which may be due to a higher food supply and sufficient amount of microhabitats for hibernation.

Scientific Review Engineering and Environmental Sciences (2024), 33 (3), 304–325

Sci. Rev. Eng. Env. Sci. (2024), 33 (3) https://srees.sggw.edu.pl

ISSN 1732-9353 (suspended) eISSN 2543-7496 DOI 10.22630/srees.5935

Received: 09.01.2024
Accepted: 29.02.2024

Matthew Ndubuisi ABONYI[1]✉

Joseph Tagbo NWABANNE[1]

Samuel Chigozie NZEKWE[1]

Clinton Chizoba ELE[1]

Blessing Chiemerie ORUNTA[1]

Lawrence Ifeanyi IGBONEKWU[2]

[1] Nnamdi Azikiwe University, Faculty of Engineering, Department of Chemical Engineering, Nigeria
[2] Nnamdi Azikiwe University, Faculty of Engineering, Department of Petroleum Engineering, Nigeria

Adsorptive removal of a nitrate ion from the aqueous solution of sodium nitrate by application of double fixed-bed column

Keywords: nitrate, rice husk, fixed-bed, double parking, adsorption

Introduction

One of the prominent global challenges in water pollution of the environment involves the contamination caused by nitrogen-containing compounds such as nitrate, nitrite, and ammonium (Ward et al., 2018). Groundwater can be susceptible to nitrate ion contamination due to excessive fertilizer usage in agriculture (El Ouardi et al., 2015; Jiaa et al., 2020). Nitrate salts, including potassium nitrate, sodium nitrate, calcium nitrates, and ammonium, find applications in the manufacturing of nitrogen-based fertilizers, specialized cement formulation, as food additives and

✉mn.abonyi@unizik.edu.ng

dyes (Daouda et al., 2018). The World Health Organization has established daily maximum acceptable limits for nitrate at 0.3–0.7 $mg \cdot kg^{-1}$. The maximum acceptable limit of nitrate in water for human consumption is set at 50 $mg \cdot l^{-1}$ (World Health Organization [WHO], 2017). Nitrate contamination poses risks to human health primarily through the conversion of nitrates to nitrites, which are highly soluble in aqueous solutions and pose threats to drinking water supplies and promote eutrophication in groundwater (El Ouardi et al., 2015).

The reduction of nitrate to nitrosamines in the stomach can lead to various health problems such as prostate, pharynx, esophagus, or colon cancer (Zheng & Wang, 2010). In infants, the conversion of nitrate to nitrite, which later reacts with hemoglobin, can cause methemoglobinemia or blue baby syndrome, resulting in blueness of the skin in newborn babies (El Ouardi et al., 2015). Nitrate-contaminated water bodies have been known to contribute to infectious diseases in humans (El Ouardi et al., 2015). Furthermore, high concentrations of nitrate in aqueous solutions have been associated with miscarriages, eutrophication, harmful algal proliferation, hypoxia, and loss of biodiversity (Tejada-Tovar et al., 2021). Consequently, there is a pressing need to reduce nitrate levels in water to meet acceptable standards.

Various techniques have been employed to remove nitrate from aqueous solutions, including electrodialysis (Koter et al., 2015), adsorption (Tong et al., 2017; Taoufik et al., 2020), biological methods (Shi et al., 2013; Li et al., 2017), ion exchange (Werth et al., 2021), reverse osmosis (Shelly et al., 2021), nano-filtration membrane (Adeniyi et al., 2022), freeze-melting (Hosseini & Mahvi, 2018), chemical reduction (El Ouardi et al., 2015), coagulation, oxidation, precipitation, and filtration (Kumar et al., 2010; Foo & Hameed, 2012). However, many of these techniques are expensive and not economically feasible for large-scale industries. Additionally, some methods result in the generation of secondary pollutants, such as residues of dead bacteria from biological approaches, which can pose challenges in subsequent processes. Therefore, there is a need to explore simple, cost-effective, efficient, and environmentally friendly techniques, such as adsorption onto micro-porous solids like activated carbon (Varsha et al., 2022).

In recent years, several adsorbents have been utilized to remove contaminants, particularly nitrate, from aqueous solutions. These include nanoparticles (Tyagi et al., 2018), modified chitosan beads (Jamka & Mohammed, 2023), local clay (Battas et al., 2019), organic resin (Li et al., 2020), mineral-based adsorbents (Chen et al., 2020), and nanostructured carbon (Liu et al., 2018). However, many of these adsorbents are expensive, non-biodegradable, and require complicated synthesis processes (Quang et al., 2022). Therefore, it is crucial to develop adsorbents

through simple synthesis methods to reduce costs. Activated rice husk presents itself as a favorable alternative due to its affordability, availability, and excellent adsorption properties.

The study of nitrate adsorption in packed columns has gained significant interest. Consequently, conducting column studies is essential to determine the necessary contact time for achieving adsorbate equilibrium. Column adsorption studies hold significance for industrial applications since findings from batch adsorption studies may not be directly applicable to field applications in treating contaminated water (Jahangiri-Rad et al., 2014). Fixed column adsorption proves to be a better, simpler, and more economical method for removing various contaminants industrially. Moreover, fixed bed columns are preferable over batch adsorption because they offer industrial feasibility for removing various contaminants from either real wastewater or synthetic effluent. Literature reveals numerous studies focused on single-parked column adsorption of nitrate from aqueous solutions, but none have explored the impact of multiple parking in a column. Introducing multiple parking in a column or utilizing serially connected columns could enhance the efficiency of the adsorption process, thereby justifying the need for this study. This research utilizes activated rice husk carbon in a double-parked fixed adsorption column to remove nitrate from aqueous solutions. The study investigates the influence of parking height, flow rate variation, adsorbate concentration, and the number of parking layers on the adsorptive removal of nitrate from aqueous solutions.

Material and methods

Adsorbent (rice husk activated carbon) preparation

The rice husk was obtained from Mgbakwu, Awka North in Anambra State, Nigeria (6°16′20″ N and 7°3′21″ E). It underwent a series of preparation steps for the experimental use. Initially, it was carefully sorted to eliminate any impurities, followed by thorough washing with clean tap water. The husk was then dried in sunlight until it reached a moisture-free state. Subsequently, the rice husk underwent thermal carbonization at 450°C in a gas oven, maintaining this temperature for a duration of 30 min. After the carbonization process, the material was allowed to cool down to room temperature and stored in an air-tight container for further use. Before being utilized, the rice husk was manually crushed and sieved to achieve a particle size of 300 μm, suitable for the experimentation. The carbonized rice husk fibers were impregnated with 1M H_2SO_4 for a 24 h,

followed by heating at 700°C with a heating rate of 10°C·min^{-1} for a period of 2.3 h. Subsequently, the samples were removed, cooled, and thoroughly washed with deionized water multiple times to eliminate any residual acid from the H_2SO_4 treatment. The pH of the material was monitored using litmus paper until it reached a neutral state. Finally, the adsorbent was dried in an oven at 105°C for 60 min and underwent separation into different sizes using a mechanical shaker.

Nitrate solution preparation

To prepare the stock solution, a 1.0 g of sodium nitrate salt was dissolved in 200 ml of distilled water in a 1,000 ml volumetric flask and shaken to dissolve. It was thereafter made up to the mark with distilled water. The stock solution was serially diluted to obtain various concentrations ranging from 100 mg·l^{-1}, 150 mg·l^{-1} and 200 mg·l^{-1} of nitrate solution for the experiment.

Characterization of the rice husk activated carbon

The functional groups present in the samples were determined by the Fourier transform infrared machine, Cary 630 model, with Agilent technology. The adsorbent's chemical compositions were determined by X-ray fluorescence. While the surface morphology of the samples were determined by a scanning electron microscope (SEM) coupled with energy-dispersive spectroscopy (EDS) of model JOEL-JSM 7600F.

Packed bed adsorption apparatus set up

The experimental setup for the packed bed column consisted of a plastic column measuring 60 cm in height and 0.9 cm in diameter (refer to Fig. 1). To secure the packing material in place and prevent the passage of activated rice husk carbon (RHAC) particles, a wire mesh and cotton wool were placed at the bottom of each packing layer. The column was clamped to a stand, and a small hose connected to a peristaltic pump was used to introduce the nitrate solution from a beaker at a flow rate of 20 ml·min^{-1} into the top of the column.

To maintain consistent flow conditions and prevent changes in the nitrate solution flow rate upon entering the second packing layer, the entire adsorption experiment was conducted with the direction of flow from the top to the bottom of the column. Residual nitrate solution samples were collected at the sample point

Abonyi, M. N., Nwabanne, J. T., Nzekwe, S. C., Ele, C. C., Orunta, B. C., Igbonekwu, L. I. (2024). Adsorptive removal of a nitrate ion from the aqueous solution of sodium nitrate by application of double fixed-bed column. *Sci. Rev. Eng. Env. Sci.*, *33* (3), 304–325. DOI 10.22630/srees.5935

located at the side of the column using a syringe for the first packing layer. For the second packing layer, the residual nitrate solution was collected at the bottom of the column using a beaker.

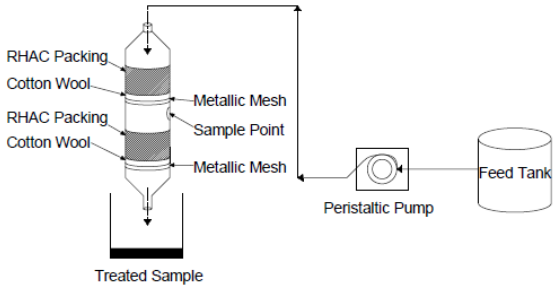

FIGURE 1. Double parked fixed bed adsorption column
Source: own work.

Finally, the initial concentration of the nitrate solution and the concentration of the nitrate solution samples obtained from both stages were analyzed using a UV spectrophotometer to determine the concentration of nitrate ions in the effluent sample.

Column experiment

Column experiment was performed to evaluate the effect of nitrate solution flow rate, number of packing, height of adsorbent packing and initial nitrate solution concentration on adsorption performance of RHAC and each of the experiment was performed as follows.

Effect of initial nitrate solution concentration

To investigate the impact of initial concentration on the adsorption performance of activated rice husk carbon (RHAC), nitrate solutions with concentrations of 100 $mg \cdot l^{-1}$, 150 $mg \cdot l^{-1}$, and 200 $mg \cdot l^{-1}$ were prepared from the stock solution. For the initial concentration of 100 $mg \cdot l^{-1}$, a 400-milliliter nitrate solution was measured and placed in a 500-milliliter beaker. The peristaltic pump was then utilized to pump the nitrate solution into the adsorption column at a constant flow rate of 10 $ml \cdot min^{-1}$. The column maintained a consistent packing height of 5 cm with the RHAC.

Samples were collected at five-minute intervals over a duration of 60 min. Each sample was collected and stored for a subsequent analysis. The analysis involved using a UV spectrophotometer at a wavelength of 220 nm to determine the nitrate ion concentration in the collected samples. This entire procedure was repeated for the initial concentrations of 150 $mg \cdot l^{-1}$ and 200 $mg \cdot l^{-1}$ of sodium nitrate solution to assess their respective adsorption performances.

Effect of bed height

To examine the impact of the height of adsorbent packing on the adsorptive performance of activated rice husk carbon (RHAC), three different packing heights were considered: 3 cm, 5 cm, and 7 cm. Throughout the experiment, a peristaltic pump was employed to transfer the nitrate solution from a beaker into the packed column. The initial concentration of the nitrate solution, flow rate, and the number of packing remained constant at 100 $mg \cdot l^{-1}$, 10 $ml \cdot min^{-1}$, and single packing, respectively.

At regular intervals of 5 min, samples were collected using sample bottles for each of the three different packing heights (3 cm, 5 cm, and 7 cm) over a total duration of 60 min. The collected samples were then analyzed using a UV-visible spectrophotometer at a wavelength of 220 nm to determine the concentrations of the samples.

Effect of number of rice activated carbon packing

To investigate the influence of the number of packing on the adsorption performance of RHAC, an adsorption column was constructed with two packings of RHAC, each 5 cm high. A 400-milliliter nitrate solution with a constant concentration of 100 $mg \cdot l^{-1}$ was measured using a measuring cylinder and placed in a beaker.

Using a peristaltic pump, the nitrate solution was continuously pumped into the adsorption column at a consistent flow rate of 10 $ml \cdot min^{-1}$. Samples were collected at two points within the column: below the first packing and at the exit bottom end. The collection of samples began at an initial time of 5 min and continued until 60 min. After the collection of samples, the nitrate ion concentration in each sample was determined using a UV spectrophotometer at a wavelength of 220 nm.

Adsorption modeling

Three adsorption modelling were employed to fit the data and describe the adsorption performance of the column. The models are Adams–Bohart, Thomas and Yoon–Nelson models. The non-linear and linear model used in this study are presented in Table 1.

TABLE 1. List of column adsorption models used

Model	Non-linear	Linear	Plot made	Eq.	Reference
Thomas	$\frac{C_t}{C_o}=\frac{1}{1+\exp\left(\frac{K_{Th}}{Q}\left(q_t x-C_o v_{eff}\right)\right)}$	$\ln\left[\frac{C_o}{C_t}-1\right]=\left[\frac{K_{Th}q_o x}{Q}\right]-K_{Th}C_o t$	$\ln\left[\frac{C_o}{C_t}-1\right]$ vs t	(1)	Swarup & Umesh, 2015
Adams–Bohart	$T=\left[\frac{N_o z}{C_o v}\right]-\left[\frac{\ln\left(\frac{C_o}{C_t}-1\right)}{C_o K_{AB}}\right]$	$\ln\left(\frac{C_t}{C_o}\right)=K_{AB}C_o t-\frac{K_{AB}N_o Z}{F}$	$\ln\left(\frac{C_t}{C_o}\right)$ vs t	(2)	Swarup & Umesh, 2015
Yoon–Nelson	$\frac{C_t}{C_o}=\frac{1}{1+e^{K_{YN}(\tau-t)}}$	$\ln\left(\frac{C_t}{C_o-C_t}\right)=K_{YN}t-\tau K_{YN}$	$\ln\left(\frac{C_t}{C_o-C_t}\right)$ vs t	(3)	Chen et al., 2017

Note: C_o – initial concentration, C_t – concentration at time (t), K_{Th} – Thomas rate constant [l·mg^{-1}·min^{-1}], Q – flow rate [ml·min^{-1}], q_t – nitrate uptake per 1 g of the adsorbent at time (t) [mg·g^{-1}], x – mass of the used adsorbent [g], v_{eff} – the effluent volume [ml], q_o – maximum nitrate uptake per 1 g of the adsorbent [mg·g^{-1}], T – the time required for 50% adsorbate breakthrough [min], N_o – saturation concentration [mg·l^{-1}], Z – bed height of column [cm], v – volume [ml], K_{AB} – the kinetic constant for the Adams–Bohart model [l·mg^{-1}·min^{-1}], F – superficial velocity calculated by dividing the flow rate by the column section area [cm·min^{-1}], e – exponent, K_{YN} – Yoon–Nelson rate constant [min^{-1}], τ – breakthrough time required for 50% adsorbate breakthrough [min].

Source: own work.

Results and discussion

Fourier transformed infrared (FTIR)

The Fourier transform infrared (FTIR) analysis of both rice husk biomass (RHB) and rice husk activated carbon (RHAC) samples was conducted within the wave number range of 500 cm^{-1} to 4,000 cm^{-1}. The results are presented in Table 2. Several significant absorption peaks were observed in the RHB sample. Notably, large absorption peaks were observed at 3,898.8 cm^{-1}, 3,749.7 cm^{-1}, and 3,313.6 cm^{-1}, which can be attributed to the overlapping stretching vibrations of hydroxyl (OH) and amino (NH_2) groups present in pure rice husk (Abonyi et al., 2023). The peak at 3,749.6 cm^{-1} corresponds to the Si-OH stretching vibration

of rice husk. Additionally, characteristic peaks of carbonyl group stretching for aldehydes and ketones were observed at 1,897.2 cm^{-1} and 1,695.9 cm^{-1}, respectively. The band at 1,568.0 cm^{-1} indicates the presence of the COO- group, which can be attributed to the H_2SO_4 used during the activation process of the rice husk. The peak at 2,322.1 cm^{-1} corresponds to the stretching vibration of Si-H, while the bands in the 1,058.6 cm^{-1} region represent the stretching vibration of Si-O. The stretching vibrations of $-NH_2$ groups were detected at 898.3 cm^{-1}.

Upon adsorption of sodium nitrate by the activated rice husk (RHA), changes in the peaks of certain functional groups were observed. Some functional groups, such as the ones at 3,898.8 cm^{-1}, 3,749.7 cm^{-1}, 3,313.6 cm^{-1}, 2,616.6 cm^{-1}, 2,448.9 cm^{-1}, 2,322.1 cm^{-1}, and 1,695.9 cm^{-1}, completely disappeared. Simultaneously, new functional groups emerged, as evidenced by the appearance of peaks at 3,268.9 cm^{-1}, 2,918.5 cm^{-1}, and 1,222.6 cm^{-1}. These changes indicate the adsorption of nitrate onto the surface of the activated rice husk (RHA), resulting in the alteration of certain functional groups and the formation of new ones.

TABLE 2. FTIR spectral of RHA and RHB

s/n	Wave number of RHB [cm^{-1}]	Wave number of RHA [cm^{-1}]	Difference in wave number [cm^{-1}]	Functional group
1	3 898.8	disappeared	3 898.8	alkane
2	3 749.7	disappeared	3 749.7	Si-OH
3	3 313.6	disappeared	3 313.6	-OH
4	absent	3 268.9	3 268.9	-O-H
5	absent	2 918.5	2 918.5	C-H
6	2 616.6	disappeared	2 616.6	N-H stretching
7	2 448.9	disappeared	2 448.9	C≡C stretching
8	2 322.1	disappeared	2 322.1	Si-H
9	2 042.4	2 109.7	66.6	-C≡C-
10	1 897.2	1 990.4	93.2	aldehyde
11	1 695.9	disappeared	1 695.9	ketone
12	1 568.0	1 576.7	8.7	COO-
13	absent	1 222.6	1 222.6	C-N
14	1 058.6	1 095.8	37.2	Si-O
14	782.7	898.3	115.6	$-NH_2$

Source: own work.

Abonyi, M. N., Nwabanne, J. T., Nzekwe, S. C., Ele, C. C., Orunta, B. C., Igbonekwu, L. I. (2024). Adsorptive removal of a nitrate ion from the aqueous solution of sodium nitrate by application of double fixed-bed column. *Sci. Rev. Eng. Env. Sci.*, *33* (3), 304–325. DOI 10.22630/srees.5935

Scanning electron microscopy (SEM-EDS)

The surface description and composition of the rice husk samples were analyzed using SEM-EDS (scanning electron microscopy-energy dispersive X-ray spectroscopy). Figure 2a shows the SEM micrograph of the untreated rice husk biomass (RHBS). It reveals that the sample exists in an amorphous silica form. Upon closer examination, the micrograph exhibits longitudinal-like fibrous particles of rice husk. Spaces and cavities are observed throughout the micrograph, which may aid in the adsorption of metals and ions in different areas of the material. These surface features indicate the potential of RHBS to retain nitrate ions.

Figure 3a depicts the SEM micrograph of the activated rice husk (RHAC). Compared to RHB in Figure 2a, the surface of RHAC shows fewer and less developed pores, as well as a less ordered and fewer flake-like structure. This variation in surface morphology between RHB and RHAC can be attributed to the adsorption of nitrate ions into the pores of the adsorbent. Thus, the observed morphologies in RHBS and RHAC present favorable surface characteristics for nitrate ion retention.

The compositions of the samples were determined using SEM-EDS, and the results are presented in Figures 2b and 3b. According to Figure 2b, RHBS primarily consists of silica (42.20%), oxygen (35.30%), and calcium (12.33%). Other components present in RHBS include carbon (5%), potassium (2.17%), and magnesium (1.25%). In Figure 3b, a larger percentage of RHAC is composed of calcium (12.33%), oxygen (20.30%), and silica (52.20%). The remaining components in RHAC are the same as in RHBS, except for the introduction of aluminum (6.30%) in RHAC.

Comparing Figures 2b and 3b, the EDS analysis reveals changes in the elemental composition of the activated rice husk after adsorption. There is a significant

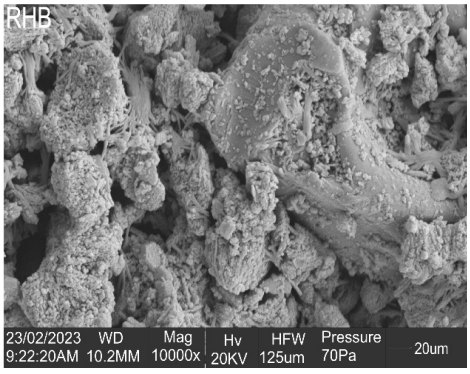

FIGURE 2a. SEM image of RHBS

Source: own work.

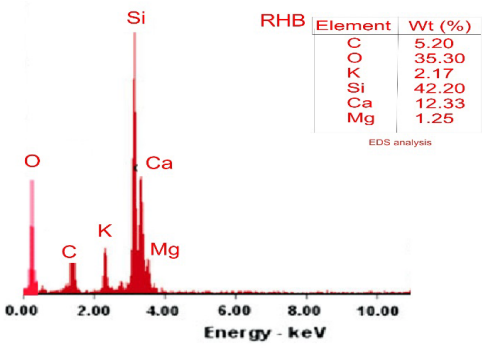

FIGURE 2b. EDS of RHBS

Source: own work.

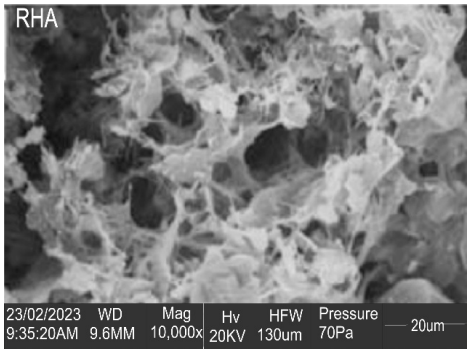

FIGURE 3a. SEM image of RHAC
Source: own work.

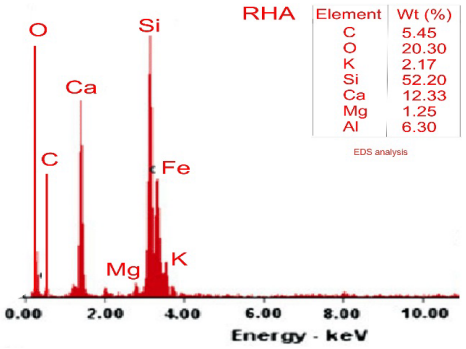

FIGURE 3b. EDS of RHAC
Source: own work.

decrease in the weight percentage [wt%] of oxygen and the introduction of aluminum (Al), which likely originated from impurities present in the nitrate salt solution used. The decrease in oxygen can be attributed to the adsorption of nitrate ions onto the surface of the activated rice husk. The increase in aluminum may be attributed to the formation of aluminum oxide or aluminum hydroxide complexes during the adsorption process. Notably, there is an increase in the weight percentage of silicon (Si) after adsorption, indicating that the adsorption process did not significantly remove Si from the activated rice husk. This is important as Si is a crucial component of the activated rice husk structure, and its removal could affect the porosity and surface area of the adsorbent. The highest peak obtained for Si occurred at 3.7 keV. The presence of potassium (K) and magnesium (Mg) before and after adsorption suggests that these elements are not significantly affected by the adsorption process and may play a lesser role in nitrate ion adsorption.

XRF analysis of rice husk

The X-ray fluorescence (XRF) analysis results for RHA and RHB are presented in Tables 3 and 4. Table 3 indicates that SiO_2, P_2O_5, CaO, and K_2O are the predominant oxides in both RHAC and RHBS. SiO_2 has the highest concentration in both RHA (71.315%) and RHBS (74.476%). It is notable that RHAC shows an increase in the concentration of SiO_2, CaO, and Al_2O_3 compared to RHBS. On the other hand, RHAC exhibits decreased concentrations of MnO, Fe_2O_3, P_2O_5, and K_2O compared to RHBS. Table 4 illustrates the elemental compositions of RHAC and RHBS as determined by the XRF analysis. Each element has characteristic X-ray peaks at different wavelengths, and the fluorescence intensity of each spectral

Abonyi, M. N., Nwabanne, J. T., Nzekwe, S. C., Ele, C. C., Orunta, B. C., Igbonekwu, L. I. (2024). Adsorptive removal of a nitrate ion from the aqueous solution of sodium nitrate by application of double fixed-bed column. *Sci. Rev. Eng. Env. Sci.*, *33* (3), 304–325. DOI 10.22630/srees.5935

line corresponds to the element concentration. The results reveal that RHAC has increased relative quantities of oxygen (O), aluminum (Al), silicon (Si), sulfur (S), calcium (Ca), and manganese (Mn), while exhibiting decreased concentrations of phosphorus (P), potassium (K), titanium (Ti), and iron (Fe).

TABLE 3. Concentrations of oxides in rice husk XRF analysis

Major oxides	Concentration [wt%]	
	RHBS	RHACS
SiO_2	71.315	74.476
MnO	0.826	0.672
Fe_2O_3	0.658	0.510
CuO	0.120	0.121
P_2O_5	7.568	6.560
SO_3	1.670	1.767
CaO	4.718	5.211
MgO	0.000	0.000
K_2O	8.037	5.881
Al_2O_3	1.497	1.744
TiO_2	0.383	0.161
ZnO	0.081	0.088

Source: own work.

TABLE 4. Concentrations of trace metals in the rice husk XRF analysis

Trace element	Concentration [ppm]	
	RHBS	RHAC
O	47.252	48.153
Al	0.792	0.923
Si	33.336	34.184
P	3.303	2.863
S	0.669	0.708
Cl	3.059	2.713
K	6.672	4.882
Ca	3.372	3.724
Ti	0.230	0.096
Mn	0.640	0.520
Fe	0.460	0.357
Cu	0.096	0.097
Zn	0.065	0.071

Source: own work.

These elemental compositions may influence the adsorption of nitrate ions onto the rice husk surface through ion exchange processes. The increased nitrate ion uptake by RHAC can potentially be attributed to the higher concentrations of more easily exchangeable elements such as Si and K. The XRF analysis provides valuable information regarding the elemental composition of the samples, which is instrumental in understanding the chemical properties of both the rice husk and the aqueous solution. The information obtained from the XRF analysis can be utilized to optimize the process, enhance product quality, and reduce waste.

Effect of initial concentration of nitrate ion on breakthrough curve

The performance of the column was evaluated at initial nitrate ion concentrations of 100 $mg \cdot l^{-1}$, 150 $mg \cdot l^{-1}$, and 200 $mg \cdot l^{-1}$. The bed height and flow rate were kept constant at 7 cm and $8.33 \cdot 10^{-8}$ $m^3 \cdot s^{-1}$, respectively. The results are depicted in Figure 4.

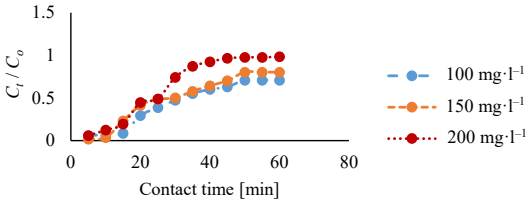

FIGURE 4. Effect of initial nitrate ion solution
Source: own work.

It can be observed that as the initial nitrate ion concentration increased from 100 $mg \cdot l^{-1}$ to 200 $mg \cdot l^{-1}$, the breakthrough time decreased. This indicates that the adsorption bed became saturated more quickly at higher initial concentrations due to the rapid saturation of binding sites within the column. At 200 $mg \cdot l^{-1}$ initial concentration, the column achieved a higher efficiency at saturation, with a value of 96.52%, compared to 70.24% and 62.99% for 150 $mg \cdot l^{-1}$ and 100 $mg \cdot l^{-1}$, respectively.

The higher efficiency at higher initial concentrations can be attributed to the increased driving force provided by the higher concentration of adsorbate (nitrate ion). This is necessary to overcome the mass transfer resistance between the aqueous solution and the RHAC adsorbent phase. As a result, there is greater collision between the nitrate ions and the active sites of the RHAC, leading to enhanced adsorption.

Abonyi, M. N., Nwabanne, J. T., Nzekwe, S. C., Ele, C. C., Orunta, B. C., Igbonekwu, L. I. (2024). Adsorptive removal of a nitrate ion from the aqueous solution of sodium nitrate by application of double fixed-bed column. *Sci. Rev. Eng. Env. Sci.*, *33* (3), 304–325. DOI 10.22630/srees.5935

In summary, the RHAC reached saturation earlier at higher initial concentrations, resulting in a reduced breakthrough time. This can be attributed to the higher initial concentrations of nitrate ions saturating the RHAC more rapidly. Conversely, lower initial concentrations of nitrate ion tend to delay the breakthrough point due to slower transport velocity and longer contact time resulting from a lower concentration gradient. Similar findings have been reported in studies conducted by Swarup and Umesh (2015), and Chen et al. (2017).

Effect of bed height on breakthrough curve

The impact of bed height on the breakthrough curve is illustrated in Figure 5. It can be observed that increasing the bed height from 3 cm to 7 cm resulted in an increase in the breakthrough time. This is because an increase in bed height leads to the addition of more sorption sites, which are necessary for the adsorption of nitrate ions. With a reduced bed height, the nitrate ions have limited time to come into contact with the RHAC surface, resulting in a decreased breakthrough time.

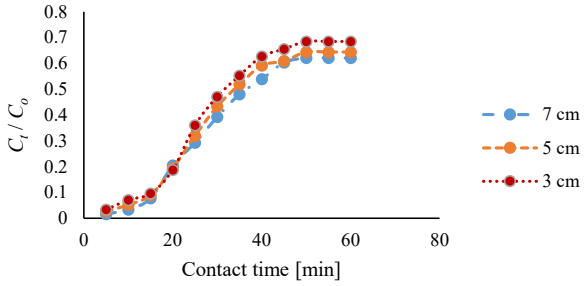

FIGURE 5. Effect of bed height on nitrate ion removal
Source: own work.

The maximum removal of nitrate from the aqueous solution using RHAC occurs in the initial stages of the adsorption process. However, over time, the sorption of nitrate ions decreases due to the depletion of available sorption sites required for nitrate ion removal. In the design and operation of a fixed bed column, a greater bed height and slower exhaustion of the adsorbent bed are desirable as they increase the adsorption capacity while extending the breakthrough time. On the other hand, a reduced bed height does not provide sufficient time for the adsorbate (nitrate ion) to diffuse into the active sites of the RHAC, resulting in a shorter breakthrough time.

Similar trends have been reported in studies conducted by Mondal (2009) and Omitola et al. (2022). They found that increasing the bed height led to an increase in breakthrough time and improved adsorption capacity.

Effect of number of parking in a column on breakthrough curve

The impact of the number of packing (or beds) in the fixed bed column was investigated under constant flow rate ($8.33 \cdot 10^{-8}$ $m^3 \cdot s^{-1}$) and initial concentration (100 $mg \cdot l^{-1}$). The configuration consisted of two packings with a height of 7 cm each, separated by a 10 cm gap, as illustrated in Figure 1. The purpose of introducing multiple packing to the column was to assess the effect of additional beds on the removal efficiency of nitrate ions.

Figure 6 demonstrates that the inclusion of an extra packing or bed tends to enhance the efficiency of the adsorption column. At saturation, the optimal removal efficiency of nitrate ions for the first bed was 60.3%, whereas the introduction of the second fixed bed increased the efficiency to 81.4%. The addition of a fixed bed to the column results in an increased amount or number of sorption sites, as well as an extended service time until breakthrough and exhaustion of the active sites.

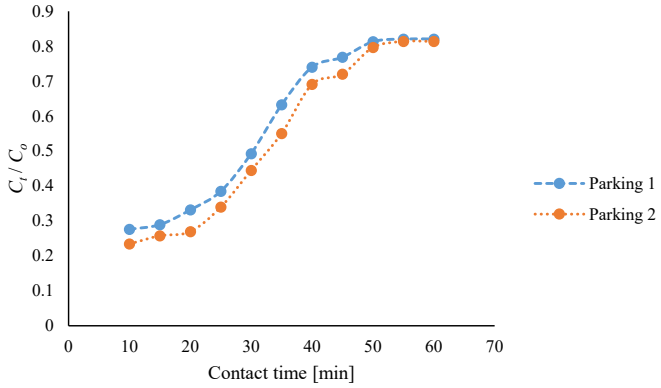

FIGURE 6. Effect of number of parking
Source: own work.

The increase in the number of beds leads to a greater amount of adsorbent within the adsorption column, providing more active sites for the removal of nitrate ions. Consequently, the overall removal efficiency of nitrate ions improves with the addition of multiple packing.

In summary, the introduction of multiple packing (beds) to the fixed bed column results in an enhanced performance and increased removal efficiency of nitrate ions. The inclusion of additional beds increases the available sorption sites and extends the service time until breakthrough and exhaustion of the active sites, leading to improved nitrate ion removal.

Column adsorption modeling

The experimental data obtained from the fixed bed adsorption experiment were analyzed using the Thomas, Adams–Bohart, and Yoon–Nelson kinetic models. The linear and non-linear forms of these models are presented in Table 1. The breakthrough behavior of the adsorption process was studied at different initial concentrations of nitrate ion, bed heights, and number of packing in the fixed bed column. The model parameters for each kinetic model were determined and are summarized in Table 5.

The Thomas model describes a rate-driving force and non-axial dispersion, assuming that internal and external diffusion are not the rate-controlling steps in the adsorption process. The q_o [mg·g^{-1}] and K_{Tb} [l·mg^{-1}·min^{-1}] constants were obtained from the plots of $\ln\left(\frac{C_o}{C_t}\right)$ versus time (t). According to Table 5, an increase in the initial concentration of nitrate ions led to a decrease in q_o, which is contrary to the findings of Omitola et al. (2022). However, the value of K_{Tb} increased with increasing initial concentration, which aligns with the reports of Chowdury et al. (2013). It was observed that a notable correlation exist between the bed height and the Thomas model constant (K_{Tb}) wherein an increase in bed height from 3 cm to 7 cm coincides with a proportional rise in K_{Tb}. Conversely, an attendant decrease in the maximum adsorption capacity (q_o) is noted under the same conditions. This observation highlights the relationship between bed height and adsorption kinetics, wherein increased column height facilitates enhanced mass transfer. This consequently increase the rate of adsorption while potentially diluting the overall adsorption capacity. Moreover, the investigation reveals a noteworthy relationship between the number of packing units within the fixed-bed column and key adsorption parameters. Specifically, an increase in packing density correlates with an increase in q_o, indicative of a heightened capacity for adsorption. Interestingly, this trend is accompanied by a decline in K_{Tb}, suggesting an observable relationship between packing density and the rate of adsorption. Such observations underline the complex dynamics governing adsorption within fixed-bed columns, wherein

the arrangement and density of packing units exert discernible influences on adsorption kinetics and capacity. Furthermore, the robustness of the Thomas model in capturing the observed trends is highlighted by the high coefficient of determination (R^2) values obtained across varied experimental conditions (Abonyi et al., 2019; Obi et al., 2024). Particularly, R^2 values ranging from 0.677 to 0.807 for initial concentrations, 0.813 to 0.883 for fixed bed heights, and close to unity (ranging from 0.915 to 0.939) for the number of packing units. These results affirm the model's efficacy in accurately predicting adsorption behavior within the fixed-bed column. The implication of this findings challenges conventional notions regarding the rate-controlling steps in the adsorption process. This suggests that internal and external diffusion mechanisms, as posited by the Thomas model, may not singularly govern adsorption kinetics within the studied system. Rather, the observed relationship between bed height, packing density, and adsorption parameters highlights the need for a good understanding of the underlying mechanisms dictating adsorption behavior in fixed-bed columns, with potential implications for optimizing industrial-scale adsorption processes.

The Adams–Bohart model was analyzed by plotting $\ln\left(\frac{C_t}{C_o}\right)$ versus t. The slope and intercept of the plots were used to evaluate the N_o [mg·l^{-1}], K_{AB} [l·mg^{-1}·min^{-1}], and R^2 parameters, which are also presented in Table 5. The study investigates the dynamic behavior of column adsorption using the Adams–Bohart model, a widely utilized framework for describing breakthrough curves in adsorption processes. The findings reveal distinct dependencies between key model parameters and experimental variables, shedding light on the intricate relationship within the system. In essence, this analysis demonstrates a discernible trend wherein the rate constant K_{AB} exhibits a decrease as the initial concentration of the adsorbate and the number of packing units are increased. Interestingly, a converse relationship emerges with respect to the bed height, showcasing an increase in K_{AB} as this parameter increase. This observation highlights the essential role bed height plays in modulating the kinetics of adsorption within the column system. Also, the characteristic parameter N_o indicative of the adsorption capacity of the column, exhibits a reduction with increasing initial concentration and bed height. Conversely, a rise is observed with an increasing number of packing units, indicating a pronounced effect of the latter on enhancing adsorption efficiency. Furthermore, the robustness of our model fitting is highlighted by the high R^2 (Abonyi et al., 2022; Ohale et al., 2023) values attained across varied experimental conditions. Specifically, the commendable R^2 values ranging from 0.669 to 0.802 for initial concentration, 0.809 to 0.880 for bed height, and 0.912 to 0.938 for

the number of packing units, affirm the reliability of the Adams–Bohart model in capturing the intricate dynamics of breakthrough curves.

The Yoon–Nelson model was utilized to determine the rate constant (K_{YN}) and the time required for 50% nitrate ion breakthrough (τ). The values of K_{YN} and τ were obtained from the slope and intercept of the Yoon–Nelson plot at different initial nitrate ion concentrations, bed heights, and number of packing, as presented in Table 5. Notably, K_{YN} exhibits a discernible trend, increasing with increased initial concentration and bed height, while witnessing a decline with an increasing number of packing units. This observation underlines the crucial influence of initial concentration and bed height on the kinetics of adsorption within the column, while highlighting the mitigating effect of packing density on the rate of adsorption.

TABLE 5. Column adsorption data

Effect of concentration									
Concentration [mg·l^{-1}]	Thomas			Adams–Bohart			Yoon–Nelson		
	q_o [mg·g^{-1}]	K_{Tb} [mg·l^{-1}]	R^2	N_o [mg·l^{-1}]	K_{AB} [l·mg^{-1}·min^{-1}]	R^2	K_{YN} [min^{-1}]	τ [min]	R^2
100	449.936	0.0277	0.807	763.247	0.0280	0.802	0.0493	101.120	0.808
150	437.564	0.0281	0.677	665.400	0.0277	0.669	0.0572	89.033	0.671
200	395.836	0.0287	0.783	609.434	0.0275	0.776	0.0587	73.310	0.780
Heigh [cm]	Effect of bed height								
3	484.438	0.0249	0.883	855.780	0.0242	0.880	0.0426	113.280	0.889
5	443.304	0.0289	0.881	845.519	0.0251	0.878	0.0495	103.520	0.882
7	382.095	0.0370	0.813	673.366	0.0360	0.809	0.0632	89.477	0.817
Parking	Effect of number of parking in a column								
Parking 1	464.874	0.0278	0.915	820.203	0.0270	0.912	0.0475	108.820	0.917
Parking 2	564.344	0.0179	0.939	1 021.100	0.0170	0.938	0.0308	132.050	0.951

Source: own work.

Furthermore, the characteristic parameter τ, indicative of the mass transfer zone length, displays a contrasting pattern, diminishing with increasing initial concentration and bed height, but growing with an increasing number of packing units. The higher τ values are indicative of enhanced performance in the adsorption of nitrate ions from the aqueous solution, highlighting the efficacy of the column under varied experimental conditions. Moreover, the commendable R^2 values obtained for the Yoon–Nelson model across different experimental parameters further emphasized the model's predictive capability. With R^2 values ranging from 0.671 to

0.809 for initial concentration, 0.817 to 0.889 for bed height, and 0.917 to 0.951 for the number of packing units, the findings revealed the robustness of the model in capturing the intricate dynamics of breakthrough curves with high reliability.

Conclusions

The comprehensive analysis of the activated rice husk's surface chemistry through FTIR, SEM, SEM-EDS, and XRF techniques provided crucial insights into the nitrate ion adsorption process. The involvement of diverse functional groups, significant morphological alterations, and elemental compositions revealed the complex mechanisms underlying adsorption. Furthermore, the application of the Thomas, Adams–Bohart, and Yoon–Nelson models revealed distinct trends in adsorption behavior concerning initial concentration, bed height, and packing density. While the models demonstrated overall suitability, challenges were observed at higher initial concentrations, particularly evident with the Adams–Bohart model. Nonetheless, the consistent performance across varying parameters highlights the potential of these models for understanding and optimizing nitrate removal processes. Notably, the efficacy of double packing emerged as a promising strategy, offering enhanced performance compared to single packing configurations. This research provides significant insights into improving the removal of nitrates from water solutions, indicating practical applications for the development of effective adsorption systems. Future research could explore refining model parameters to address challenges at higher initial concentrations and further investigate the applicability of double packing configurations in larger-scale systems. Such advancements hold promise for addressing nitrate contamination challenges effectively.

Acknowledgments

We acknowledge the department of Chemical Engineering Nnamdi Azikiwe University, Awka for given us access to their laboratories for this research.

References

Abonyi, M. N., Nwabanne, J. T., Igbonekwu, L. I., Ohale, P. E., Nwachukwu, J. O., Ezechukwu, C. M., & Ndibe, I. O. (2023). Parametric and kinetic study of hybrid dye uptake by activated mango seed endocar. *UNIZIK Journal of Engineering and Applied Sciences*, *2* (2), 285–300.

Abonyi, M. N., Menkiti, M. C., Nwabanne, J. T., & Akomie G. K. (2022). Kinetic modeling and half-life study on bioremediation of crude oil dispersed by palm bunch enhanced stimulant, *Cleaner Chemical Engineering*, *2*, 100031. https://doi.org/10.1016/j.clce.2022.100031

Abonyi, M. N., Aniagor, C. O., Menkiti, M. C. (2019). Effective Dephenolation of Effluent from the Petroleum Industry Using Ionic-Liquid-Induced Hybrid Adsorbent. *Arabian Journal of Science and Engineering*, *44* (12), 10017–10029. https://doi.org/10.1007/s13369-019-04000-8

Adeniyi, A., Ortiz, D. G., Bohatier, C. P., Mbakop, S., & Onyango, M. S. (2022). Preparation of nanofiltration membrane modified with sawdust-derived cellulose nanocrystals for removal of nitrate from drinking water. *Membranes*, *12* (7), 670. https://doi.org/10.3390/membranes12070670

Battas, A., Gaidoumi, A. E., Ksakas, A., & Kherbeche, A. (2019). Adsorption study for the removal of nitrate from water using local clay. *The Scientific World Journal*, *2019*, 9529618. https://doi.org/10.1155/2019/9529618

Chen, W., Luan, J., Yu, X., & Wang, X. (2020). The preparation of novel mineral-based mesoporous microsphere by microencapsulation technology and its application in the adsorption of dye contaminants. *Water Science and Technology*, *81* (5), 985–999. https://doi.org/10.2166/wst.2020.188

Chen, Y., Wu, ., Liu, C., Guo, L., Nie, J., & Ren, R. (2017). Continuous fixed-bed column study and adsorption modeling: Removal of arsenate and arsenite in aqueous solution by organic modified spent grains. *Polish Journal of Environmental Studies*, *26* (4), 1847–1854. https://doi.org/10.15244/pjoes/68869

Chowdhury, Z. Z., Zain, S. M., Rashid, A. K., Rafique, R. F., & Khalid, K. (2013). Breakthrough curve analysis for column dynamics sorption of Mn (II) ions from wastewater by using Mangostana garcinia peel-based granular-activated carbon. *Journal of Chemistry*, *2013*, 959761. https://doi.org/10.1155/2013/959761

Daouda, K., Rahman, A. N., Valery, H. G., Nsami, N. J., Wahabou, A., & Mbadcam, K. J. (2018). Adsorption Equilibrium of Nitrates Ions onto Oil Palm Shells-based Activated Carbons. *Global Journal of Science Frontier Research: B Chemistry*, *18* (B2), 37–52.

El Ouardi, M., Qourzal, S., Alahiane, S., Assabbane, A., & Douch, J. (2015). Effective removal of nitrates ions from aqueous solution using new clay as potential low-cost adsorbent. *Journal of Encapsulation and Adsorption Sciences*, *5* (4), 178–190. http://dx.doi.org/10.4236/jeas.2015.54015

Foo, K. Y., & Hameed, B. H. (2012). Textural porosity, surface chemistry and adsorptive properties of durian shell derived activated carbon prepared by microwave assisted NaOH activation. *Chemical Engineering Journal*, *187*, 53–62. https://doi.org/10.1016/j.cej.2012.01.079

Hosseini, S. S., & Mahvi, A. H. (2018). Freezing process-a new approach for nitrate removal from drinking water. *Desalination and Water Treatment*, *130*, 109–116. https://doi.org/10.5004/dwt.2018.22963

Koter, S., Chojnowska, P., Szynkiewicz, K., & Koter, I. (2015). Batch electrodialysis of ammonium nitrate and sulfate solutions. *Journal of Membrane Science*, *496*, 219–228. https://doi.org/10.1016/j.memsci.2015.08.064

Kumar, K. V., Valenzuela-Calahorro, C., Juarez, J. M., Molina-Sabio, M., Silvestre-Albero, J., & Rodriguez-Reinoso, F. (2010). Hybrid isotherms for adsorption and capillary condensation of N_2 at 77K on porous and non-porous materials. *Chemical Engineering Journal*, *162* (1), 424–429. https://doi.org/10.1016/j.cej.2010.04.058

Li, Q., Li, X., Sun, J., Song, H., Wu, J., Wang, G., & Li, A. (2020). Removal of organic and inorganic matters from secondary effluent using resin adsorption and reuse of desorption eluate using ozone oxidation. *Chemosphere*, *251*, 126442. https://doi.org/10.1016/j.chemosphere.2020.126442

Li, Y., Wang, Y., Fu, L., Gao, Y., Zhao, H., & Zhou, W. (2017). Aerobic-heterotrophic nitrogen removal through nitrate reduction and ammonium assimilation by marine bacterium *Vibrio* sp. Y1-5. *Bioresource Technol*ogy, *230*, 103–111. https://doi.org/10.1016/j.biortech.2017.01.049

Liu, X., He, C., Yu, X., Bai, Y., Ye, L., Wang, B., & Zhang, L. (2018). Net-like porous activated carbon materials from shrimp shell by solution-processed carbonization and H_3PO_4 activation for methylene blue adsorption. *Powder Technology*, *326*, 181–189. https://doi.org/10.1016/j.powtec.2017.12.034

Jahangiri-Rad, M., Jamshidi, A., Rafiee, M., & Nabizadeh, R. (2014). Adsorption performance of packed bed column for nitrate removal using PAN-oxime-nano Fe_2O_3. *Journal of Environmental Health Science and Engineering*, *12* (90), 1–5. https://doi.org/10.1186/2052-336X-12-90

Jamka, Z. N., & Mohammed, W. T. (2023). Assessment of the feasibility of modified chitosan beads for the adsorption of nitrate from an aqueous solution. *Journal of Ecological Engineering*, *24* (2), 265–278. https://doi.org/10.12911/22998993/156886

Jiaa, L., Jiangb, B., Huangb, F., & Hub, X. (2020). Adsorption and mechanism of nitrate from groundwater onto Si–Al porous clay mineral material as ceramic waste: characterization, kinetics, and adsorption isotherms, *Desalination and Water Treatment*, *202*, 251–263. https://doi.org/10.5004/dwt.2020.26184

Mondal, M. K. (2009). Removal of Pb (II) ions from aqueous solution using activated tea waste: Adsorption on a fixed-bed column. *Journal of Environmental Management*, *90* (11), 3266–3271. https://doi.org/10.1016/j.jenvman.2009.05.025

Obi, C. C., Nwabanne, J. T., Igwegbe, C. A., Abonyi, M. N., Umembamalu, C. J., & Kamuche, T. T. (2024). Intelligent algorithms-aided modeling and optimization of the deturbidization of abattoir wastewater by electrocoagulation using aluminium electrodes. *Journal of Environmental Management*, *353*, 120161. https://doi.org/10.1016/j.jenvman.2024.120161

Omitola, O. B., Abonyi, M. N., Akpomie, K. G., & Dawodu, F. A. (2022). Adams-Bohart, Yoon-Nelson, and Thomas modeling of the fix-bed continuous column adsorption of amoxicillin onto silver nanoparticle-maize leaf composite. *Applied Water Science*, *12* (5), 94. https://doi.org/10.1007/s13201-022-01624-4

Ohale, P. E., Chukwudi, K., Ndive, J. N., Michael, M. E., Abonyi, M. N., Chukwu, M. M., Obi, C. C., Onu, C. E., Igwegbe, C. A., & Azie, C. A., & Azie, C. O. (2023). Optimization of Fe_2O_3@BC-KC composite preparation for adsorption of Alizarin red S dye: Characterization, kinetics, equilibrium, and thermodynamic studies. *Results in Surfaces and Interfaces*, *13*, 100157. https://doi.org/10.1016/j.rsurfi.2023.100157

Quang, H. H. P., Phan, K. T., Ta, P. D. L., Dinh, N. T., Alomar, T. S., AlMasoud, N., Huang, C. W., Chauchan, A., & Nguyen, V. H. (2022). Nitrate removal from aqueous solution using watermelon rind derived biochar-supported ZrO_2 nanomaterial: Synthesis, characterization, and mechanism. *Arabian Journal of Chemistry*, *15* (10), 104106. https://doi.org/10.1016/j.arabjc.2022.104106

Shelly, Y., Kuk, M., Menashe, O., Zeira, G., Azerrad, S., & Kurzbaum, E. (2021). Nitrate removal from a nitrate-rich reverse osmosis concentrate: Superior efficiency using the bioaugmentation of an Acinetobacter biofilm. *Journal of Water Process Engineering*, *44*, 102425. https://doi.org/10.1016/j.jwpe.2021.102425

Shi, Z., Zhang, Y., Zhou, J., Chen, M., & Wang, X. (2013). Biological removal of nitrate and ammonium under aerobic atmosphere by *Paracoccus versutus* LYM. *Bioresource Technology*, *148*, 144–148. https://doi.org/10.1016/j.biortech.2013.08.052

Swarup, B., & Umesh, M. (2015). Continuous fixed-bed column study and adsorption modeling: removal of lead ion from aqueous solution by charcoal originated from chemical carbonization of rubber wood sawdust. *Journal of Chemistry*, *2015*, 907379.

Taoufik, N., Elmchaouri, A., Korili, S. A., & Gil, A. (2020). Optimizing the removal of nitrate by adsorption onto activated carbon using response surface methodology based on the central composite design. *Journal of Applied Water Engineering and Research*, *8* (1), 66-77. https://doi.org/10.1080/23249676.2020.1723446

Tejada-Tovar, C., Villabona-Ortíz, Á., & Gonzalez-Delgado, Á. D. (2021). Removal of nitrate ions using thermally and chemically modified bioadsorbents. *Applied Sciences*, *11* (18), 8455. https://doi.org/10.3390/app11188455

Tong, X., Yang, Z., Xu, P., Li, Y., & Niu, X. (2017). Nitrate adsorption from aqueous solutions by calcined ternary Mg-Al-Fe hydrotalcite. *Water Science and Technology*, *75* (9), 2194-2203. https://doi.org/10.2166/wst.2017.082

Tyagi, S., Rawtani, D., Khatri, N., & Tharmavaram, M. (2018). Strategies for nitrate removal from aqueous environment using nanotechnology: a review. *Journal of Water Process Engineering*, *21*, 84–95. https://doi.org/10.1016/j.jwpe.2017.12.005

Varsha, M., Kumar, P. S., & Rathi, B. S. (2022). A review on recent trends in the removal of emerging contaminants from aquatic environment using low-cost adsorbents. *Chemosphere*, *287*, 132270. https://doi.org/10.1016/j.chemosphere.2021.132270

Ward, M. H., Jones, R. R., Brender, J. D., De Kok, T. M., Weyer, P. J., Nolan, B. T., Villanueva, C. M., & Van Breda, S. G. (2018). Drinking water nitrate and human health: an updated review. *International Journal of Environmental Research and Public Health*, *15* (7), 1557. https://doi.org/10.3390/ijerph15071557

Werth, C. J., Yan, C., & Troutman, J. P. (2020). Factors impeding replacement of ion exchange with (electro) catalytic treatment for nitrate removal from drinking water. *Acs Es&T Engineering*, *1* (1), 6–20. https://doi.org/10.1021/acsestengg.0c00076

World Health Organization. (2017). *Guidelines for drinking-water quality, 4th edition, incorporating the 1st addendum.* WHO. https://www.who.int/publications/i/item/9789241549950

Zhang, Y., Zheng, R., Zhao, J., Ma, F., Zhang, Y., & Meng, Q. (2014). Characterization of H_3PO_4-treated rice husk adsorbent and adsorption of copper (II) from aqueous solution. *BioMed Research International*, *2014*, 496878. https://doi.org/10.1155/2014/496878

Zheng, Y., & Wang, A. (2010). Nitrate adsorption using poly (dimethyl diallyl ammonium chloride)/polyacrylamide hydrogel. *Journal of Chemical & Engineering Data*, *55* (9), 3494-3500. https://doi.org/10.1021/je100169r

Summary

Adsorptive removal of a nitrate ion from the aqueous solution of sodium nitrate by application of double fixed-bed column. This study focuses on the removal of nitrate ions from aqueous solutions using rice husk activated carbon (RHAC). The RHAC was subjected to characterization via Fourier transform infrared (FTIR), scanning electron microscopy coupled with energy dispersive spectroscopy (SEM-EDS), and X-ray florescence (XRF) to ascertain its functional groups, surface morphology, and oxide/elemental composition, respectively. Batch experiments were conducted to assess the impact of nitrate concentration, bed height, and number of packing layers on removal efficiency. FTIR spectra revealed favorable sorption-related functional groups within RHAC, while SEM analysis indicated the presence of effective sorption sites on its surface. EDS analysis of the rice husk adsorbent before adsorption (RHBS) demonstrated a significant composition of Si (42.20%), O (35.30%), and Ca (12.33%). The batch study unveiled a concentration--dependent decrease in nitrate removal efficiency, alongside the enhanced performance with increased bed height and number of packing layers. Kinetic data fitting favored the Yoon–Nelson and Adams–Bohart models. Overall, RHAC exhibited efficient nitrate ion removal, with column performance notably improved by utilizing multiple packing layers. These results will enhance our understanding of the mechanisms involved in removing nitrate ions and highlight the potential effectiveness of RHAC, especially when utilized with multiple packing arrangements in column setups.

Instruction for Authors

The journal publishes in English languages, peer-reviewed original research, critical reviews and short communications, which have not been and will not be published elsewhere in substantially the same form. Author of an article is required to transfer the copyright to the journal publisher, however authors retain significant rights to use and share their own published papers. The published papers are available under the terms of the principles of Open Access Creative Commons CC BY-NC license. The submitting author must agree to pay the publication charge (see Charges).

The author of submitted materials (e.g. text, figures, tables etc.) is obligated to restricts the publishing rights. All contributors who do not meet the criteria for authorship should be listed in an Acknowledgements section of the manuscript. Authors should, therefore, add a statement on the type of assistance, if any, received from the sponsor or the sponsor's representative and include the names of any person who provided technical help, writing assistance, editorial support or any type of participation in writing the manuscript.

Uniform requirements for manuscripts

The manuscript should be submitted by the Open Journal System (OJS) at https://srees.sggw.edu.pl/about/submissions. All figures and tables should be placed near their reference in the main text and additionally sent in a form of data files (e.g. Excel, Visio, Adobe Illustrator, Adobe Photoshop, CorelDRAW). Figures are printed in black and white on paper version of the journal (color printing is combined with an additional fee calculated on a case-by-case basis), while on the website are published in color.

The size of the manuscript should be limited up to 10 pages including overview, summary, references and figures (the manuscript more than 13 pages is unacceptable); Please set the text format in single column with paragraphs (A4 paper format), all margins to 25 mm, use the font Times New Roman, typeface 12 points and line spacing one and half.

The submitted manuscript should include the following parts:

- name and SURNAME of the author(s) – up to 5 authors
- affiliation of the author(s), ORCID Id (optional)
- title of the work
- key words
- abstract (about 500 characters)
- text of the paper divided into: Introduction, Material and Methods, Results and Discussion, Conclusions, References and Summary
- references in APA style are listed fully in alphabetical order according to the last name of the first author and not numbered; please find the details below
- post and mailing address of the corresponding author:

  Author's address:
  Name, SURNAME
  Affiliation
  Street, number, postal code, City
  Country
  e-mail: adress@domain

- Plagiarism statement (https://srees.sggw.edu.pl/copyright)

Reference formatting

In the Scientific Review Engineering and Environmental Sciences the APA 7th edition style is used.

Detailed information

More information can be found: https://srees.sggw.edu.pl